Timing, variability and cross-protection in bacteria –

Insights from dynamic gene expression responses to antibiotics

by

Karin Mitosch

July 24, 2017

A thesis presented to the
Graduate School
of the
Institute of Science and Technology Austria, Klosterneuburg, Austria
in partial fulfillment of the requirements
for the degree of
Doctor of Philosophy

Abstract

Antibiotics have diverse effects on bacteria. At high concentrations, they mostly stop bacterial growth or kill bacteria. However, in the human body or in nature, they are frequently found at lower concentrations, where they induce massive changes in bacterial metabolism, macromolecular composition, and gene expression. Whereas the gene expression changes under many antibiotics have been measured, the temporal organization of these responses and their dependence on the bacterial growth rate are unclear. Here, we initially quantified the temporal gene expression changes in the bacterium *Escherichia coli* in response to the sudden exposure to antibiotics. We chose four antibiotics representing diverse mechanisms of action and measured gene expression using a fluorescent reporter library and a robotic system. Our data show temporally structured gene expression responses, with response times for individual genes ranging from tens of minutes to several hours. The overall dynamics of these gene expression changes is mainly determined by the rate at which the antibiotic initially inhibits bacterial growth, but is also affected by antibiotic-specific mechanisms.

We observed that many stress response genes were activated in response to antibiotics. Some of these were expected based on the antibiotic mode of action; others, like the rapid and transient acid stress response under the folate synthesis inhibitor trimethoprim, were more surprising. It is unclear whether such stress responses are activated because bacteria experience and sense the particular stress, or whether they are activated via different regulons in a more unspecific way. Using genetic manipulations, a ratiometric pH sensor, and microfluidics, we showed that bacteria indeed experience an intracellular pH drop in response to trimethoprim due to the depletion of purine nucleotides, a downstream effect of folate synthesis inhibition.

It is known that certain stress responses cross-protect bacteria from other stressors. We therefore asked whether cellular responses to antibiotics have a similar protective role. Indeed, we found that the trimethoprim-induced acid stress response protects bacteria from subsequent acid stress. We then combined microfluidics with time-lapse imaging to monitor survival, intracellular pH, and acid stress response in single cells. This approach revealed that the variable expression of the acid resistance operon *gadBC* strongly correlates with single-cell survival time. Cells with higher *gadBC* expression following trimethoprim maintain higher intracellular pH and survive the acid stress longer. The seemingly random single-cell survival under acid stress can therefore be predicted from *gadBC* expression and rationalized in terms of GadB/C molecular function. Overall, we provide a way to identify single-cell cross-protection between antibiotics and environmental stressors from temporal gene expression data, and show how antibiotics can increase bacterial fitness in changing environments.

While gene expression changes to antibiotics show a clear temporal structure at the population-level, it is unclear whether this clear temporal order is followed by every single cell. We developed and validated a dual-reporter method for the efficient integration of

pairs of promoters into the bacterial chromosome. Using these strains, we measured the gene expression dynamics of promoter pairs in the same cells using microfluidics and microscopy. This revealed that some genes are activated in a clear temporal order, while others do not adhere to the temporal order suggested by population experiments. The oxidative stress response and the DNA stress response showed little timing variability and a clear temporal order under the antibiotic nitrofurantoin. In contrast, the acid stress response under trimethoprim ran independently from all other activated response programs including the DNA stress response, which showed particularly high timing variability in this stress condition. In summary, this approach provides insight into the temporal organization of gene expression programs at the single-cell level and suggests dependencies between response programs and the underlying variability-introducing mechanisms.

Altogether, this work advances our understanding of the diverse effects that antibiotics have on bacteria. These results were obtained by taking into account gene expression dynamics, which allowed us to identify general principles, molecular mechanisms, and dependencies between genes. Our findings may have implications for infectious disease treatments, and microbial communities in the human body and in nature.

About the author

Karin Mitosch was born in Landshut, Germany, and received her BSc in Molecular Medicine from the University of Ulm, Germany in 2007. With an increased interest in quantitative biology, she then joined an MSc program in Systems Biology at the Free University Amsterdam, and conducted her master research project in the group of Matthias Heinemann at ETH Zurich on stochastic modeling of a metabolic pathway in bacteria. From 2009 to 2010, she spent a research year in Japan, with a fellowship from the Riken institute in Yokohama. There, she worked in the group of Mariko Okada-Hatakeyama on the single-cell characterization of a signaling pathway in cancer cells. In 2011 she joined IST Austria to work with Tobias Bollenbach. Her research interests are drug-induced physiological changes, cell-to-cell heterogeneities, and metabolism. Her PhD research has been published in the high-impact Systems Biology journal *Cell Systems*.

Acknowledgments

First of all, I would like to express great gratitude to my PhD supervisor Tobias Bollenbach. Through his open and trusting attitude I had the freedom to explore different scientific directions during this project, and follow the research lines of my interest. I am thankful for constructive and often extensive discussions and his support and commitment during the different stages of my PhD.

I want to thank my committee members, Călin Guet, Terry Hwa and Nassos Typas for their interest and their valuable input to this project. Special thanks to Nassos for career guidance, and for accepting me in his lab.

A big thank you goes to the past, present and affiliated members of the Bollenbach group: Guillaume Chevereau, Marjon de Vos, Marta Lukačišinová, Veronika Bierbaum, Qi Qin, Marcin Zagórski, Martin Lukačišin, Andreas Angermayr, Bor Kavčič, Julia Tischler, Dilay Ayhan, Jaroslav Ferenc, and Georg Rieckh. I enjoyed working and discussing with you very much and I will miss our lengthy group meetings, our inspiring journal clubs, and our common lunches. Special thanks to Bor for great mental and professional support during the hard months of thesis writing, and to Marta for very creative times during the beginning of our PhDs. May the 'Bacterial Survival Guide' decorate the walls of IST forever! A great thanks to my friend and collaborator Georg Rieckh for his enthusiasm and for getting so involved in these projects, for his endurance and for his company throughout the years.

Thanks to the FriSBi crowd at IST Austria for interesting meetings and discussions. In particular I want to thank Magdalena Steinrück, and Anna Andersson for inspiring exchange, and enjoyable time together.

Thanks to everybody who contributed to the cover for *Cell Systems:* The constructive input from Tobias Bollenbach, Bor Kavčič, Georg Rieckh, Marta Lukačišinová, and Sebastian Nozzi, and the professional implementation by the graphic designer Martina Markus from the University of Cologne.

Thanks to all my office mates in the first floor Bertalanffy building throughout the years: for ensuring a pleasant working atmosphere, and for your company!

In general, I want to thank all the people that make IST such a great environment, with the many possibilities to shape our own social and research environment.

I want to thank my family for all kind of practical support during the years, and my second family in Argentina for their enthusiasm. Thanks to my brother Bernhard and my sister Martina for being great siblings, and to Helena and Valentin for the joy you brought to my life.

My deep gratitude goes to Sebastian Nozzi, for constant support, patience, love and for believing in me.

List of publications

i. Mitosch, K., and Bollenbach, T. (2014). Bacterial responses to antibiotics and their combinations. Environ. Microbiol. Rep. *6*, 545–557.

ii. Mitosch, K., Rieckh, G., and Bollenbach, T. (2017). Noisy response to antibiotic stress predicts subsequent single-cell survival in an acidic environment. Cell Syst. *4*, 393–403.e5.

The journal *Cell Systems* chose our suggestion for the cover of April 2017, which can be seen below.

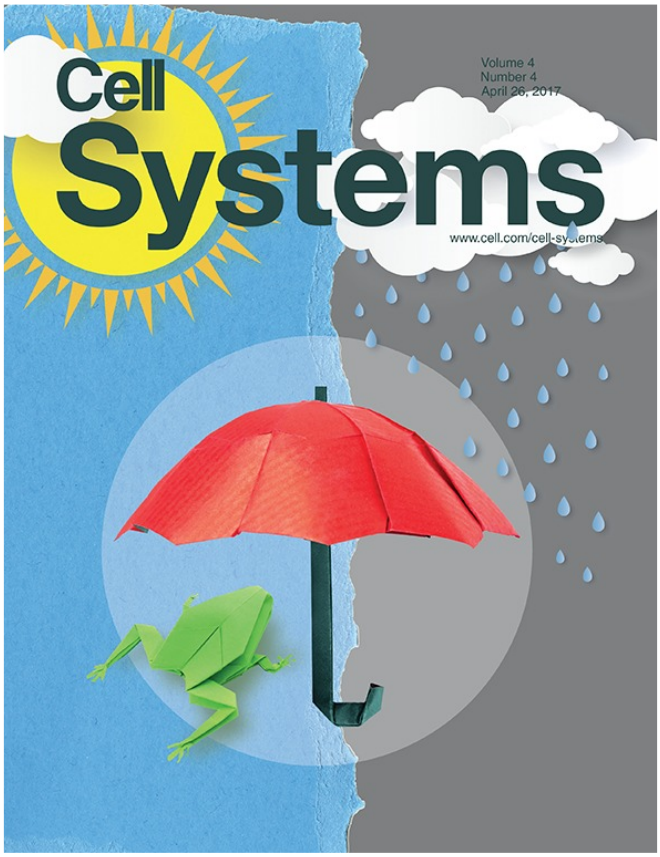

Idea of the cover: An umbrella, used as a parasol when it's sunny, provides protection when the weather suddenly changes to rain. Analogously, bacteria's response to an antibiotic challenge also helps them survive future acid stress.

List of abbreviations

TMP Trimethoprim

TET Tetracycline

NIT Nitrofurantoin

CHL Chloramphenicol

AMP Ampicillin

KAN Kanamycin

FA Formic acid

IPTG Isopropyl β-D-1-thiogalactopyranoside

GFP Green fluorescent protein

YFP Yellow fluorescent protein

RFP Red fluorescent protein

PCA Principal component analysis

PC Principal component

A_{600} Absorbance at 600nm

GO Gene ontology

PCR Polymerase chain reaction

H_2O_2 Hydrogen peroxide

HCl Hydrochloric acid

Table of contents

General introduction

Parts of this general introduction have been published as a review paper in *Environmental Biology Reports* (Mitosch and Bollenbach, 2014). In addition to this general introduction, every thesis chapter has an introduction specific to the presented results.

i. Antibiotics inhibit bacterial growth and restrict infection

Bacteria are small unicellular microorganisms that can populate most ecological niches on Earth (Newman and Banfield, 2002), including our human body. They are omnipresent on human skin and can be found extensively in our digestive tract (Dethlefsen et al., 2007), nostrils (Costello et al., 2009) and lungs (Beck et al., 2012). Many bacterial species are beneficial to health (Kong, 2011; Parvez et al., 2006) like the bacterial microbiota in the human digestive tract which are essential for our digestion (Neish, 2009). In addition, bacteria play an important role in shaping our immune system (Mazmanian et al., 2005). However, if bacteria reach locations such as our bloodstream, the urinary tract or the peritoneum (O'Boyle et al., 1998), they can be highly detrimental. More importantly, some bacteria have genes specialized for pathogenesis and can lead to life-threatening infections (Kaper et al., 2004).

Since the first half of the 20th century, antibiotics with diverse mechanisms of action have been developed (Clatworthy et al., 2007). Antibiotics are small molecules that inhibit essential cellular processes - ideally exclusively in bacteria without harming mammalian cells. The first line of discovery of antibiotics originated from nature when Alexander Fleming accidentally discovered the antibacterial properties of a penicillin-producing fungus (Fleming, 1929). In a second line of discovery, chemists developed synthetic molecules with antibacterial action based on dyes which led to the antibiotic class of sulfa drugs (Henry, 1943). Since then, many different classes of antibiotics have been developed and deployed in the clinic (Figure 1; (Clatworthy et al., 2007)).

Using antibiotics, medical practitioners were suddenly able to treat bacterial infections and control diseases like pneumonia, tuberculosis and enteritis, which were the most common causes of death in the United States until the end of the 19th century (Hinman, 1990). This saved millions of lives, and some overly optimistic and enthusiastic voices at the time even claimed that the era of infectious diseases was over (Spellberg and Taylor-Blake, 2013).

ii. Bacteria can circumvent the effect of antibiotics

But just a few years after the introduction of the first antibiotics, it became increasingly apparent that bacteria have ways to fight back: they can circumvent the action of antibiotics by evolving or acquiring resistance mechanisms (Figure 1; (Clatworthy et al., 2007)). Another challenge to antimicrobial therapy are biofilms: bacteria can produce and thrive in these

extracellular polymeric matrices that often attach to surfaces (Costerton et al., 1999). These biofilms shield them from antibiotics and other antimicrobial agents and thereby constitute a collective protection strategy (Costerton et al., 1999). Many chronic infections are consequences of bacterial biofilms, which often appear in hosts with a compromised immune system (Costerton et al., 1999). This suggests more complex interactions between bacteria, antibiotics, and host factors. In addition, complex interactions also emerge between our health-promoting bacterial communities and antibiotics. In particular, even short-term antibiotic treatments can harm our microbiome and lead to long-lasting perturbations (Jakobsson et al., 2010).

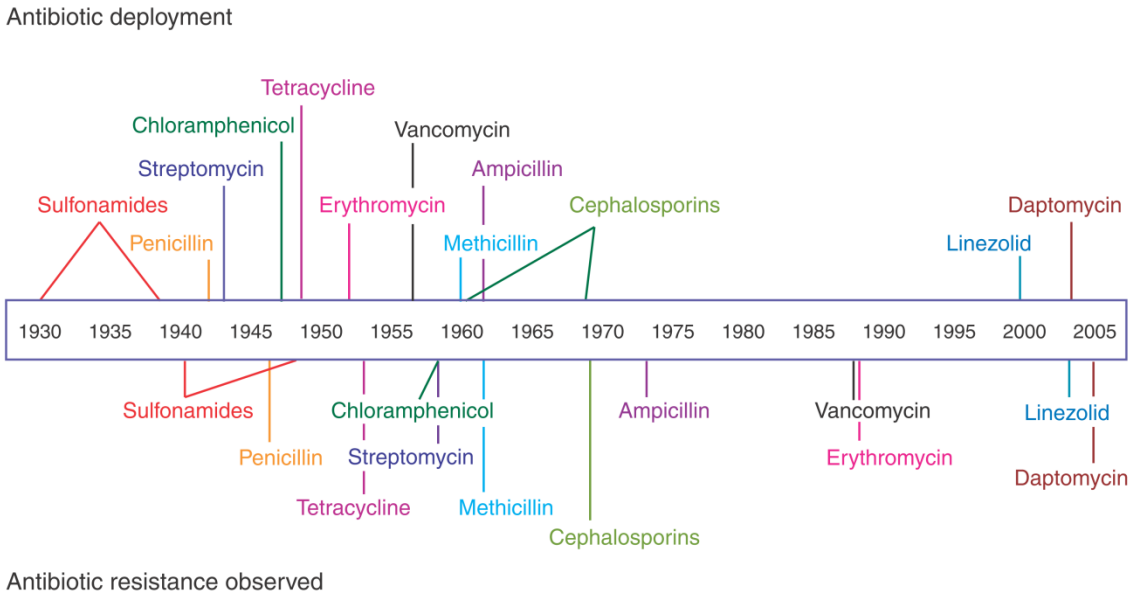

Figure 1. Timeline of antibiotic deployment and antibiotic resistance evolution. The box in the middle shows the years after the first clinical use of antibiotics. The lines connecting the timeline from above show when certain antibiotics were first deployed, and the lines connecting from below show when the first resistant strains were found. The development of resistance does not, however, mean that this antibiotic has lost all its clinical utility. Figure from Clatworthy (2007).

iii. Antibiotic mechanisms of action

As a response to the increased prevalence of treatment failures (Levy and Marshall, 2004; Mégraud, 2004), recent research is focusing on understanding the detailed mechanisms of antibiotics' actions on bacteria, and the complex interactions between bacteria, antibiotics and their abiotic or biotic environment (Adams et al., 2011; Allison et al., 2011; Helaine et al., 2014; Justice et al., 2008; McMahon et al., 2007). Antibiotics-mediated detrimental effects on bacterial growth begin with the physical interaction between a drug molecule and its molecular target in bacteria. The antibiotic concentrations needed for bacterial growth inhibition or killing vary strongly between drugs and across bacterial species (Dantas et al., 2008). Most known antibiotics inhibit bacterial growth by targeting one of the following

main mechanisms: DNA replication, RNA synthesis, protein synthesis, cell wall synthesis, folic acid biosynthesis, or they harm bacteria by depolarization of the membrane potential (Figure 2; (Walsh, 2003)). An alternative mechanism applies to nitrofuran antibiotics, which enter the cell in the form of prodrugs and are activated by intracellular enzymes into nitro anion radicals. These radicals introduce diverse damage to bacterial cells (Youngman et al., 1982).

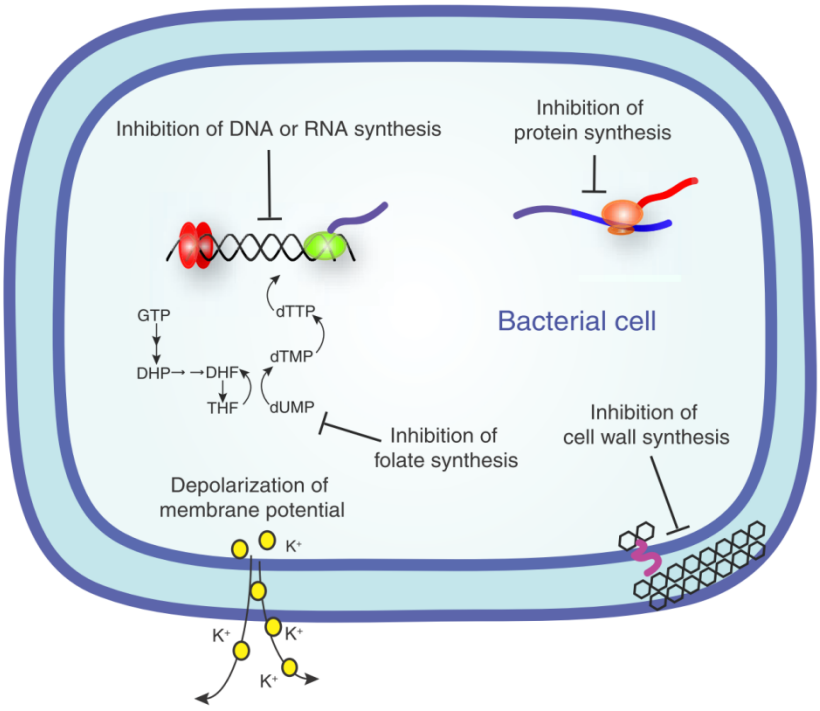

Figure 2. Antibiotic mechanisms of action. Figure from Clatworthy (2007).

The abundance of the corresponding cellular drug targets is substantially different for the different mechanisms of action. For example, an *Escherichia coli* bacterium contains about 10,000 ribosomes (Bremer and Dennis, 2008), but fewer than 50 DNA gyrases (Maier et al., 2011; Taniguchi et al., 2010) which are the target of quinolone antibiotics. In addition, drugs have different binding affinities for their targets as well as different chemical properties which affect the drug's ability to enter cells (Nikaido and Vaara, 1985). In general, gram-negative bacteria are better protected than gram-positive bacteria due to their additional lipopolysaccharide layer (Costerton and Cheng, 1975; Gupta, 2011). Consequently, the bacterial response is specific to each antibiotic as well as bacterial species and, therefore, needs to be quantified accordingly.

iv. Antibiotics induce multilayered downstream effects with implications for fitness and virulence

The initial target inhibition by antibiotics leads to downstream effects, which alter the affected bacterium at the biochemical, molecular and macromolecular levels, and can

change the bacterial cell composition (Kohanski et al., 2010; Scott et al., 2010). These effects are specific to each antibiotic (Kohanski et al., 2010). Whereas the main cellular targets are well understood for most antibiotics, the diverse downstream effects are far less studied. Yet, it is conceivable that these downstream effects could modify the lethal effects of antibiotics or have implications on bacterial virulence.

For example, the unexpected induction of the bacterial SOS response (DNA damage response) in the presence of cell-wall synthesis inhibitors was suggested to induce a transient reduction in growth, resulting in a decrease in bacterial susceptibility to the drugs (Miller et al., 2004). This stress response further increases the probability for the horizontal transfer of virulence genes (Maiques et al., 2006). Likewise, exposure to low concentrations of the gyrase inhibitor ciprofloxacin can increase the percentage of persister cells, which are normally found in small frequencies in the absence of ciprofloxacin (Dörr et al., 2010). Persister cells are dormant isogenic and multi-drug resistant cells, usually present at frequencies as low as 10^{-5}, which can repopulate after drug removal (Lewis, 2010). Further, the application of antibiotics can induce biofilm formation (Hoffman et al., 2005), toxin production (Zhang et al., 2000), or mutagenesis and resistance evolution (Cirz et al., 2005; Ysern et al., 1990). Conversely, the downstream effects can also amplify the lethality of antibiotics, as is the case for aminoglycoside antibiotics: the initial binding of aminoglycosides to the ribosome leads to a reduction in translation accuracy. Defective proteins are subsequently inserted into the cell membrane and facilitate the further uptake of these antibiotics (Busse et al., 1992). All these examples show the diversity of effects that antibiotics can have on bacterial virulence, survival, and growth.

v. Quantifying the effect of antibiotics on bacterial growth

The concentration-dependent effects of antibiotics on bacterial growth *in vitro* are commonly quantified using dose-response curves (Figure 3), with bacterial growth rate, growth yield or survival on the y-axis and the drug concentration on the x-axis. Dose-response curves are usually well-fit by Hill functions, with the key parameters IC_{50} (the concentration at which growth is reduced by 50%) and m, corresponding to the steepness of the curve (Ankomah and Levin, 2012; Greco et al., 1995). Another commonly used scalar quantity is the minimal inhibitory concentration (MIC), the lowest concentration at which no growth occurs following a standardized inoculation procedure and incubation time (Andrews, 2001). Depending on the antibiotic, the transition from slight to complete growth inhibition can occur over several orders of magnitude of drug concentrations (e.g. this is the case for the folic acid synthesis inhibitor trimethoprim in *E. coli* (Chevereau et al., 2015)) or over a very narrow concentration window in which growth ceases in a step-like fashion ('all-or-nothing' growth inhibition, as observed e.g. for aminoglycosides in *E. coli* (Lázár et al., 2013)). It is the subject of active research how the shape of the dose-response curve comes about mechanistically. Parameters that certainly affect the shape of the dose-response curve are the drug-to-target ratio, the degree of target inhibition required to block cell growth (Wei et al., 2011), and the kinetics of drug uptake and binding to the target (Elf et al., 2006; Greulich et al., 2017). Additional factors that can influence the sensitivity of

bacterial cells to antibiotics are the specific composition of the growth environment (Allison et al., 2011; Harvey, 1973), cell density (Tan et al., 2012), and cellular growth rate (Evans et al., 1990; Greulich et al., 2015; Tuomanen et al., 1986).

Another aspect that can vary considerably is the rate at which bacterial growth rate is inhibited after the exposure to antibiotics. This effect can be immediate, as observed for the ribosome inhibitor tetracycline (Inoue et al., 1970), but may also take hours, as seen for folate biosynthesis inhibiting sulfa drugs (Greenwood and O'Grady, 1976) or the cell-wall biosynthesis inhibitor ampicillin (Rolinson, 1980). This aspect, combined with the so-called post-antibiotic effect – the delayed regrowth of bacteria after removal of the drug (MacKenzie and Gould, 1993) should be considered for effective treatment intervals in clinical settings (Vogelman and Craig, 1986).

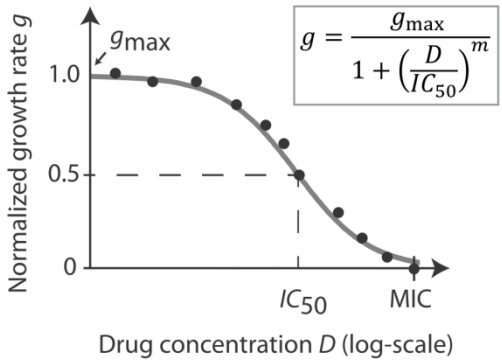

Figure 3. Schematic of a typical dose-response curve. Measurements can be fit with a Hill function with parameters IC_{50} (drug concentration at which growth is inhibited by 50%) and m (a parameter corresponding to the steepness of the curve). The minimal inhibitory concentration (MIC) is the lowest concentration at which no growth occurs.

Even low concentrations of antibiotics can lead to diverse downstream effects in bacteria (Andersson and Hughes, 2014; Lorian, 1975; Mathieu et al., 2016). During antimicrobial therapy, the drug concentration in the infected host is ideally high enough to quickly eradicate all harmful bacteria. In practice, however, low concentrations of antibiotics are probably very common during therapy: concentrations at the infection sites in the human body may be variable in time and space due to the different abilities of body tissues and compartments to absorb or degrade drugs (Delacher et al., 2000). Further, the concentrations recommended for fast clearance may not be reached in the body due to poor patient compliance (McNulty et al., 2007; Pichichero and Casey, 2007). In addition, we are also exposed to low concentrations of antibiotics even without an intended antibiotic therapy: antibiotics are produced by bacteria and fungi in the environment (Martín and Liras, 1989; Waksman, 1961), and due to our use of antibiotics in medical therapy and agriculture, trace amounts of these drugs end up in many lakes, rivers and soils, and finally also in our food (Andersson and Hughes, 2014).

vi. Temporal gene expression measurements as a means to study cellular responses to changing environments

The detailed investigation of drug-induced effects has helped in the past to reveal specific and global mechanisms in bacterial physiology (Bollenbach and Kishony, 2011; Falconer et al., 2011; Scott et al., 2010). This is because antibiotics target essential cellular processes which cannot easily be studied using deletion mutants of these processes. Additionally, with most antibiotics it is possible to gradually inhibit their target and therefore study the reaction to the gradual inhibition of essential cellular processes. The many downstream effects of antibiotics mentioned above are reflected in massive changes at the bacterial gene expression level (Goh et al., 2002; Shaw et al., 2003). As changes in growth rate alone can already lead to gene expression changes (Esquerré et al., 2013; Hua et al., 2004), and the level of growth rate inhibition can determine the extent of gene expression changes (Bollenbach and Kishony, 2011), growth rate changes should be taken into account. Measuring gene expression changes in response to antibiotics while monitoring growth rate changes, gives us a means to dissect stress-induced molecular events.
The gene expression changes happening in response to many antibiotics have been characterized (Brazas and Hancock, 2005; Shaw et al., 2003). However, in most cases, the sequence of molecular events and their interaction with bacterial growth are not well understood. For example, how long does it take until bacteria have adapted to an antibiotic stress condition, and what is the temporal organization of the differentially expressed genes? A clear temporal organization is common for developmental processes in bacteria and higher organisms (Bar-Joseph et al., 2012; Sinai et al., 2015), and has also been shown for nutrient shifts in bacteria (Zampar et al., 2013; Zaslaver et al., 2004). Antibiotics are stressors to which sensitive bacteria have probably not evolved. It is therefore yet unknown whether a clear temporal organization is also observable for such stressors.

vii. Cellular strategies, optimality, and protective responses in changing environments

While many gene expression levels change in response to antibiotics, it is generally unclear if these changes are advantageous, i.e. if they lead to increased growth or survival compared to no regulation. Alternatively, these gene expression changes could also be induced by cross-activation from others regulons as an inevitable consequence of the limited regulatory network that has evolved for other situations. Recent experimental studies have suggested that gene regulation responses to stressful environments are often nonoptimal with respect to growth rate maximization (Bollenbach et al., 2009; Price et al., 2013). Genome-wide and temporal data, combined with growth rate data, can be very valuable in addressing these questions, as they contain information on the simultaneity, and the order of events occurring.

Further, temporal gene expression data can provide insight into dependencies, causality (Bar-Joseph et al., 2012) or cellular strategies in response to changing environments (Zaslaver et al., 2004). One strategy to cope with stress would be to precisely sense the current stress level and react accordingly. However, such a strategy can be deadly when the

time it takes to initiate the response is greater than the time it takes for the stress to act. An alternative strategy in fluctuating environments is anticipation (Mitchell et al., 2009; Tagkopoulos et al., 2008; Venturelli et al., 2015): due to the frequent co-occurrence of two stressful environments in their evolutionary history, cells may have evolved to express genes that protect them from the second environment already during the first stressful environment.

A similar principle to anticipation is cross-protection, where a culture adapted to one stressful environment confers a fitness benefit when exposed to another stressful environment (Figure 4). In contrast to anticipation, however, observing cross-protection does not imply an evolutionarily beneficial strategy: it might simply be that both stressful conditions share the same stress protection genes. Cross-protection is commonly found between environmental stressors such as starvation, acid, or heat stress in bacteria (Battesti et al., 2011; Jenkins et al., 1988; Leyer and Johnson, 1993; Wang and Doyle, 1998), but has recently also been observed between the antibiotic ampicillin and heat or oxidative stress (Mathieu et al., 2016). Pre-adaptation to certain environmental stressors has also been found to decrease bacterial susceptibility to antibiotics (Al-Nabulsi et al., 2015; McMahon et al., 2007). While little is known yet about potential cross-protection between antibiotics and environmental stressors, temporal gene expression data can enable predictions about stressors against which a prestress might cross-protect.

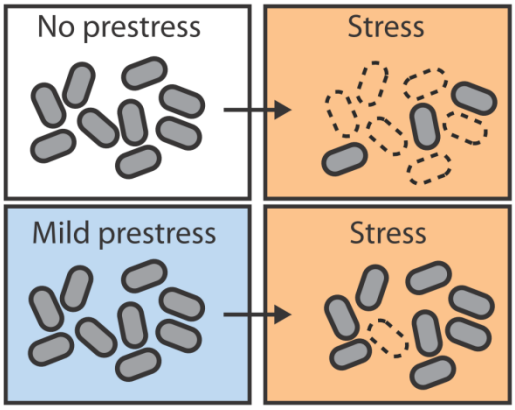

Figure 4. Cross-protection between a mild prestress and a subsequent stress. Exposure to a mild prestress (blue environment) improves survival of single cells in an otherwise lethal stress condition (orange environment). Gray ovals depict living cells, ovals with a dashed border depict dead cells.

Temporal gene expression data can further propose time-windows in which bacteria would be particularly tolerant or vulnerable to environmental changes (Mathis and Ackermann, 2016; Meredith et al., 2015; Miller et al., 2004). Understanding the sequence of molecular events that occur in response to antibiotics might therefore lead to the discovery of new and more elaborate treatment strategies, for example, by applying antibiotics or adjuvants in a time-window in which bacteria are particularly sensitive (Gefen et al., 2008), or avoiding certain treatment intervals (Fridman et al., 2014).

viii. Single-cell studies reveal cell-to-cell variabilities and their effects on bacterial fitness

With the advent of single-cell techniques, it has become clear that individual cells do not necessarily behave similarly (Brehm-Stecher and Johnson, 2004). In general, such cell-to-cell variability may be genetic (Read and Taylor, 2001) and introduced by random mutations or phase variation (Henderson et al., 1999). Phase variation is a means to induce a phenotype switch in fluctuating environments, and can be achieved by mechanisms like gene inversion or site-specific recombination; it is much more frequent than random mutation and is for example found in the *Salmonella* flagellin locus (Zieg et al., 1977). A further variability introducing factor can be bacterial cell age, as certain proteins tend to accumulate at the cell poles (Bergmiller et al., 2017). However, recent research has revealed numerous examples in which stochastic mechanisms induce cell-to-cell variability at the phenotype-level ('noise'), owing to the mere fact that biochemical reactions ultimately rely on random collisions between diffusing molecules (Arnoldini et al., 2014; Balaban et al., 2004; Ni et al., 2012). High heterogeneity has also been detected in host-pathogen interactions during an infection (Claudi et al., 2014). This heterogeneity may be introduced from the side of the host, for example by differences in microenvironments within the host (Snijder et al., 2009) or phenotypic differences in immune cells (Gog et al., 2012), but may also stem from cell-to-cell variability in bacteria (Avraham et al., 2015).

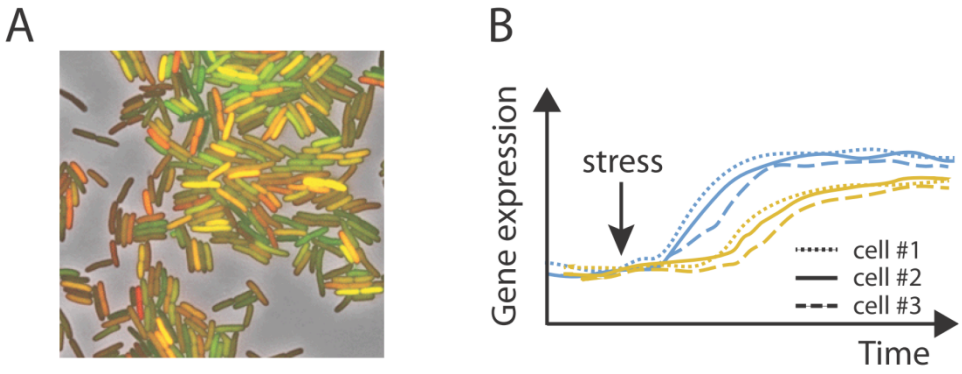

Figure 5. Stochastic gene expression in single cells, and schematic on the coupled response of genes with a clear temporal order. A. Bacterial cells expressing two different fluorescent proteins (red and green) from identical promoters in a constant environment; cells that express both fluorescent proteins equally strongly appear yellow. Because of noise gene expression, expression from two nearly identical promoters is not the same. Figure taken from Elowitz et al. (2002). **B.** Schematic on the expression of two genes (blue and yellow lines) in response to stress in three single cells. The timing shows variability between the cells, yet the genes are coupled. Coupling can be seen as cell #1 activates expression from both genes first relative to the other cells, cell #2 activates both genes later, and cell #3 activates both genes last. Expression follows a clear temporal order in that the first gene (blue) is expressed before the second gene (yellow) in every single cell.

Noise in gene expression can be detected using fluorescent reporters and single-cell methods like flow cytometry or microscopy, and noise sources can be quantified by tagging the same transcript with two different fluorescent proteins in the same cell (Figure 5A; (Elowitz et al., 2002)). Using such single-cell methods, many examples in the literature attribute a functional role for noise in gene expression in bacterial and eukaryotic cells (Eldar and Elowitz, 2010). For example, the transient dynamics of *Bacillus subtilits* bacterial competence, i.e. the ability to take up DNA from the environment, is induced by an excitable genetic circuit that amplifies noise in single cells (Süel et al., 2006).

Cell-to-cell variability at the gene expression level can lead to subpopulations of cells with different phenotypes, and certain phenotypes may have a fitness benefit. For example, the expression of virulence genes in *Salmonella* was shown to be bistable and only those cells with a high expression of these genes survive an antibiotic treatment (Arnoldini et al., 2014). Similarly, dormant persister cells can survive antibiotic treatment, whereas their growing sister cells cannot (Balaban et al., 2004). Notably, antibiotics might also increase cell-to-cell variability in gene expression (Ni et al., 2012), or induce certain genes that are intrinsically noisy. For example, it has been shown that variability in gene expression is particularly high for some stress response genes (Newman et al., 2006; Silander et al., 2012). It is therefore relevant to study bacterial responses to stress, such as antibiotics, at the single-cell level.

Also the time at which individual cells respond to an external signal can be variable (Amir et al., 2007; Boulineau et al., 2013). This variability may be tuned with the concentration of the external signal (Mader et al., 2015; Megerle et al., 2008). Alternatively, the temporal response may also be very similar in individual cells (Friedman et al., 2005; Young et al., 2013). In a response in which certain genes are expressed with a clear temporal order at the population level, it is therefore not clear if this clear temporal order is followed by every single cell (Figure 5B). This question has hardly been addressed before, but provides important information for population experiments: any notion that a temporal response is adaptive or even optimal only makes sense if the response tends to run in a clear temporal order in individual cells.

In general, high cell-to-cell variability in a certain trait may be an evolved strategy to increase the overall fitness of a population (Blake et al., 2006), or may just be the consequence of different physiological constraints (Uphoff et al., 2016). When comparing variable genes from different stress response programs, they might fluctuate together or they might fluctuate independently of each other (Martins et al., 2017; Stewart-Ornstein et al., 2012). If every stress response also comes with a fitness cost (Kussell and Leibler, 2005), such a ‘multi-dimensional variability’ might be beneficial: every cell is well prepared for a different future environment. In response to an external signal, responding genes may be coupled in their response times (Figure 5B), or their response times may be independent. The quantification of these measures can provide new insights into the sources of variability that introduce timing variability into the system, and the dependencies between different genes, such as the connection by regulatory links (Dunlop et al., 2008).

ix. Goals of this thesis

This thesis aims at using temporal gene expression data to advance our understanding of bacterial gene expression changes in response to antibiotics: their temporal structure, their underlying mechanisms, their variability and dependencies, and their consequences for bacterial fitness in constant and changing environments.

Chapter 1 of this thesis describes the temporal structure of genome-wide temporal gene expression changes in response to antibiotics and their interaction with the bacterial growth rate. In Chapter 2, we predict from these data stressors against which antibiotics-prestressed bacteria might be protected and study an antibiotics-induced, highly variable acid stress response system at the single-cell level. We further investigate the consequences of this variable response for bacterial survival in an acidic environment. In Chapter 2, we also identify a previously unknown molecular link between the depletion of nucleobases and the specific activation of the acid stress response. In Chapter 3, we describe a method to study the timing of pairs of genes at the single cell level. This method is then applied in Chapter 4, where we explore the temporal organization of different gene pairs during complex stress responses induced by low concentrations of antibiotics.

1. Chapter 1: Dynamics of global gene expression response to antibiotics

The work presented in this chapter was performed by KM and part of the work presented here has been published in an article in *Cell Systems* (Mitosch et al., 2017).

1.1 Introduction

In this first chapter, we focus on the analysis of dynamic gene expression changes in response to low concentrations of different antibiotics, obtained by measuring a genome-wide promoter library of *Escherichia coli.* In contrast to the following chapters, which all deal with the gene expression dynamics of selected genes at the single-cell level, this chapter reports on experiments at the population level and gives a genome-wide overview of dynamic gene expression changes. In particular, we compare the identity of differentially expressed promoters between different antibiotics. We also describe the overall dynamics and identify global factors influencing the expression dynamics of many promoters. Finally, we highlight the exceptional expression of acid stress promoters in response to one antibiotic, trimethoprim, which is investigated further in Chapter 2.

Antibiotics, i.e. small molecules that inhibit or kill bacteria, exert their action by disturbing essential cellular processes (Walsh, 2003). Although antibiotics have a limited number of target processes, they can induce massive downstream effects in bacterial metabolism (Belenky et al., 2015; Kwon et al., 2010; Zampieri et al., 2017), cell composition (Bollenbach et al., 2009; Scott et al., 2010), and gene expression (Goh et al., 2002). Antibiotics have also been shown to induce changes in the cell-to-cell variability (Dörr et al., 2010; Ni et al., 2012). Gene expression changes in response to antibiotics have been quantified before using DNA microarrays (Shaw et al., 2003), transcriptional reporters (Goh et al., 2002) or proteomics (Bandow et al., 2003) and many genes involved in the stress responses to diverse antibiotics have been determined.

Previous studies did not, however, put much focus on the temporal structure of gene expression changes in response to antibiotics. Many studies only analyzed one or a few time-points shortly after the addition of the antibiotic (Bandow et al., 2003; Lin et al., 2005; Sangurdekar et al., 2011; Shaw et al., 2003). It is therefore not clear on which time-scales gene expression changes happen. Knowing the overall timing of expression changes to the antibiotic stress might also help us understand which determinants affect global gene expression. Such factors could be the bacterial growth rate or dynamic changes in the concentrations of metabolites, second messengers, or transcriptional global regulators (Mitosch and Bollenbach, 2014). In addition, the temporal sequence of molecular events happening in response to antibiotics, from target inhibition to effects further downstream is poorly understood for most antibiotics. Characterizing these dynamic changes in response to antibiotics will ultimately provide means to manipulate and aggravate the early effect of antibiotics on bacteria (Allison et al., 2011; Morones-Ramirez et al., 2013).

In order to quantify the overall temporal gene expression response of *E. coli*, we used a dilution protocol on a robotic system to measure the genome-wide promoter-GFP reporter library (Zaslaver et al., 2006) in response to four antibiotics (trimethoprim, tetracycline, nitrofurantoin, and chloramphenicol). We found that each antibiotic induces different specific promoters, including many stress response promoters, with a defined temporal order. Characteristic response times range from tens of minutes to several hours. The expression level changes of most promoters follow a permanent shift and the dynamics of this shift is determined by the initial rate at which the growth rate drops under antibiotic stress. This work thus sheds light on the overall temporal gene expression response to antibiotics, the interplay between growth rate and gene expression and gives insight into the dynamics of complex bacterial stress responses. This provides a basis for the further investigation of underlying molecular processes inducing these gene expression changes.

1.2 Results

1.2.1 Automated dilution protocol for the quantification of genome-wide gene expression changes to antibiotics

In order to quantify the dynamics of gene expression changes in response to antibiotics, we used a genome-wide promoter-GFP library (Zaslaver et al., 2006). This technique has several advantages for our purpose of tracking the effect of antibiotics on gene expression with high time resolution. First, the promoter-GFP library mainly reports on changes at the transcription level, the first step in gene expression, although the GFP signal requires protein expression and is therefore subjected to all processes that affect the growth physiology of the cell. But as the promoter-GFP library combines different promoters with the same tandem of ribosomal binding site and fluorescent protein, GFP, the majority of observed changes must stem from differences in promoter activities. While measuring protein levels generally gives better information on the phenotype of a cell, measuring the transcriptional response can provide valid information on the early changes in gene expression and their inducing processes during a stress response. Such information may be hidden by measurements at the protein level, where the readout is a combination of transcriptional and translational changes, each including gene-specific parameters like mRNA stability, strength of ribosomal binding site, or protein stability. Measurements at the transcriptional level therefore reduce the complexity of gene expression and are ideal if one is interested in the temporal sequence of gene expression changes. Also in contrast to transcriptional methods like DNA microarrays or RNA sequencing (Ozsolak and Milos, 2011; Ramsay, 1998), this method does not deal with the problem of low mRNA stability, which can make sample preparation delicate (Cho et al., 2013). Further, the same culture can be measured over time as measurements are done in living cells, in contrast to all other methods for measuring gene expression mentioned above, which start by lysing the cells. This allows direct comparison of subsequent time-points without separate normalization for each time-point which might introduce fluctuations. Last, the use of fluorescent proteins

makes the transition from population-level measurements to measurements at the single-cell level straightforward and allows for direct comparison between these methods.

The method of choice has, however, some drawbacks that must be considered during data interpretation. In this library, putative *E. coli* promoters are taken out of their natural context and put onto plasmids. Therefore, promoters with long-range regulation like the *lac* promoter (Oehler et al., 1990) are not complete in the plasmid library and may behave differently from the chromosomal promoter. In addition, gene expression changes that depend on the chromosomal context (Bryant et al., 2014; Conway et al., 2014) are not captured. Further, the plasmid-based system might introduce biases due to higher copy numbers of the promoter (Brewster et al., 2014) or due to plasmid copy-number changes. In order to perform genome-wide screens, this method needs as many cultures as there are genes or promoters in *E. coli.* Such a large number of strains might therefore make robotic systems indispensible. This is in stark contrast to methods like RNA sequencing that can deliver genome-wide data from a single culture.

For the automated determination of genome-wide gene expression changes, we developed a protocol on a robotic liquid handling system. We used the antibiotics trimethoprim (TMP), tetracycline (TET), nitrofurantoin (NIT), and chloramphenicol (CHL), representing diverse modes of action (Table 1). We maintained bacterial cultures of the genome-wide promoter-GFP library based on the *E. coli* strain K-12 MG1655 (Zaslaver et al., 2006), growing in 96-well plates, in exponential growth by four successive 10-fold dilutions (Figure 1A,B; Methods). Before the addition of antibiotics, the cultures grew at a growth rate of ~0.65/h (M9 minimal medium with glucose and amino acids, 30°C). Antibiotics were added after ~10 hours, which corresponds to ~8 mass doublings. Because the level of inhibition, i.e. the resulting growth rate under antibiotic stress, can strongly affect gene expression (Bollenbach and Kishony, 2011), we tuned antibiotic concentrations to result in 40-50% growth inhibition for all conditions. Like this, we were able to reliably measure gene expression changes and compare the data from different antibiotics with each other (Figure 3B). This protocol enabled us to quantify the expression changes of ~1,000 promoters (out of ~1800 promoters in total) at a temporal resolution of ~25 minutes (Methods).

Table 1. Antibiotics used in this and the following chapters. Concentrations were adjusted so that they led to a growth rate inhibition of 40-50%; TMP 1 µg/mL reduced growth rate to ~38%.

Antibiotic	Abbreviation	Mechanism of action	Concentration
Trimethoprim	TMP	Folate synthesis inhibition	0.5 µg/mL (1 µg/mL)
Tetracycline	TET	Ribosome inhibition (30S)	0.7 µg/mL
Nitrofurantoin	NIT	Nitro radical formation	4.0 µg/mL
Chloramphenicol	CHL	Ribosome inhibition (50S)	1.0 µg/mL

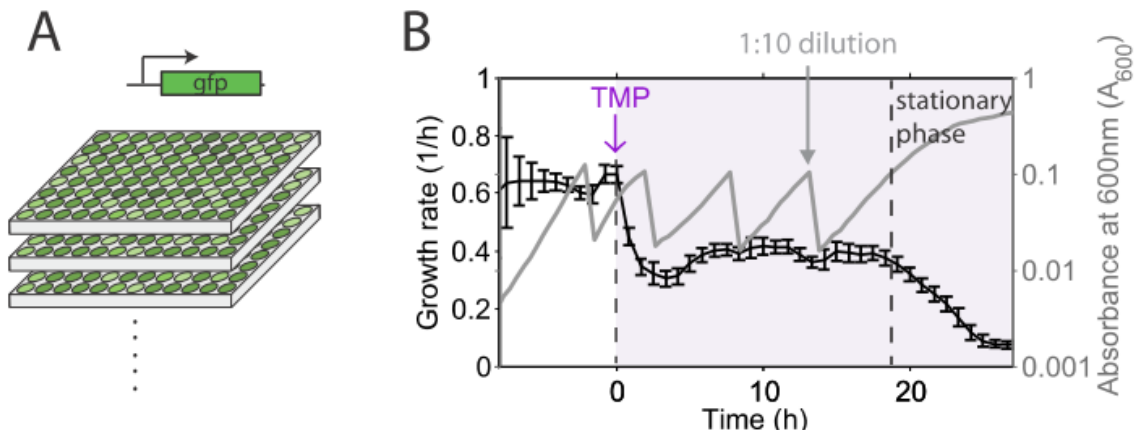

Figure 1. Dynamic measurements of genome-wide transcriptional response to several antibiotics using a dilution protocol. A. Schematic of the genome-wide promoter-GFP library (Zaslaver et al., 2006). This library has in total 1,800 strains, organized in 21 96-well plates, each strain with a different expression level of GFP. **B.** Growth rate (black line, error bars are standard deviation from all strains) and absorbance (A_{600}) (grey line) of one reporter strain (P_{aroH}-*gfp*) over time in response to sustained TMP stress, added at t = 0. The dashed black line on the right indicates the entry into stationary phase.

1.2.2 Gene expression changes are specific to each antibiotic

We quantified which proportion of promoters had a more than two-fold up- or down-regulation of their GFP concentration (determined as normalized GFP/A_{600}; Methods) under our different stress conditions. While only ~5% of the ~1,000 tested library promoters responded to CHL, about 20% of promoters were up- or down-regulated by more than 2-fold for TMP and TET (Table 2). When we measured the whole library without any added antibiotic using the same dilution protocol, only 3% of all promoters exceeded the 2-fold threshold. When applying a 3-fold threshold, we detected 5% (TMP), 6% (TET) and 3% (NIT) differentially expressed promoters, which is comparable to previous results reporting that ~5% of genes were > 3-fold up-regulated for different antibiotics (Goh et al., 2002). Whereas the percentage of responding promoters under TMP, TET, and NIT was significantly higher than in the control without added antibiotic (Table 2), the results for CHL were less striking. Especially for promoters with > 3-fold up- or down-regulation, the response to CHL was not significantly different than in the control without added antibiotic. We note that there were small, but significant negative correlations between the absolute expression levels before antibiotic exposure and the fold change of promoters for TMP, TET, and NIT. These correlations were -0.14, $p = 7.5 \times 10^{-7}$ (TMP); -0.27, $p = 2.5 \times 10^{-19}$ (TET); -0.20, $p = 2.1 \times 10^{-9}$ (NIT). These negative correlations are explained by the fact that strong down-regulation can only be detected for promoters with a high basal expression. In general, we conclude that antibiotics can induce massive changes in bacterial gene expression. Most of the molecular mechanisms leading to these substantial gene expression changes are however unclear.

Table 2. Percentage of differentially expressed promoters for all four antibiotics and a control without antibiotic stress. The p-values were determined with a one-sided binomial test, taking the percentage of 'no antibiotic' as probability.

	TMP	TET	NIT	CHL	No antibiotic
> 2-fold up- or down-regulation	19%	25%	12%	5%	3%
p-value	1.2×10^{-108}	9.3×10^{-155}	2.8×10^{-33}	1.0×10^{-4}	
> 3-fold up- or down-regulation	5%	6%	3%	0.6%	0.6%
p-value	6.1×10^{-29}	8.9×10^{-44}	1.0×10^{-9}	0.16	

To find out if gene expression changes result from a general stress response and growth rate changes common to all antibiotics, or if gene expression changes are rather specific to each antibiotic, we identified promoters that were differentially expressed under all four conditions. The intersection of promoters that were up- or down-regulated > 2-fold for all four antibiotics consisted only of three genes (*gadB, ydiE, nrdH*). The *ydiE* and *nrdH* genes both belong to the Fur regulon, which is the major regulator for iron homeostasis in *E. coli* (Keseler et al., 2013). All Fur-regulated promoters fluctuated strongly with the dilutions in our experimental protocol, probably due to traces of iron in our growth medium, which is consumed during growth. The common activation of these iron-regulated genes under all antibiotics is therefore probably unrelated to the drug mode of action.

In general, these data suggest that gene expression changes are specific to each antibiotic. However, certain pairs of antibiotics shared more differentially expressed promoters: the expression levels from promoters with > 2-fold expression changes under the ribosome inhibitors TET and CHL were strongly correlated ($\rho = 0.66$, $p = 0.0008$, Figure 2). This pair had 22 overlapping promoters, which corresponds to 8% of the differentially expressed promoters for TET and 45% for CHL. This likely reflects their similar mode of action and suggests that these gene expression changes are a general response to translation inhibition. Also NIT and TET ($\rho = 0.47$, $p = 0.008$, 31 overlapping promoters, Figure 2) were positively correlated with high significance, whereas TMP and CHL showed a strong anticorrelation ($\rho = -0.79$, $p = 2 \cdot 10^{-5}$; 21 overlapping promoters, Figure 2). As a reference, promoters induced by two different concentrations of TMP (0.5 µg/mL and 1 µg/mL) showed a very strong correlation ($\rho = 0.98$, $p = 1 \cdot 10^{-99}$, 135 overlapping promoters). Consistent with previous studies (Goh et al., 2002; Shaw et al., 2003), these data suggest that different antibiotics do not activate a common set of promoters; however, certain pairs of antibiotics seem to act on similar cellular processes and therefore activate similar promoters.

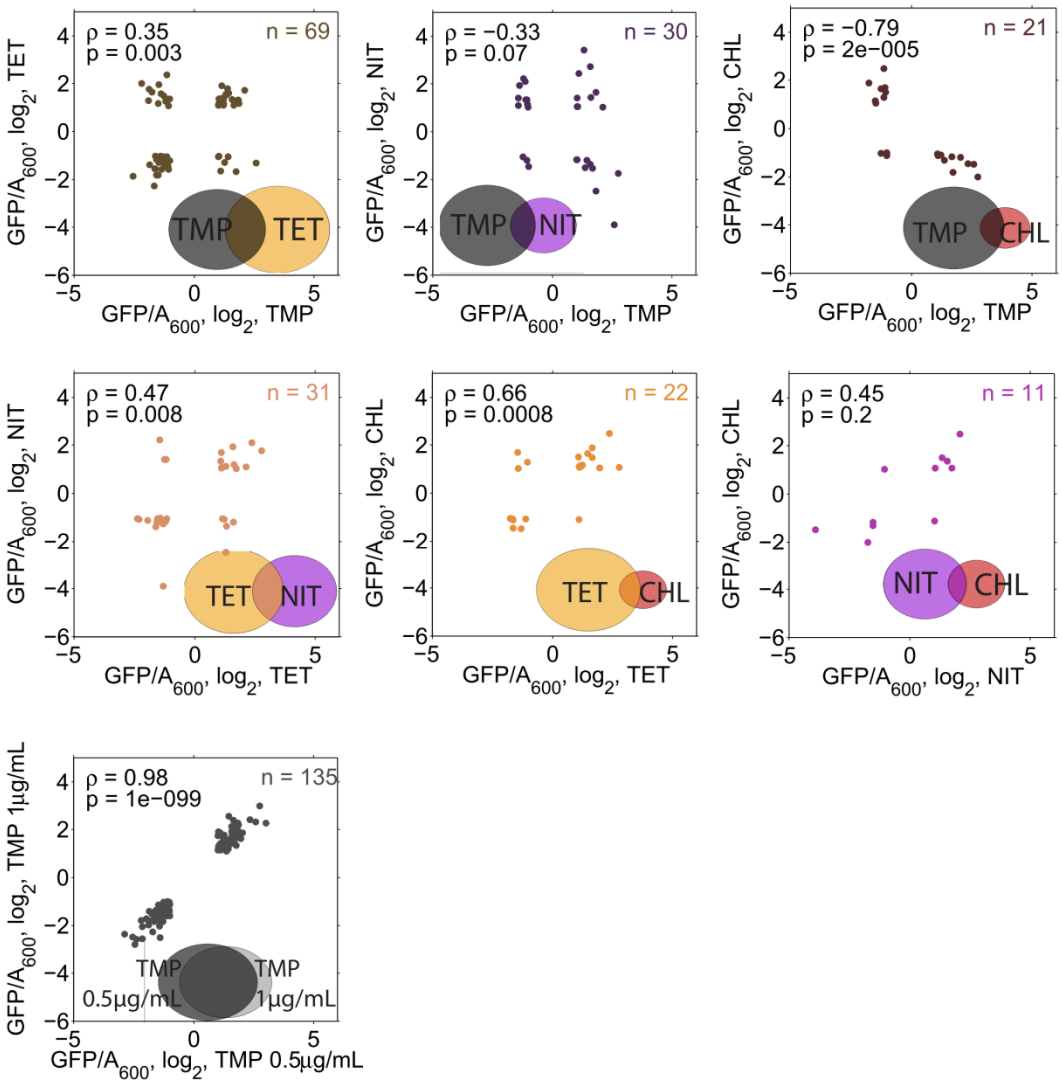

Figure 2. Correlation of promoters with > 2-fold expression changes in two conditions. Dots are promoters with > 2-fold expression changes in both conditions; n is the size of the intersecting set in the two conditions. The Pearson correlation coefficient ρ and its p-value are given. The pair with the highest negative correlation is TMP-CHL; the pairs with the highest significant positive correlations are TET-NIT, TET-CHL and the reference TMP 1 µg/mL-TMP 0.5 µg/mL. Insets: The size of each ellipse reflects the number of differentially expressed promoters in that condition. The size of the intersection of both ellipses corresponds to the number of promoters with > 2-fold expression changes in two conditions.

1.2.3 Principal component analysis reveals low dimensionality of the data, and the effect of the initial growth rate drop on response times

To quantitatively describe the overall dynamics of our data set, we used principal component analysis (PCA, Methods), a statistical analysis technique that identifies a lower dimensional space capturing as much variance as possible (Quackenbush, 2001). The data

are transformed so that each curve, i.e. the gene expression over time for a specific promoter, can be described by a linear combination of linearly uncorrelated variables, called principal components (PCs), which are ordered by decreasing fraction of variance explained. An original response curve R is therefore described by

$$R = s1 \times PC1(t) + s2 \times PC2(t) + s3 \times PC3(t) + \ldots$$

where s1, s2, s3, … are the scores and PC1(t), PC2(t), PC3(t), … are so-called loadings, corresponding to the directions in the multidimensional space. The first principal component, PC1, which explains the biggest fraction of variance, described more than 80% of the variance in the data for TMP, TET, and NIT, and more than 65% for CHL (Figure 3A). If a low number of PCs can describe a big fraction of the variance in the data, the data has rather low dimensionality and the data representation can be greatly collapsed into only a few dimensions. In our case, dimensions could be collapsed greatly from around 50 (corresponding to the number of measurements over time) for TMP, TET, and NIT: the first two principal components explained around 90% of the variance for these stressors (Figure 3A). The data set for CHL was less well described by the first two PCs (Figure 3A), as relatively few promoters had clear changes in their expression; the analysis for CHL was therefore influenced by global fluctuations in the data that may stem from the dilution protocol alone, from additional fluctuations originating from measurement noise or data normalization. Overall, we concluded that the responses for most promoters are composed of only a few superimposed response modes.

The shape of PC1 was similar for all antibiotics: it described a permanent shift. However, this shift had a greater slope for CHL and NIT compared to TMP and TET (Figure 3C). This coincided with faster and more severe initial growth rate changes induced by TMP and TET (Figure 3B). An increase in cell volume dilutes protein levels and the growth rate therefore corresponds to an effective degradation rate; the degradation rate of a protein sets the time scale for relaxation to steady-state for proteins without autoregulation (Rosenfeld et al., 2002). We therefore hypothesized that a slower initial growth rate drop and thereby a higher instantaneous growth rate, as seen for NIT and CHL, allows the cells to reach their protein target levels more quickly. Indeed, when we performed PCA on the data set of gene expression over generations instead of time, thereby taking into account the effect that growth rate determines the rate of protein accumulation or reduction, the difference in PC1 between the antibiotics with a strong initial growth rate drop (TMP, TET) and the ones with a weaker initial growth rate drop (NIT, CHL) was nearly absent (Figure 3D). This suggests that the overall response rate to an antibiotic is affected by the initial rate at which this antibiotic inhibits growth: a weaker initial growth inhibition leads to a faster response.

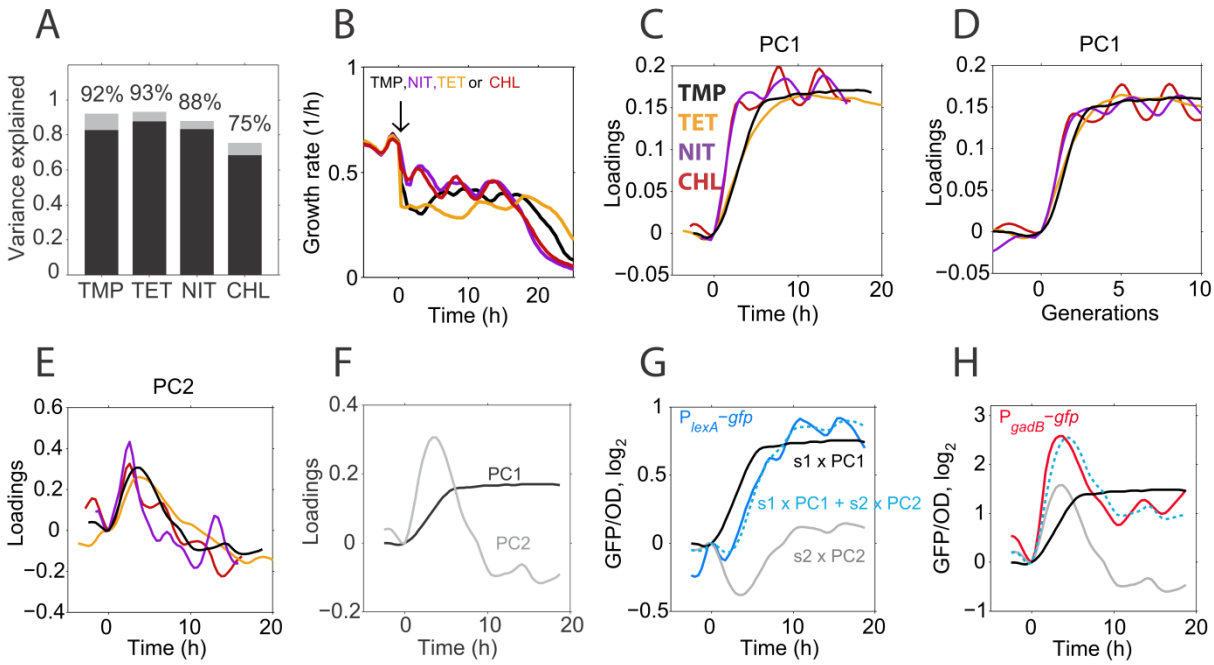

Figure 3. Principal component analysis on the data sets obtained by TMP, TET, NIT, or CHL stress. **A.** Fraction of variance explained by PC1 (black) and PC2 (gray) for TMP, TET, NIT and CHL. The fraction of variance explained by the 3rd to 5th PC was already as low as 1-3% for all antibiotics except for CHL (4-6%). **B.** Growth rate changes in response to antibiotics. Fluctuations in the growth rate curves are due to our dilution protocol, where cells grew a bit slower shortly before the dilution and picked up fast growth after the dilution into fresh medium. **C.** PC1 for TMP (black), TET (orange), NIT (purple), and CHL (red) shows a permanent shift. **D.** PC1, taken over generations instead of time, which assimilates the rate of PC1 for all antibiotics. **E.** PC2 describes a transient pulse for all stressors. **F.** PC1 and PC2 for TMP, also depicted in G-H. **G-H.** Response curves are well described as a linear combination of PC1 and PC2 for exemplary promoters (*lexA* (G)*, gadB* (H)) with very different dynamic responses. The solid line is the measured curve, blue for P_{lexA}-*gfp*, red for P_{gadB}-*gfp*. The dashed blue line is the reconstructed curve combined of PC1 and PC2.

1.2.4 TMP induces a response pulse in promoters from the acid stress response

Under TMP, TET, or NIT stress, the response curves for each promoter could consequently be described by a linear combination of two PCs: a permanent shift (PC1; Figure 3C) and a transient pulse (PC2; Figure 3E). Whereas some promoters behaved similar to only one of the PCs, most promoters were described by a combination (Figure 3F-H). For example, the dynamics of the *lexA* promoter under TMP stress was described by a permanent shift; however, PC2 mainly introduced a slight temporal shift (Figure 3G). In contrast, the dynamics of the *gadB* promoter had a strong contribution of PC2; PC1 only contributed to lift the final expression level to which this promoter returned.

To determine if there were differences in the contribution of PC1 and PC2 for the individual stressors, we plotted the scores for each promoter for PC1 and PC2 (Figure 4). While the

role of PC2 was mainly to move the permanent shift in time for TET, NIT, and CHL, similar as described before for the *lexA* promoter (Figure 3G), TMP induced some promoters that had a high score for PC2, but relatively low scores for PC1: these promoters responded with pulse-like dynamics, similar to the *gadB* promoter (Figure 3H). The promoters with a strong contribution of PC2 (score > 4) were *aidB* (present twice in the data set)*, focA, gadB, gadA,* and *slp.* Interestingly, three of them (*gadB, gadA, slp*) are related to the glutamate-dependent acid stress response system in *E. coli; focA* (a formate channel) plays a role in the prevention of intracellular acidification (Keseler et al., 2013) and *aidB* has been reported to respond to acetate stress (Smirnova et al., 1994). We therefore concluded that promoters related to acid stress show a pulse-like response under TMP. The further analysis of this TMP-induced acid stress response pulse is the subject of Chapter 2.

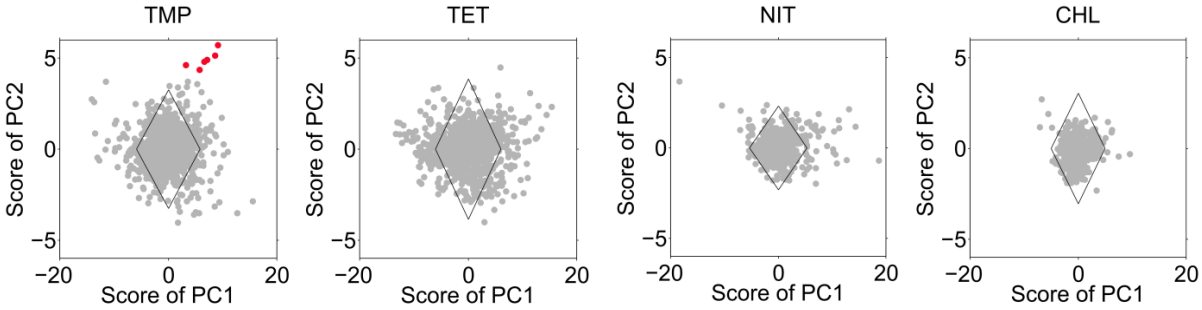

Figure 4. Data sets for TMP, TET, NIT, and CHL depicted as scores of the first two PCs. Promoters outside the diamond are the ones whose response curves (normalized GFP/A_{600} over time in response to the stress) had a > 2-fold up-or down-regulation when described as a superposition from PC1 and PC2. Note that the x- and the y-axis have different scales. Red dots in the panel for TMP are promoters with a PC2 score of > 4.

1.2.5 Differentially expressed promoters are more likely to be regulated by transcription factors and are enriched for stress response promoters

As we did not find many promoters that were differentially regulated in all four stress conditions, we hypothesized that promoters with a strong differential expression (> 2-fold) were specifically regulated by transcription factors, instead of reacting to global cellular changes, like changes in the growth rate (Klumpp et al., 2009). To quantify how prevalent the regulation by transcription factors was among all differentially expressed promoters, we calculated the average number of transcription factors controlling the differentially expressed promoters, and compared that number to the average number of transcription factors controlling all measured promoters. Counts of transcription factors was done based on the database RegulonDB (Gama-Castro et al., 2011). This measure told us how prevalent regulation by transcription factors was among the differentially expressed promoters. For all stress conditions, regulation by transcription factors was significantly enriched among the differentially expressed promoters (Table 3), with the highest enrichment for CHL stress.

Such enrichment is consistent with the notion that promoters that strongly respond to antibiotic stress are actively regulated by transcription factors, compared to passive regulation by growth rate or other means of gene regulation.

Table 3. Enrichment of the regulation by transcription factors among the promoters with > 2-fold expression changes. The p-value was determined with a one-sided binomial test.

	TMP	TET	NIT	CHL
Enrichment of regulation by transcription factors	1.69-fold	1.33-fold	1.88-fold	2.55-fold
p-value	1.4×10^{-23}	1.8×10^{-7}	4.8×10^{-22}	2.3×10^{-22}

As a next step, we wanted to know which specific biological processes were activated or suppressed by the individual antibiotics. We performed a gene ontology enrichment analysis as described before ((Chevereau and Bollenbach, 2015); Table S1; Methods). In this enrichment analysis, the molecular function terms of the differentially expressed promoters are determined and checked for over-representation compared to the molecular function terms of all measured promoters. The analysis yielded enrichment of promoters functioning in bacterial stress response, and other processes (see Table S1). Promoters with the gene ontology term 'responding to drugs', transcription-related promoters and DNA damage-related promoters were enriched for all antibiotics. The response to TMP was enriched for genes functioning in intracellular pH elevation in the up-regulated genes; NIT and CHL in the down-regulated genes. The response to TET was enriched for protein folding related processes in the up-regulated genes, whereas TMP had an enrichment of cold shock promoters in the down-regulated genes. TET and TMP also showed enrichment for promoters related to oxidative stress in the up-regulated promoters. Overall, we see diverse processes responsive in all four stress conditions; however, other processes seem specific for the individual antibiotics. The fact that well-known stress responses like DNA-damage, acid, oxidative or heat/cold shock response are triggered by antibiotics could mean that bacteria experience stress in response to antibiotics that is similar to the stress normally introduced by common environmental stressors. Alternatively, these stress response might be activated as a by-product of the activation of other processes (Price et al., 2013).

1.2.6 Promoters respond with vastly different response times

Next, we wanted to know how strongly and how rapidly promoters responded to antibiotics and if different biological processes followed a clear temporal order. We therefore defined a measure for the response time of each promoter, which was measured as the time until half maximum expression level change was reached (Figure 5A, Methods). Response times in our data set ranged from tens of minutes to several hours (Figure 5B), considerably exceeding the generation time of ~100 minutes in antibiotic stress. The detection of the response times for down-regulated genes was less sensitive than for up-regulated promoters: as the used GFP is stable (Zaslaver et al., 2006), its concentration can maximally decrease at the

rate of dilution due to growth. Consistent with that, we see the fastest response times for up-regulated promoters (Figure 5B).

We further wanted to know whether promoters from certain biological processes were up- or down-regulated together in time. We focused on the biological processes identified in the gene ontology enrichment analysis: acid stress response, oxidative stress response, DNA stress response, and chaperones functioning in heat and cold shock**.** For the acid, oxidative and DNA stress response, we included all promoters regulated by major stress response transcription factors: the glutamate-dependent acid stress transcription factors GadE, GadW and GadX (GadEWX) for acid stress, OxyR and SoxS for oxidative stress and LexA for DNA stress. Additionally, we looked into regulation by the general stress response sigma factor SigmaS (RpoS).

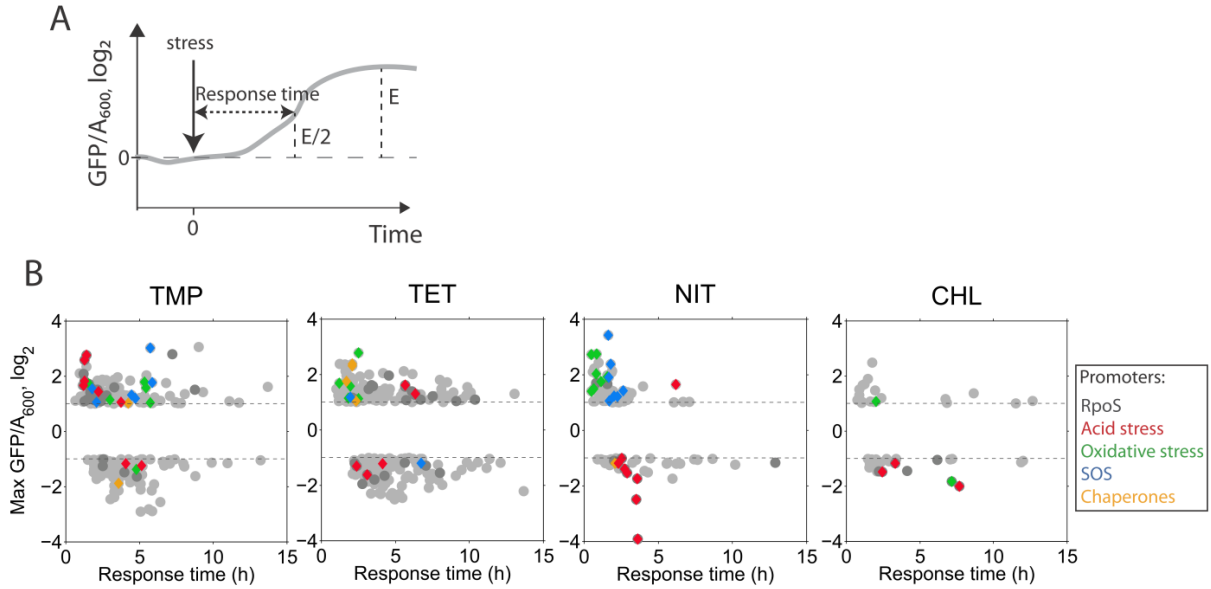

Figure 5. Genome-wide gene expression changes and response times upon sudden addition of different antibiotics (TMP, TET, NIT, CHL). A. Schematic illustrating response time determined as the time until half maximum expression on a $\log_2$ scale. **B.** Shown are all promoters that changed expression by > 2-fold; dark grey dots are promoters from the regulon of the general stress response sigma factor RpoS, red diamonds GadEWX-regulated, green diamonds are SoxS or OxyR-regulated, blue diamonds are LexA-regulated (SOS response), and orange diamonds are chaperones. Note the rapid acid stress response to TMP and the clear temporal sequence of stress responses for NIT. Response times, fold changes and absolute expression values are provided in Table S2.

Promoters belonging to the same specific stress responses tended to be activated at a similar time-point (Figure 5B). Specifically, NIT and TET triggered an early oxidative stress response. NIT has been shown before to induce oxidative stress in both prokaryotes and eukaryotes (Rossi et al., 1988; Streker et al., 2005; Youngman et al., 1982), probably due to oxidative damage by nitro anion radicals. In contrast, TET has previously not been associated with oxidative stress (Demple, 1991; Dridi et al., 2015). In addition, there is a

disputed hypothesis that bactericidal, but not bacteriostatic antibiotics induce oxidative stress (Kohanski et al., 2007). This would further support that the bacteriostatic antibiotic tetracycline does not induce oxidative stress. It therefore remains to be shown whether TET really induces oxidative stress or whether the oxidative stress response is upregulated unspecifically as a by-product of the activation of other processes. This question is addressed in Chapter 4.

TMP and NIT induced a delayed LexA-regulated SOS response (Figure 5B). DNA damage for NIT and TMP has been described before (Bryant and McCalla, 1980; Lewin and Amyes, 1991; Sangurdekar et al., 2011): NIT causes oxidative DNA damage, leading to interstrand cross-links in the DNA (Basak and Chatterjee, 1994; Sengupta et al., 1990); in the case of TMP, DNA damage likely comes from the depletion of thymine bases needed in DNA replication and subsequent stalling of the replication fork (Lewin and Amyes, 1991).

TET induced an early activation of chaperones functioning in heat and cold shock (Figure 5B). The activated promoters were *cspA, dnaK, htpG,* and *groS.* This is in contrast to previous studies measuring protein levels in response to translation inhibitors (VanBogelen and Neidhardt, 1990). Drugs that lead to a change in the translational capacity of the cell can increase the levels of either heat or cold shock proteins. TET, in particular, has been reported to induce a cold shock response at a similar concentration and temperature (0.8 µg/mL TET at 28°C) as in our protocol (0.7 µg/mL TET at 30°C), but to repress a heat shock response when TET prestressed cultures were shifted from 28°C to 42°C (VanBogelen and Neidhardt, 1990). We speculate that the unknown mechanism repressing heat shock promoters might be post-transcriptional, which could explain the discrepancy between our data and the literature. Alternatively, the induction of heat shock under TET may be so delayed that it has not been detected before, as measurements have only been reported up to 75 min (VanBogelen and Neidhardt, 1990).

Promoters from the glutamate-dependent acid resistance system, which provides protection at pH-values as low as 2.5 (Lin et al., 1996), showed particularly strong changes for TMP and NIT: they were down-regulated under NIT, but rapidly and transiently up-regulated under TMP (Figure 5B). This acid stress response pulse coincided with an initially aggravated growth rate drop under TMP (Figure 1B). Similarly to the acid stress genes, promoters regulated by the general stress sigma factor RpoS were up-regulated by TMP (2.3-fold enrichment in the up-regulated promoters, $p = 1.6 \times 10^{-4}$), but mostly repressed by NIT (2.8-fold enrichment in down-regulated promoters, $p = 2.9 \times 10^{-3}$). To our knowledge, these changes in the glutamate-dependent acid stress response in response to TMP and NIT have not been described before.

From these results we conclude that antibiotics can trigger the induction of temporally structured stress responses. Some of these stress responses, like the oxidative stress response for NIT or the DNA stress response for NIT and TMP, are a direct reaction to underlying drug-induced damage. For other stress responses, however, it is unclear whether they are a reaction to underlying damage, or if they get activated less specifically (Price et al., 2013). Such an unspecific activation could, for example, be the result of a cross-activation between transcription factors in the intricate gene regulatory network, as it is known for the

oxidative stress transcription factor SoxS with MarA/MarR, the transcription factors for multiple antibiotic resistance (Keseler et al., 2013). It therefore remains to be shown which molecular events lead to these stress responses. In Chapter 2, we address this question for one such stress response: the activation of the acid stress response under TMP. In addition to identifying the mechanism that leads to acid stress activation in response to TMP, we also explore physiological consequences for bacterial fitness in changing environments.

1.3 Discussion

In this chapter, we described the timing of global bacterial gene expression in response to diverse antibiotics. We found some general principles that seem to hold across drugs. Specifically, we saw that global gene expression mostly follows a permanent up- or downshift and that the initial growth rate drop has an impact on the dynamics of this shift. The strength of the initial growth rate drop is specific to each antibiotic and might be influenced, for example, by the permeability of the bacterial membrane to this antibiotic (Nikaido and Vaara, 1985), by the binding properties of the antibiotic to its target or by the rate at which downstream essential metabolites get depleted. These results also suggest that if the antibiotic concentration increases more slowly, not step-wise, thereby slowly inhibiting the growth rate, bacteria might in some situations respond faster. If the set of differentially expressed genes remains the same or could also change under a slower growth rate inhibition, as has been shown for the response to salt or ethanol stress in *Bacillus subtilis* (Young et al., 2013), remains to be shown.

In addition, we found that each antibiotic induces specific genes, and we could not find a general response common to all antibiotics. This complexity is consistent with previous results (Goh et al., 2002; Shaw et al., 2003). We detected that many genes belonging to well-characterized stress response systems specifically respond to antibiotics. This could either mean that the bacteria really experience the respective stresses like acid stress, oxidative stress, or DNA damage stress. We know that this is true or at least plausible for some cases: TMP induces DNA damage and the SOS response is a direct reaction to this damage (Lewin and Amyes, 1991). In addition, NIT is known to produce nitro radicals which are known to cause damage on macromolecules and DNA, with subsequent activation of oxidative stress response and DNA damage response (Bryant and McCalla, 1980; Streker et al., 2005). Alternatively, these stress response genes could be induced indirectly due to their membership in global stress regulons that evolved for responding to other environments (Price et al., 2013). Characterizing the temporal sequence of these molecular events, their interplay and their interactions with the environment in response to antibiotics can ultimately allow us to exploit vulnerabilities during this adaptation process and thereby improve the efficacy of antibiotics.

1.4 Methods

1.4.1 Strains and growth conditions

The strains used were from a GFP-promoter library (Zaslaver et al., 2006) with the parent strain K12 MG1655. All experiments were performed in minimal M9 medium (1x M9 salts, 2 mM $MgSO_4$, 0.1 mM $CaCl_2$, supplemented with 4 g/L glucose and 0.1% amicase, pH ~7.1). For experiments in 96-well plates, Triton X-100 was added at 0.001% (v/v) to reduce surface tension in the microplate wells; this had no detectable effect on growth or gene expression. Antibiotics for dynamic measurements were dissolved in ethanol (TMP, TET, CHL) or in dimethylformamide (NIT) and added from concentrated stocks (stored at -20°C in the dark) at the indicated concentrations; Sigma Aldrich catalog numbers are trimethoprim (92131), tetracycline (268054), nitrofurantoin (N7878), and chloramphenicol (C0378). Antibiotics for selection and glycerol stocks were dissolved in water; kanamycin (catalog # A9518) was used at 25 μg/mL. For dynamic experiments, no selection antibiotic was added. All chemicals were obtained from Sigma Aldrich except when stated otherwise.

1.4.2 Gene expression measurements with robotic system

Cultures were diluted ~1:1000 (with a VP408 pin tool, V&P Scientific, Inc.) from M9 medium glycerol stocks into fresh M9 medium. All reporter library strains were grown in 200 μL in transparent flat-bottom 96-well plates (Nunc) at 30°C with rapid shaking. Absorbance at 600 nm (A_{600}) and GFP fluorescence (excitation 485 nm(20), emission 535 nm (25)) were measured every ~25 minutes using an automated robotic system (Tecan Freedom Evo150) and a plate reader (Tecan infinite 500). Whenever the threshold absorbance (A_{600}) of 0.13 (which corresponds to a background corrected A_{600} of ~0.093) was exceeded, the cultures were diluted 10-fold into fresh M9 medium using a 96-channel pipetting head (Figure 1B). After the first dilution, 2 μL of antibiotic stock adjusted to 100-fold the desired concentration was added to all wells when they exceeded an absorbance threshold of 0.08 (background corrected A_{600} ~0.043). The subsequent dilutions were done into medium containing antibiotics at the same concentration.

1.4.3 Normalization and data analysis of the population-level data

All data analysis was performed using custom MATLAB (MathWorks) software. Absorbance background was measured before each experiment in each plate (filled with 200 μL M9 medium per well) before inoculation and subtracted in a well-specific manner. GFP background subtraction was done as described (Zaslaver et al., 2006). Only promoters with a mean signal-to-noise ratio (GFP/A_{600} divided by the standard deviation of GFP/A_{600} from the two promoter-less strains on each library plate) greater than 5 and exclusively positive GFP/A_{600} values were analyzed, reducing the number of promoters to ~1000 (1102 for TMP, 1111 for TET, 900 for NIT, 993 for CHL). Parts of growth curves that clearly suffered from

technical problems (e.g. due to air bubbles in the well), were automatically exchanged with the same part of the closest growth curve from another strain; this was unproblematic as nearly all strains from the library grew at the same rate in our conditions.

After each of the four 10-fold dilution steps in our protocol (Figure 1B), the background subtracted absorbance and GFP values dropped to ~1/10 of the value before the dilution (Figure 1B). This resulted in meaningless values at the point of dilution when differentiating the whole measurement curve. As we needed these differentiated data for later normalization and correction of the data (see below), we compensated for this drop in absorbance and GFP values by adding an offset to all the measurements after each dilution. This offset was calculated by extrapolating a linear fit (using the MATLAB function *robustfit*) from the last 4 absorbance measurements on a log scale before the dilution to the next time point. Further, using our protocol with recurring dilutions and the addition of antibiotics, it was impossible to keep the measurement intervals at exactly 25 minutes at all times. In order to have a common time axis for all measurements, we interpolated all measured A_{600} and GFP data onto a time axis with the fixed interval of 25 minutes, counting forward in time after the time point when antibiotics were added, and backwards in time before. This was unproblematic, as the real measurement points were close to 25 minutes for all data. All data were subsequently smoothed with a moving average filter with a span of 3 (using the MATLAB function *smooth*).

Using a plasmid-based GFP reporter system, unspecific effects can occur (like plasmid copy number changes (Bollenbach et al., 2009)) affecting all strains in a similar way. We corrected for these unspecific effects in our data using the following procedure. Without any unspecific effects, the total cellular protein concentration, and in approximation the median GFP concentration over all measured strains behaves as

$$\frac{\mathrm{d}\widetilde{\mathrm{GFP}}}{\mathrm{dt}} = \widetilde{\mathrm{PA}} - \mu \cdot \widetilde{\mathrm{GFP}},$$

where $\widetilde{\mathrm{PA}}$ is the median promoter activity over all strains, obtained from the individual strain promoter activities $\mathrm{PA} = \frac{\frac{\Delta \mathrm{GFP}}{\Delta \mathrm{t}}}{\mathrm{A}_{600}}$, where A_{600} is the absorbance value at the later time point of Δt. Further, μ is the growth rate and $\widetilde{\mathrm{GFP}}$ is the median GFP concentration over all strains. Based on the assumption that the total cellular protein concentration does not change over time (Basan et al., 2015), the median promoter activity $\widetilde{\mathrm{PA}}$ is directly proportional to the growth rate μ:

$$\widetilde{\mathrm{PA}} = \mu \cdot \widetilde{\mathrm{GFP}}$$

For each experimental condition, we corrected our data for deviations from this equation by subtracting the difference between $\log_2(\widetilde{\mathrm{PA}})$, shifted to zero for t = 0 and $\log_2(\mu)$, also shifted to 0 for t = 0, from the $\log_2$-transformed promoter activity $\log_2(\mathrm{PA})$ of each strain. From this corrected PA of each strain, we calculated back the GFP concentration by multiplication with

the absorbance values and numerical integration using the MATLAB function *trapz*. To compare relative changes in gene expression upon drug addition, all GFP/A_{600} data were $\log_2$-transformed and shifted to zero for t = 0.

Information on gene regulation was from (Gama-Castro et al., 2011; Keseler et al., 2013; Seo et al., 2015). Maximum fold-change in expression was determined as the maximum (for upregulated promoters) or minimum (for down-regulated promoters) GFP/A_{600} change on a $\log_2$ scale after the addition of stress. Response times were determined as the time until the half maximum expression on a $\log_2$ scale was reached (Figure 5A). Instantaneous growth rates in Figure 1B and 3B were determined by dividing the difference between subsequent log-transformed absorbance measurements by the respective time interval for each strain and averaging over all measured strains.

Before performing principal component analysis, the data were normalized and $\log_2$ transformed as described above. Principal component analysis was performed with the MATLAB function *princomp*, using each time series as an observation and each time point as a variable. This function did not rescale the variables.

The gene ontology database used in our analysis was retrieved from geneontology.org (released 31/03/2017) and the gene association file linking gene names to GO numbers from ecocyc.org (GOC Validation Date: 03/31/2017) (Hu et al., 2014; Keseler et al., 2013). The *p*-values were obtained using a custom implementation of Sherlock and Weng's GO:Termfinder software (Tavazoie et al., 1999) and Bonferroni corrected for the number of GO terms tested.

1.5 Supplement

Table S1: Biological processes enriched in the differentially expressed promoters (separately for up- and down-regulation) identified with gene ontology enrichment analysis (Methods). Only biological processes with > 2 promoters detected and with a Bonferroni-corrected p-value of < 0.05 are shown.

P-value	Counts	Promoters	Biological process
TMP: up-regulated promoters			
1.8×10^{-6}	14/63	*aidB, dctA, dinB, emrE, katE, mutM, mutS, recA, recN, sbmC, sulA, ybiJ, yfbU, yqjI*	Cellular response to DNA damage stimulus
1.7×10^{-3}	4/9	*dinB, recA, recN, uvrD*	SOS response
9.9×10^{-3}	2/3	*katE, osmC*	Hyperosmotic response
9.9×10^{-3}	2/3	*ldtA, ldtB*	Peptidoglycan-protein cross-linking
9.9×10^{-3}	2/3	*dkgB, yeaE*	Methylglyoxal catabolic process
0.01	5/19	*cysD, katE, osmC, gpmM, ychF*	Response to oxidative stress
0.012	3/7	*emrE, fpr, gyrB*	Response to drug
0.038	2/4	*fruB, treB*	Phosphoenolpyruvate-dependent sugar phosphotransferase system
0.038	2/4	*gadA, gadB*	Intracellular pH elevation
TMP: down-regulated promoters			
0.01	2/3	*cspA, rfaH*	Transcription antitermination
0.014	3/7	*cspA, cspB, rbfA*	Response to cold
0.019	4/13	*codB, lacY, setA, adeP*	Proton transport
TET: up-regulated promoters			
6.7×10^{-8}	16/56	*add, aidB, asnA, blc, elaB, fepB, glgB, htpG, hupA, pflA, yafN, ldtD, ycjW, yggE, yohC, yqjI*	Cellular response to DNA damage stimulus
0.013	3/6	*groS, htpG, trxC*	Protein folding
0.02	2/3	*sodA, sodB*	Superoxide metabolic process
0.02	2/3	*sodA, sodB*	Removal of superoxide radicals
0.02	2/3	*dnaK, groS*	Chaperone mediated protein folding requiring cofactor
0.02	2/3	*katG, ygiW*	Cellular response to hydrogen peroxide
TET: down-regulated promoters			
0.00023	4/6	*dcuS, glnL, torS, dgcE*	Peptidyl-histidine phosphorylation
0.00035	5/10	*dctA, nanT, pitA, setA, adeP*	Proton transport
0.00043	6/15	*dcuS, glnL, norR, prpR, torS, dgcE*	Phosphorelay signal transduction system
0.00077	4/7	*dcuS, glnL, torS, dgcE*	Signal transduction by protein phosphorylation
0.0023	8/32	*rseP, feaR, hcaR, nac, norR, prpR, ydeO, yeiE*	Positive regulation of transcription, DNA-templated

0.016	2/3	*glnL, torS*	Protein dephosphorylation
0.016	2/3	*puuA, patA*	Putrescine catabolic process
0.028	8/43	*cytR, fabR, hcaR, hipB, nac, prpR, bluR, ygaV*	Negative regulation of transcription, DNA-templated
0.048	3/8	*entS, yadC, yojI*	Response to antibiotic
NIT: up-regulated promoters			
2.9×10^{-9}	6/8	*dinG, lexA, polB, recA, ruvA, uvrD*	SOS response
2.9×10^{-5}	3/4	*dinG, ruvA, uvrD*	DNA duplex unwinding
0.0012	2/3	*cysD, cysP*	Sulfur compound metabolic process
0.0012	2/3	*comR, bhsA*	Response to copper ion
0.0012	2/3	*ftsK, marR*	Cellular response to antibiotic
0.0047	2/4	*recA, rmuC*	DNA recombination
0.0078	6/45	*fepB, idi, lexA, recA, ybiJ, yqiJ*	Cellular response to DNA damage stimulus
0.015	5/35	*lexA, marR, comR, nimR, dmlR*	Negative regulation of transcription, DNA-templated
0.039	2/7	*bhsA, yoaB*	Single-species biofilm formation
0.039	2/6	*kilR, ybjG*	Response to antibiotic
NIT: down-regulated promoters			
0.00012	2/3	*gadA, gadB*	Intracellular pH elevation
0.00047	2/4	*arcB, dcuS*	Peptidyl-histidine phosphorylation
0.00047	2/4	*arcB, dcuS*	Signal transduction by protein phosphorylation
0.00061	4/23	*gadX, nac, ydeO, yeiE*	Positive regulation of transcription, DNA-templated
0.0063	2/8	*arcB, dcuS*	Phosphorelay signal transduction system
0.0099	4/40	*gadW, gadX, ydeO, yeiE*	Transcription, DNA-templated
0.017	4/45	*asnA, gadW, gadX, ompC*	Cellular response to DNA damage stimulus
CHL: up-regulated promoters			
-	-	-	-
CHL: down-regulated promoters			
4.7×10^{-5}	2/3	*gadA, gadB*	Intracellular pH elevation
0.00019	2/4	*fruB, manX*	Phosphoenolpyruvate-dependent sugar phosphotransferase system
0.0038	2/9	*fsr, mdtK*	Response to antibiotic
0.0052	4/48	*dctA, deoC, fsr, udp*	Cellular response to DNA damage stimulus

Table S2. Fold change and absolute GFP/OD_{600} data for promoters in Figure 5. Absolute GFP/OD_{600} values are given for the respective antibiotics condition. Note that *hdeA* falls into two categories: acid stress and chaperone promoter. It is depicted in the category of acid stress promoters as a red diamond in Figure 5 for TMP, TET, and NIT stress.

Promoter	Response time (h)	Fold change, $\log_2$	GFP/OD_{600} at t = 0
TMP: up-regulated promoters			
Acid stress promoters (regulated by GadEWX)			
hdeD	1.20	1.67	0.57×10^4
slp	1.25	1.82	0.61×10^4
gadB	1.26	2.58	1.79×10^4
gadA	1.38	2.77	0.50×10^4
hdeA	2.19	1.44	0.38×10^4
cyoA	3.75	1.06	1.55×10^4
Oxidative stress promoters (regulated by OxyR or SoxS)			
dps	1.56	1.72	1.96×10^4
ychF	2.99	1.14	1.34×10^4
nfo	5.33	1.79	0.09×10^4
soxS	5.44	1.58	0.14×10^4
fpr	5.74	1.05	0.34×10^4
DNA stress promoters (regulated by LexA)			
dinB	1.76	1.55	0.03×10^4
uvrD	2.06	1.06	0.15×10^4
recA	4.47	1.31	0.55×10^4
smbC	4.72	1.20	0.08×10^4
recN	5.72	3.02	0.03×10^4
sulA	5.85	1.77	0.15×10^4
Chaperone promoters			
hdeA	2.19	1.44	0.38×10^4
stpA	4.22	1.02	0.25×10^4
TMP: down-regulated promoters			
Acid stress promoters (regulated by GadEWX)			
btuB	4.06	-1.16	0.16×10^4
adiC	5.12	-1.23	0.06×10^4
Oxidative stress promoters (regulated by OxyR or SoxS)			
grxA	4.77	-1.38	0.14×10^4
Chaperone promoters			
cspA	3.57	-1.88	4.68×10^4
TET: up-regulated promoters			
Acid stress promoters (regulated by GadEWX)			
hdeA	5.66	1.61	0.34×10^4
slp	6.34	1.31	0.55×10^4

Oxidative stress promoters (regulated by OxyR or SoxS)			
sodA	1.18	1.68	0.32×10^4
trxC	1.80	1.15	0.14×10^4
grxA	1.95	1.58	0.11×10^4
katG	2.50	1.13	0.08×10^4
ahpC	2.50	2.78	0.18×10^4
DNA stress promoters (regulated by LexA)			
uvrA	1.95	1.17	0.44×10^4
Chaperone promoters			
cspA	1.67	1.76	4.01×10^4
dnaK	2.06	2.39	0.28×10^4
groE	2.08	2.30	0.32×10^4
htpG	2.32	1.04	0.46×10^4
hdeA	5.66	1.61	0.34×10^4
TET: down-regulated promoters			
Acid stress promoters (regulated by GadEWX)			
gadB	2.37	-1.30	1.74×10^4
gadW	3.07	-1.61	4.07×10^4
uspE	4.14	-1.22	1.73×10^4
DNA stress promoters (regulated by LexA)			
dinG	6.72	-1.20	0.38×10^4
NIT: up-regulated promoters			
Acid stress promoters (regulated by GadEWX)			
rcsA	6.17	1.65	0.13×10^4
Oxidative stress promoters (regulated by OxyR or SoxS)			
soxS	0.48	2.73	0.07×10^4
fpr	0.48	1.42	0.21×10^4
inaA	0.65	1.50	0.21×10^4
ybjC	0.80	2.04	0.16×10^4
marR	0.83	2.74	0.07×10^4
ahpC	1.12	1.76	0.09×10^4
grxA	1.56	1.94	0.11×10^4
DNA stress promoters (regulated by LexA)			
recA	1.62	3.42	0.35×10^4
polB	1.65	1.92	0.10×10^4
uvrD	1.67	1.06	0.15×10^4
lexA	1.77	2.39	0.26×10^4
ruvA	1.99	1.23	0.29×10^4
ftsK	2.22	1.22	0.59×10^4
dinG	2.62	1.42	0.21×10^4

NIT: down-regulated promoters			
Acid stress promoters (regulated by GadEWX)			
hdeA	2.29	-1.19	0.24×10^4
gadX	2.52	-1.01	4.06×10^4
gadW	2.73	-1.39	2.84×10^4
hdeD	2.88	-1.53	0.36×10^4
slp	3.52	-2.49	0.39×10^4
gadA	3.58	-1.73	0.29×10^4
gadB	3.60	-3.91	1.28×10^4
Chaperone promoters			
stpA	2.06	-1.18	0.17×10^4
hdeA	2.29	-1.19	0.24×10^4
CHL: up-regulated promoters			
Oxidative stress promoters (regulated by OxyR or SoxS)			
ahpC	2.02	1.08	0.15×10^4
CHL: down-regulated promoters			
Acid stress promoters (regulated by GadEWX)			
gadB	2.44	-1.47	1.31×10^4
hdeD	3.32	-1.17	0.59×10^4
gadA	7.67	-1.99	0.45×10^4
Oxidative stress promoters (regulated by OxyR or SoxS)			
dps	7.15	-1.82	2.08×10^4

2. Chapter 2: Noisy response to antibiotic stress predicts single-cell survival in an acidic environment

The work described in this chapter was performed by KM. It uses the method for chromosomal integration of promoters described in the following chapter 3. This method was conceived and developed by Georg Rieckh. The work from this chapter has been published in an article in *Cell Systems* (Mitosch et al., 2017).

2.1 Introduction

In the second chapter, we investigate one of the antibiotic-induced stress responses in more detail: the induction of the glutamate-dependent acid stress response genes under trimethoprim (TMP) stress. Based on data from the first chapter, we ask which underlying mechanisms lead to the activation of this stress response. In addition, we investigate the physiological consequences of this acid stress response when cells are exposed to a sudden change in the environment. We address these questions at the single-cell level thereby exploring the relevance of cell-to-cell variability in this stress response and exploiting natural variability to identify causal chains of molecular events.

Microbes regularly encounter harsh environmental conditions. Both general and specific stress response programs help them survive the current stress; these responses may also protect them against subsequent higher levels of the same stress (Begley et al., 2002; Berry and Gasch, 2008; Goodson and Rowbury, 1989) or against different stresses (Al-Nabulsi et al., 2015; Battesti et al., 2011; Jenkins et al., 1988; Leyer and Johnson, 1993; McMahon et al., 2007; Wang and Doyle, 1998). Certain stress response programs are also specifically coupled, suggesting frequent co-occurrence of the corresponding stressors in the environment over the bacterium's evolutionary history (Mitchell et al., 2009; Tagkopoulos et al., 2008). As shown in Chapter 1 and in the literature, antibiotics trigger massive and complex changes in metabolism and global gene expression (Belenky et al., 2015; Brazas and Hancock, 2005; Goh et al., 2002; Kwon et al., 2010), including the induction of specific stress response genes. The physiological consequences are, however, unknown for most antibiotics-induced gene expression changes, and it is unclear if they can change the microbes' ability to survive environmental changes such as low pH, oxidative stress, or heat.

Such environmental stresses and their sudden fluctuations are commonplace challenges for commensal and pathogenic bacteria. For example, bacteria entering the mammalian stomach suddenly experience an acidic environment with pH values as low as pH 2 (Weinstein et al., 2013). Antibiotics are a similarly widespread impediment for bacterial growth: they are often produced by other microbes in the environment (Martín and Liras, 1989; Waksman, 1961) and their occurrence is further increased by their use in treating human infections and in agriculture with its resultant contaminations of water and soil (Andersson and Hughes, 2014). It is therefore relevant to study the combined effects of antibiotics and environmental stressors on bacteria. In particular, the bacterial stress

response programs triggered by antibiotics can indicate changes in bacterial susceptibility and new vulnerabilities to specific environmental stressors.

Most stress response mechanisms were elaborated at the population level. However, the expression of stress response genes tends to be highly variable from cell to cell (Locke et al., 2011; Newman et al., 2006; Silander et al., 2012) which can result in different phenotypes at the single-cell level and varying probabilities of an individual's survival (El Meouche et al., 2016; Sánchez-Romero and Casadesús, 2014). For example, in response to low concentrations of streptomycin, the expression level of a heat shock promoter in *E. coli* increased and became more variable and negatively correlated with survival (Ni et al., 2012). In another study, *Salmonella* bacteria variably expressed virulence genes in response to nutrient prestress (Arnoldini et al., 2014); those individual bacteria that most highly expressed the virulence genes had a lower growth rate and a more than 1,000-fold higher probability to survive clinically relevant ciprofloxacin concentrations (Arnoldini et al., 2014). This is an example of 'cross-protection': adaptation to one stressful environment (spent medium) provides a fitness benefit when cells are exposed to a second stressor (antibiotics).

Here, we ask if cross-protection can occur in the opposite direction: can antibiotic-induced gene expression changes provide protection against environmental stressors? We are also interested in disentangling the molecular events that lead to such cross-protection. As described in Chapter 1, we measured the genome-wide transcriptional regulation dynamics in response to four antibiotics using a fluorescent reporter library. From these data, we identified gene expression changes that might cross-protect from different stressors. In particular, we saw that TMP triggered an exceptionally strong and fast acid stress response pulse. Here, we report that this acid stress response indeed leads to cross-protection from extreme acid stress. We found that expression from the acid resistance operon *gadBC* was highly variable and that the expression level just before the exposure to acid stress predicted single-cell survival in this new environment. Survival of single cells also correlated with the intracellular pH of individual cells. This observation thus directly connects the function of TMP-induced GadB/C in pH homeostasis to survival following acid stress. We also investigated the mechanism of acid stress induction under TMP and found that it results from the intracellular depletion of purine nucleotides, a downstream effect of TMP. The cross-protection between TMP and acid stress presented here shows how antibiotics can increase bacterial fitness in a changing environment.

2.2 Results

2.2.1 Induction of the acid stress response under TMP is independent of RpoS

In the first chapter, we showed that many stress responses are induced in response to antibiotics. The induction of the glutamate-dependent acid stress response under TMP stress was particularly strong and unexpected since TMP does not acidify the medium, is unlikely to act as a potent acid (pK_a ~ 7; (Qiang and Adams, 2004)) and its mechanism of

action (inhibition of folate synthesis) is not obviously related to intracellular acidification. As a first step towards understanding how TMP induces the acid stress response, we asked whether this response was part of the general stress response induced by RpoS or if it was activated more specifically and independently of RpoS. To this end, we measured the expression of a key acid stress promoter, P_{gadB}, following TMP-treatment in an *rpoS* deletion strain (Baba et al., 2006). During acid stress P_{gadB} controls the expression of one of the glutamate decarboxylases in *E. coli*, GadB, and the glutamate:4-aminobutyrate antiporter GadC in an RpoS-dependent manner. The presence of both enzymes is essential for survival at low external pH (Castanie-Cornet et al., 1999; Richard and Foster, 2004): GadB catalyzes the proton-consuming decarboxylation on glutamate and GadC exchanges the product Gamma-aminobutyric acid (GABA) for glutamate, thereby increasing intracellular pH (Hersh et al., 1996; Tsai et al., 2013). GadB has a homolog, GadA, with highly similar regulation and redundant function (Keseler et al., 2013). In contrast, there is no homolog for GadC in *E. coli* which renders a *ΔgadC* strain extremely sensitive to acid (Castanie-Cornet et al., 1999). We observed that this system is activated by TMP independently of RpoS: the basal expression of *gadBC* was 6-fold lower in the Δ*rpoS* strain but this strain still upregulated *gadBC* by 7-fold in response to TMP (compared to 13-fold in the wild type, Figure 1). Thus, we conclude that while RpoS is needed for the basal expression of *gadBC* and amplifies the acid stress response activation, consistent with previous results (Burton et al., 2010), it is not essential for triggering the response to TMP.

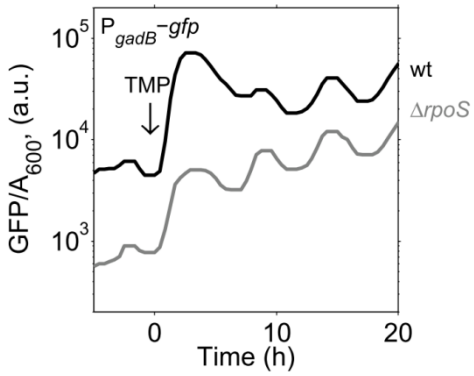

Figure 1. RpoS is important for the basal level of *gadBC* expression, but not for its induction after TMP stress. *GadBC* expression in an *rpoS* deletion strain. Using the same protocol as in Figure 1 of Chapter 1, *gadBC* expression over time in response to TMP in an *rpoS* deletion mutant (Δ*rpoS,* gray) was compared to the wild type BW25113 (wt, black). The basal expression level is much lower in the *rpoS* mutant, but the pulse-like induction in response to TMP is still present. Fluctuations in gene expression stem from our dilution protocol, as described in Chapter 1.

2.2.2 Organic acid stress induces similar acid stress response pulse as TMP

To confirm the specific activation of the acid stress response by TMP, we compared it to the dynamic response triggered by a common organic acid, formic acid. We adjusted the concentration of formic acid to achieve a similar initial growth rate drop as with TMP (Figure 2A). Following this challenge, bacterial growth rate thereafter recovered similarly as to the

TMP challenge, but to a higher final growth rate. Under these conditions, formic acid induced a strikingly similar pulse in the same acid stress and RpoS-regulated promoters as TMP (Figure 2B). Expression after this pulse settled back to slightly higher levels than before the stress. These pulse-like dynamics may result from autoregulation and the short half-life of the acid stress regulator GadE (Heuveling et al., 2008; Hommais et al., 2004; Ma et al., 2004) and confirm previous reports (Stincone et al., 2011). Promoters that are related to acid stress but independent of RpoS and GadE, such as the pH-sensitive formate channel FocA and the alternative sigma factor RpoE, had similar dynamics (Figure 1B). Overall, these data show that the dynamic response to a common organic acid is similar to the acid stress response induction under the antibiotic TMP.

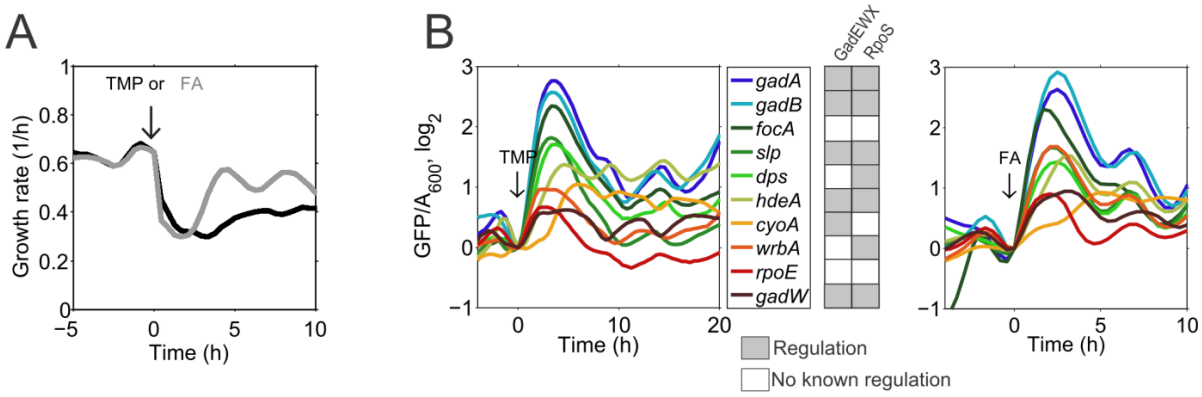

Figure 2. Growth rate and gene expression changes over time in response to TMP and formic acid. **A.** Growth rates over time in response to sustained exposure to TMP (0.5 µg/mL , black), or formic acid (FA, gray), titrated to pH 6.4, suddenly added at t = 0. Curves are mean growth rate over all measured strains. Fluctuations in growth rate are due to dilutions of the cultures into fresh medium whenever the threshold A_{600} was reached. **B.** Normalized gene expression over time for selected acid stress and RpoS-regulated promoters in response to sustained TMP stress or FA stress. The table shows known transcriptional regulation (gray squares) or no known regulation (white squares) by GadEWX or RpoS, according to (Keseler et al., 2013; Seo et al., 2015).

2.2.3 TMP cross-protects bacteria from subsequent acid stress

We thus hypothesized that the acid stress response induced by TMP could cross-protect bacteria from subsequent acid stress, similar to the effect of a mild acid prestress (Arnold et al., 2001; Leyer and Johnson, 1993; Ryu and Beuchat, 1998). To test this idea, we stressed microcolonies growing in a microfluidics device with TMP and, after three hours, switched to medium at pH 3 without antibiotic (Figure 3A; Methods). Under this acid stress, bacteria stopped growing and started lysing within minutes. Lysis was detected by the sudden loss of fluorescence of the fluorophore used for segmentation (Lowder et al., 2000) (Figure 3B). The survival curves approximately followed an exponential decay characteristic of a Poisson process for which the probability of cell death remains constant over time (Figure 3C). Cells that had not been prestressed lysed rapidly (half-life 31 ± 2 min); in contrast, cells prestressed with TMP had greatly extended survival times (half-lives of 107 ± 6 min and 320

± 11 min for 0.5 µg/mL and 1 µg/mL TMP, respectively; Figure 3C). Thus, pre-exposure to TMP strongly protects bacteria from subsequent acid stress. By contrast, pre-treatment with NIT, which down-regulates acid stress promoters (Figure 5B of Chapter 1), caused individual cells to lyse even faster than in the control (half-life 9.8 ± 0.8 min; Figure 3B,C). Taken together, these data show that antibiotics can protect or sensitize bacteria to subsequent acid stress in a way that can be explained by their transcriptional response.

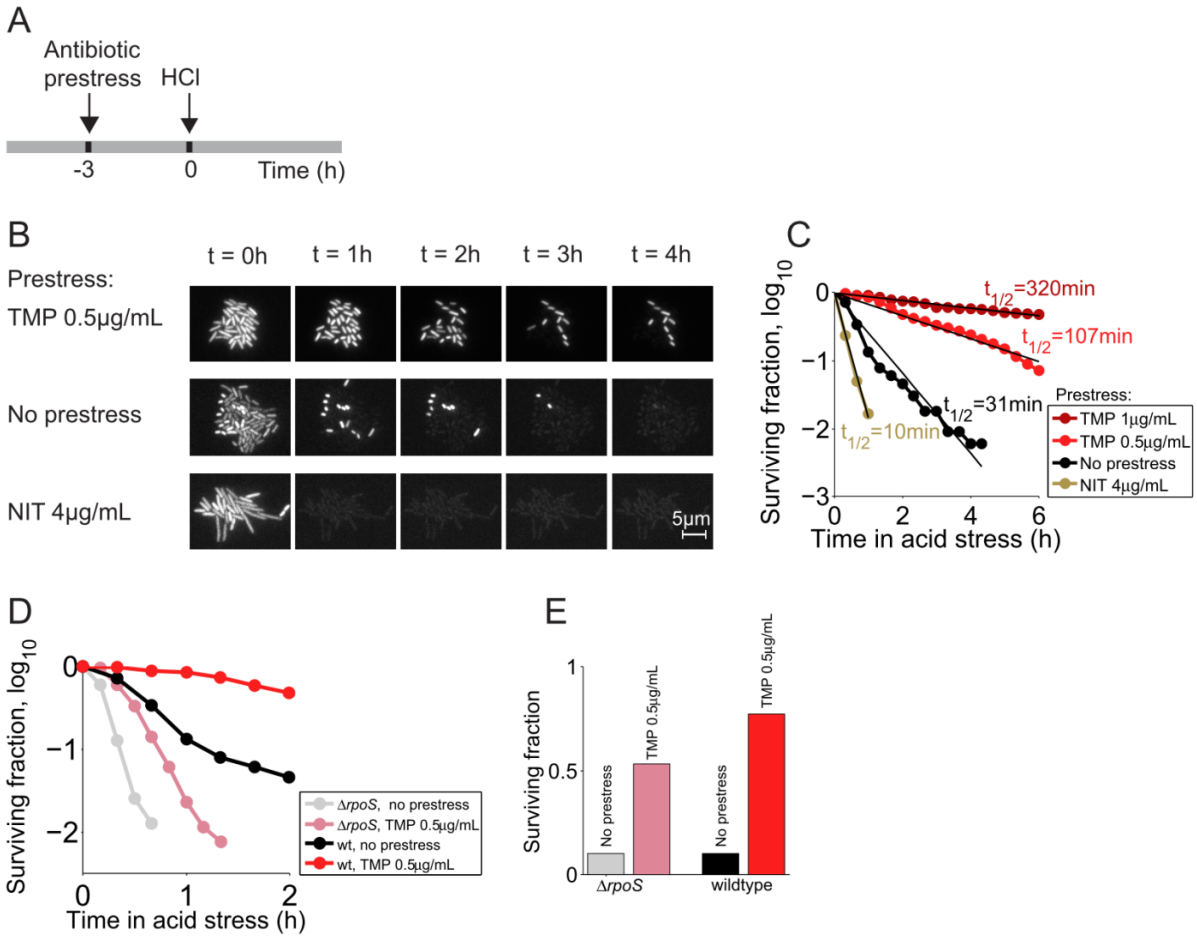

Figure 3. TMP prestress cross-protects bacteria from subsequent acid challenge, and the induction of cross-protection is largely independent of *rpoS*. A. Experimental procedure: bacteria growing in microcolonies in a microfluidics device were prestressed for three hours and then subjected to extreme acid stress with HCl at pH 3 (Methods); the antibiotic was not present during the extreme acid stress. **B.** Microscopy images of cells at various time points during the acid stress, with or without 0.5 µg/mL TMP or 4 µg/mL NIT prestress (white is the segmentation fluorophore). Scale bar is 5 µm. **C.** Fraction of surviving bacteria after addition of HCl and linear fits to the $\log_{10}$ values ($t_{1/2}$ is the half-life) after prestress with 1 µg/mL TMP (dark red, number of analyzed single cells n = 91), 0.5 µg/mL TMP (light red, n = 181), 4 µg/mL NIT (ocher, n = 60) or bacteria without prestress (black, n = 330). **D.** Fraction of surviving bacteria over time after addition of HCl on a $\log_{10}$ scale for MG1655 Δ*rpoS* and the wild type MG1655, prestressed with 0.5 µg/mL TMP (Δ*rpoS*: n = 261 from six microcolonies; wt: n = 181 from 5 microcolonies; data for wt taken from Figure 3C) or without prestress (Δ*rpoS*: n = 157 from four microcolonies; wt: n = 330 from four microcolonies; data for wt taken from Figure 3C). **E.** Surviving fraction in acid stress for Δ*rpoS* (rose bar) and MG1655 wild type

(red bar) with 0.5 μg/mL TMP prestress determined at 10% survival of Δ*rpoS* (gray bar) and MG1655 wild type (black bar) without prestress.

To test the role of RpoS in acid protection under our conditions, we measured TMP-induced acid protection in an *rpoS* deletion strain (Methods). Consistent with the lower basal levels of *gadBC* in an *rpoS* deletion strain (Figure 1), this strain was more sensitive to acid without TMP prestress. TMP prestress protected the *rpoS* deletion strain, albeit less than the wild type (Figure 3D,E); this is consistent with the weaker *gadBC* induction in an *rpoS* deletion strain (Figure 1). Acid stress is known to increase *rpoS* transcription (Hommais et al., 2004) and a drop in intracellular ATP levels, a downstream effect of folate biosynthesis inhibition by TMP (Kwon et al., 2010), can additionally enrich RpoS due to decreased degradation by the ATP-dependent ClpXP protease (Peterson et al., 2012). These data support the findings from above that RpoS is not essential for the TMP-induced cross-protection, but it increases the basal level of acid protection, and its induction in response to TMP amplifies the cross-protection.

2.2.4 Expression of the acid stress operon *gadBC* under TMP is highly variable and predicts single-cell survival

Promoters from the glutamate-dependent acid stress response system were previously found to be highly variable from cell to cell under unstressed conditions (Silander et al., 2012). We therefore wanted to know how variable the expression of this acid stress response was under TMP stress. To this end, we integrated a transcriptional yellow fluorescent protein (YFP) reporter for the *gadB* promoter (P_{gadB}-*yfp*) into the chromosome (Method described in Chapter 3). We selected the *gadB* promoter as it controls the expression of two proteins, GadB and GadC, which act together to lower the intracellular proton concentration (Figure 4A). Using time-lapse microscopy, we observed that the *gadB* promoter was upregulated within three hours after TMP addition (Figure 4B), consistent with our population-level experiments (Figure 2B); fold-changes varied drastically among cells, ranging from virtually no change to a > 30-fold increase. Variability in *gadBC* expression (quantified as coefficient of variation three hours after TMP addition) was high compared to the RpoS-regulated promoters *wrbA* and *dps* (Figure 3C) which also showed pulse-like dynamics in their average response (Figure 2B). Further, *folA* which codes for dihydrofolate reductase (DHFR, the target of TMP) and is not regulated by acid stress or RpoS, but upregulated under TMP (Keseler et al., 2013), was considerably less variable than *gadBC* (Figure 4C). In addition, this high variability in *gadBC* expression was independent of RpoS, as the coefficient of variation of the expression level in an *rpoS* deletion strain was still extremely high (Figure 4C). In the Δ*rpoS* strain, the basal *gadBC* expression level was considerably lower (Figure 1), which can explain the even higher variability compared to the wild type (Figure 4C and (Taniguchi et al., 2010)). These data show that *gadBC* induction in response to TMP is highly variable, consistent with previous results on GadEWX-regulated genes in other conditions (Silander et al., 2012), and that this variability is independent of RpoS.

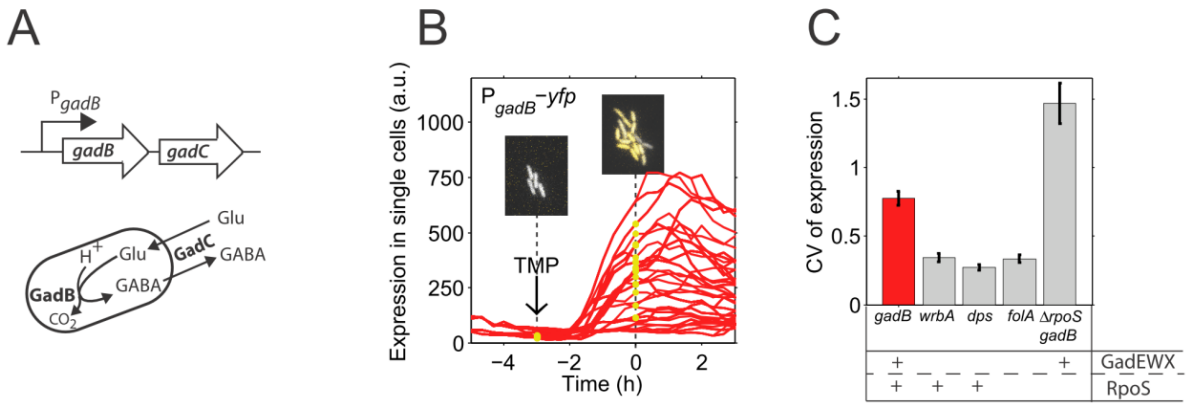

Figure 4. Expression of the acid stress operon *gadBC* is highly variable. A. Schematic of the *gadBC* operon and the function of GadB and GadC. Upon intracellular acidification, GadB catalyzes a proton-consuming reaction on glutamate (Glu) decreasing the intracellular proton concentration in concert with the antiporter GadC that exchanges the product gamma-aminobutyric acid (GABA) for glutamate. **B.** Expression of P_{gadB}-*yfp* in response to sudden TMP addition (0.5 µg/mL) at time point -3h in single cells of two microcolonies. Microscopy images of one microcolony at time points -3h and 0h are shown; segmentation fluorophore is gray, YFP is yellow. Yellow dots are *gadBC* expression of cells in the depicted microcolony. **C.** Coefficient of variation (CV) as a measure for cell-to-cell variability in gene expression 3h after TMP addition for different promoter-*yfp* constructs (P_{gadB}-*yfp*, P_{wrbA}-*yfp*, P_{dps}-*yfp*, P_{folA}-*yfp*, Δ*rpoS* P_{gadB}-*yfp*). For each promoter, at least 78 cells from at least three microcolonies were analyzed; error bars are from bootstrapping (Methods). Regulation by GadEWX and/or RpoS is shown by '+'.

We reasoned that the highly variable *gadBC* expression in response to TMP might explain the variability in single-cell survival times under subsequent acid stress (Figure 3B,C). Indeed, single-cell *gadBC* expression right before the acid stress was strongly correlated with the survival time ($\rho = 0.73$, $p = 3 \cdot 10^{-21}$; Figure 5A,B). A two-fold increase in *gadBC* expression prolonged survival on average by almost 2 hours. A similar correlation occurred in a control without prestress ($\rho = 0.62$, $p = 3 \cdot 10^{-25}$; Figure 5C) and when pooling data from different prestresses (TMP, NIT) and no prestress ($\rho = 0.75$, $p = 2 \cdot 10^{-81}$; Figure 5C). In contrast, *wrbA, dps*, or *folA* expression correlated only moderately with survival (Figure 5D), with the weakest correlation for *folA* which is neither regulated by RpoS nor GadEWX. The weaker correlation of the RpoS-regulated promoters *wrbA* and *dps* compared to *gadB* may be explained by their smaller dynamic range. Overall, these data show that the specifically variable *gadBC* expression under TMP predicts single-cell survival upon sudden acid stress, supporting the functional importance of GadB/C in cross-protection and suggesting an important role of these proteins in phenotypically diversifying the bacterial population.

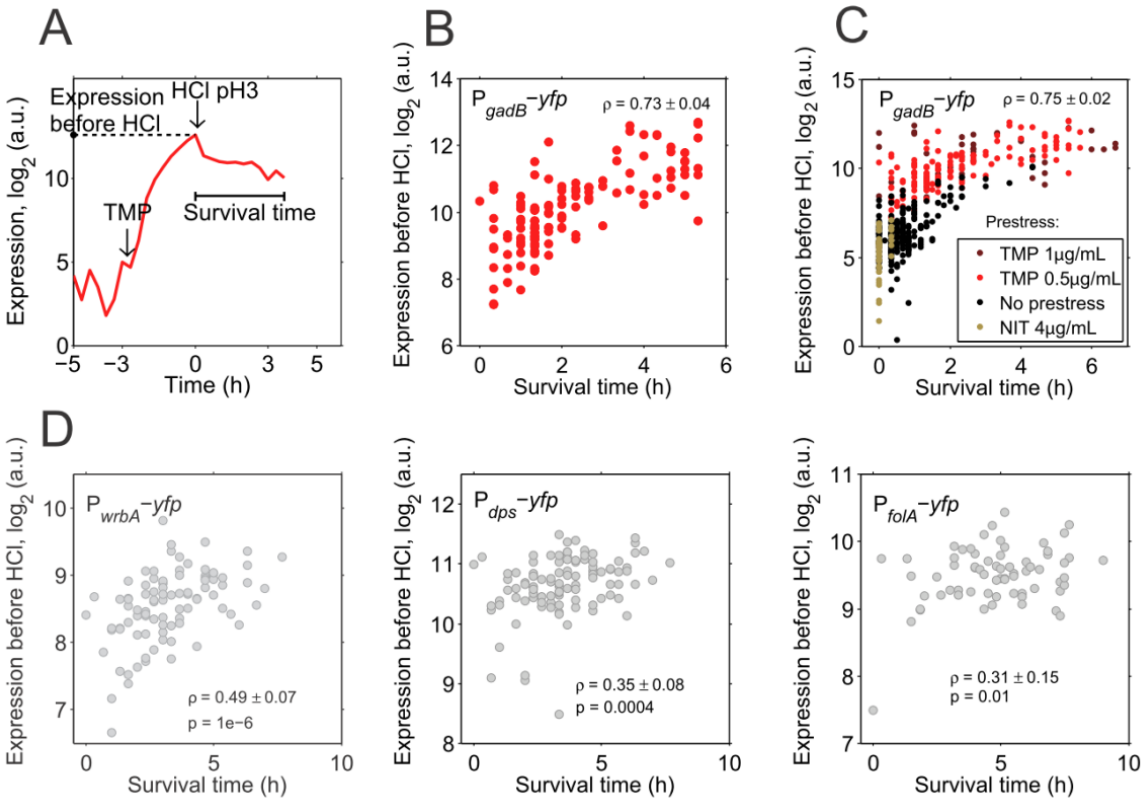

Figure 5. *GadBC* expression predicts single-cell survival under acid stress. A. Representative trace of a cell expressing P_{gadB}-*yfp* prestressed with TMP and 3h later with HCl at pH 3. Survival time is the time from HCl addition until cell lysis; expression level before HCl was measured as shown. **B.** Expression of P_{gadB}-*yfp* right before HCl addition versus single cell survival time. Data are from 122 cells in three microcolonies; only cells dying during the time course of the experiment are shown and analyzed. Pearson correlation coefficient is $\rho = 0.73 \pm 0.04$, $p = 3 \cdot 10^{-21}$. **C.** Same as for **B**, but for additional prestressors: 1 µg/mL TMP, 4 µg/mL NIT, and no prestress. For each condition, at least two microcolonies were analyzed. Pearson correlation coefficient for the combined data is $\rho = 0.75 \pm 0.02$, $p = 2 \cdot 10^{-81}$. **D.** Expression of promoters P_{wrbA}-*yfp*, P_{dps}-*yfp*, and P_{folA}-*yfp* after 3h of 0.5 µg/mL TMP prestress (1 µg/mL TMP for *folA*) right before HCl addition versus single-cell survival time in acid. Correlations are significant but weak to moderate ($\rho < 0.5$). Data from at least 69 cells in three microcolonies were analyzed for each promoter. The errors of the Pearson correlation coefficient ρ in B, C and D were calculated from bootstrapping (Methods).

2.2.5 Higher intracellular pH under HCl entails longer survival times and correlates with *gadBC* expression before HCl

To test whether single-cell survival depends directly on the function of GadB/C, namely the reduction of the intracellular proton concentration, we monitored the intracellular pH using *pHluorin*, a ratiometric GFP variant which was calibrated as described (Figure 6A; Methods) (Martinez et al., 2012; Miesenböck et al., 1998). When TMP-prestressed cells were exposed to sudden acid stress, their intracellular pH dropped strongly and showed high cell-to-cell

variability (> 5-fold increase in standard deviation; Figure 6B). The mean pH of cells that survived for at least 10 minutes was 3.9 ± 0.7, consistent with population-level measurements (Richard and Foster, 2004) and close to the pH optimum of GadB (McCormick and Tunnicliff, 2001; Pennacchietti et al., 2009). The intracellular pH right after HCl addition correlated with each cell's survival time (Figure 6C, $\rho = 0.60$, $p = 1.4 \cdot 10^{-12}$) and pH was significantly higher for cells that survived for longer than 1.5 hours (Figure 6D; $p = 10^{-11}$); no such relation held for the intracellular pH right before the acid stress (Figure 6E). The relation between pH and survival in acid was however not perfect (Figure 6C,D), consistent with previous results that pH is not the sole factor influencing survival (Richard and Foster, 2004); this imperfect relation might also be due to limitations in intracellular pH measurement with *pHluorin* below pH 5 (Figure 6A; (Martinez et al., 2012; Miesenböck et al., 1998)). When switching back to normal growth medium, some surviving bacteria resumed growth during the time course of the experiment while others did not resume growth or lost fluorescence. In contrast, cells classified as dead based on their loss of fluorescence during the acid stress never resumed growth.

To test whether higher intracellular pH after HCl addition is caused by high *gadBC* expression levels before the HCl stress, we measured P_{gadB}-*mCherry* expression and intracellular pH in the same cell. Even though *mCherry* has a longer maturation time which impedes dynamic measurements (see Chapter 3, Figure 1), we still detected a strong correlation ($\rho = 0.58$, $p = 1 \cdot 10^{-17}$; Figure 6F). Together with the correlation between *gadBC* expression and survival, these results directly connect the function of the acid stress proteins GadB/C to survival: higher *gadBC* expression enables cells to maintain higher intracellular pH under severe acid stress, which in turn prolongs survival.

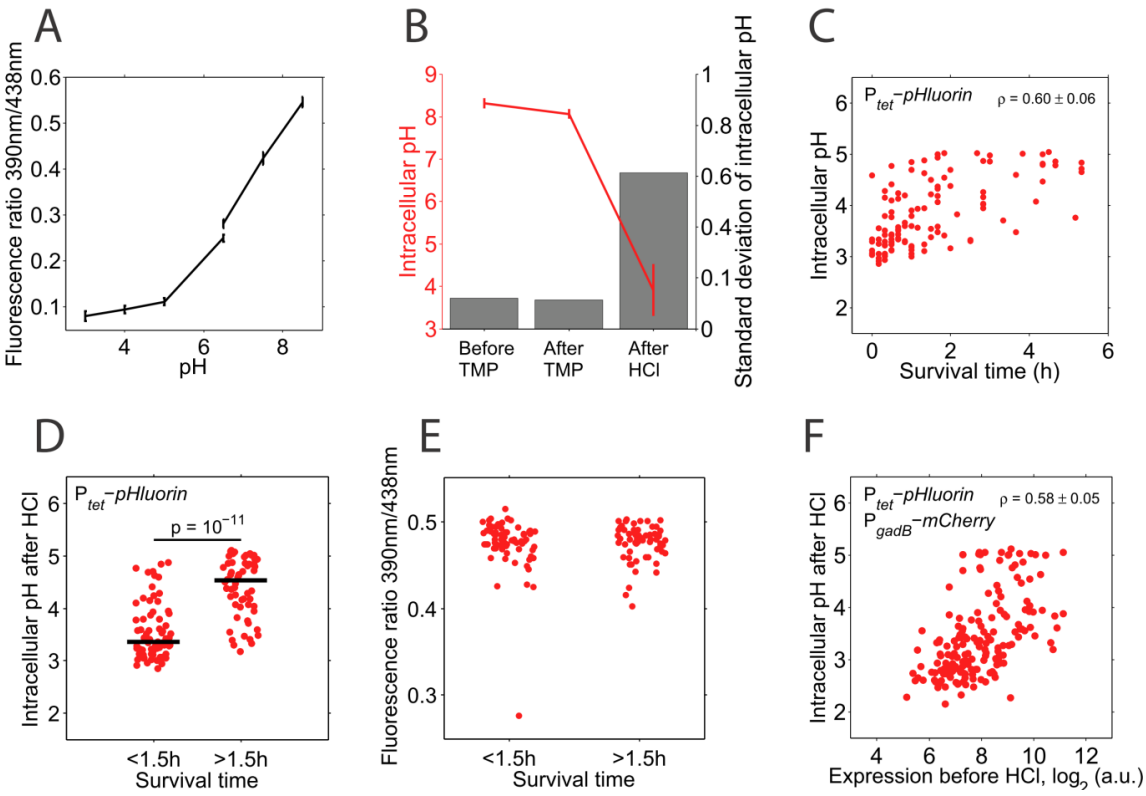

Figure 6. Higher intracellular pH after HCl prolongs survival and is correlated with *gadBC* expression. A. Fluorescence ratio over pH as determined for pH 3 to 6.5 and for pH 6.5 to pH 8.5, measured on different days (Methods). As calibration values, we used the mean over several time points and many cells (n = 34 for pH 3 to 6.5; n = 32 for pH 6.5 to 8.5), error bars are the highest standard deviations of all the standard deviations (taken at each time point) in the specific pH environment. Calibration was done for each experiment separately, due to day-to-day variations in illumination. The calibration curve is flatter for lower pH values; this alone can, however, not explain the increase in variability among different cells in HCl stress (Methods). **B.** Red line (corresponding to the left y-axis): mean and standard deviation of intracellular pH, calibrated based on Figure 6A; bars (corresponding to the right y-axis): standard deviation of single-cell intracellular pH right before TMP addition, right before HCl addition and 10 min after HCl addition. Data before and after HCl addition are from separate experiments (number of single cells analyzed is n = 56 before HCl addition and n = 29 after HCl). **C.** Intracellular pH of individual cells 10 min after HCl addition, measured with *pHluorin* (Methods) versus survival time. Only cells that died before the end of the experiment (6h after HCl addition) are included. Pearson correlation coefficient is $\rho = 0.60 \pm 0.06$, $p = 1.4 \cdot 10^{-12}$; error from bootstrapping (Methods). **D.** Intracellular pH of individual cells 10 min after HCl addition, measured with *pHluorin* (Methods); left: cells that survived < 1.5 hours; right: cells that survived > 1.5 hours. Medians (black lines) are significantly different ($p = 10^{-11}$, Wilcoxon rank sum test). Data are from 127 cells in six microcolonies, with no significant differences between the microcolonies. **E.** Fluorescence ratio, determined with *pHluorin* before HCl addition. Cells were grouped into cells with survival < 1.5 hours and survival > 1.5 hours as in **C**. Each dot is the fluorescence ratio of a single cell (total n = 134) right before HCl addition. The median of the two groups was not significantly different (Wilcoxon rank sum test). **F.** Intracellular pH 10 min after HCl addition versus expression of P_{gadB}-*mCherry* right before HCl addition in single cells. Spearman correlation coefficient is $\rho = 0.58 \pm 0.05$, $p = 1 \cdot 10^{-17}$; error from bootstrapping (Methods). Intracellular pH values < pH 3 occur due to large measurement errors and low sensitivity of *pHluorin* at these low pH values (Figure 6A).

2.2.6 Depletion of adenine bases leads to a pH drop and activation of the acid stress response

Which molecular pathways and physiological changes lead to the activation of acid stress promoters in response to TMP? The main downstream effects of dihydrofolate reductase (DHFR or FolA) inhibition are the depletion of amino acids, purine bases and thymine (Amyes and Smith, 1974; Kwon et al., 2010). We first confirmed that DHFR inhibition by TMP in our conditions could be rescued by supplementing purine bases and thymine: we observed only minor growth rate changes in response to even high concentrations of TMP when inosine (a purine base) and thymine were added to the growth medium (Figure 7A). Next, to distinguish whether thymine or purine depletion induced the acid stress response, we supplemented either component separately to the growth medium: thymine had little effect, but when inosine was supplemented, acid stress and RpoS-regulated promoters were not upregulated anymore (Figure 7C,D). Under these conditions, also the growth rate response to TMP changed drastically (Figure 7B) in that growth was unaffected for ~4 hours, but completely halted afterwards. With supplemented inosine, TMP is bactericidal and leads to 'thymineless death': in contrast to purine depletion which results in growth arrest, bacteria cannot sense the depletion of thymine bases and incur severe DNA damage (Amyes and Smith, 1974; Kwon et al., 2010). We thus hypothesized that the acid stress response to TMP is activated as a downstream effect of the depletion of purine bases.

To further pinpoint whether guanine nucleotide depletion or adenine nucleotide depletion cause an acid stress response induction, we mimicked the inhibitory effect of TMP on each of these biosynthesis pathways separately. Specifically, we measured *gadBC* expression under sudden guanine and adenine nucleotide depletion, respectively, using the deletion mutants *ΔguaB* and *ΔpurA* (Baba et al., 2006). Both enzymes are downstream of the reaction catalyzed by PurH which consumes 10-formyltetrahydrofolate (10-formyl-THF) (Figure 8A): GuaB is the first enzyme in the synthesis of guanine nucleotides from inosine monophosphate (IMP) and PurA catalyzes the first step in the synthesis of adenine nucleotides from IMP. We grew these mutants in medium supplemented with their respective purine base (guanine for *ΔguaB* and adenine for *ΔpurA*) and induced depletion by sudden removal of these purine bases in the microfluidics device (Methods). In both cases, growth rates dropped (Figure 8B), presumably due to the complete depletion of purine bases. While *gadBC* expression stayed low and showed virtually no response to sudden guanine removal, it strongly increased upon adenine depletion (Figure 8C).

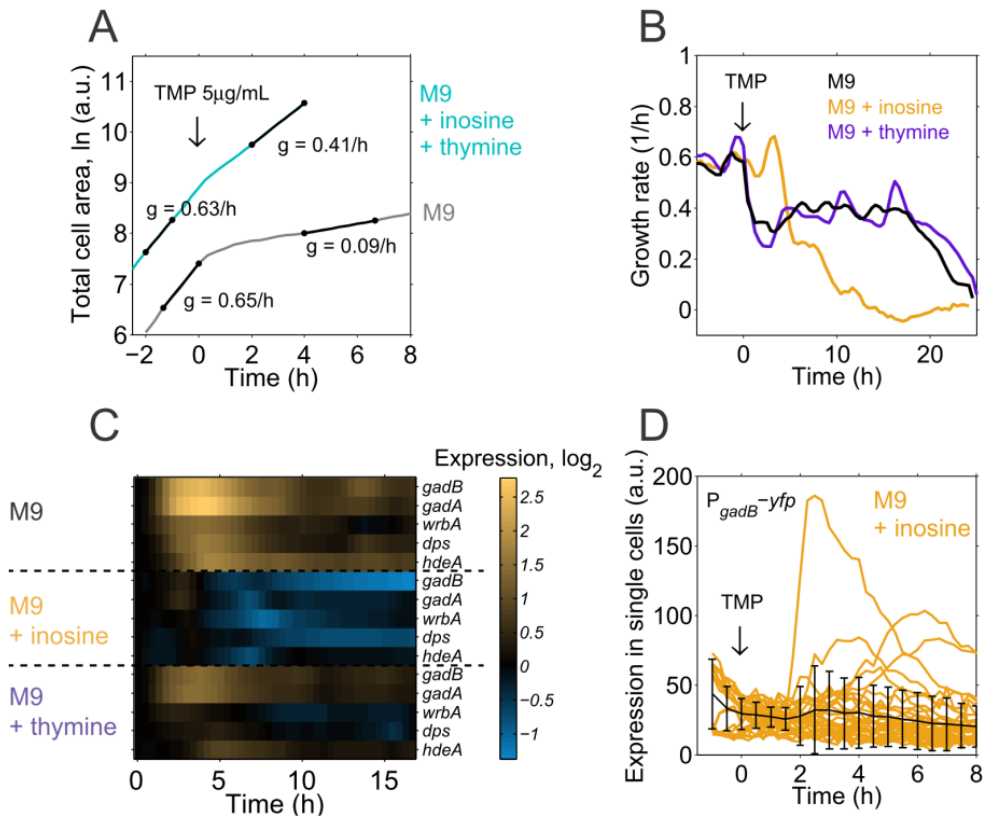

Figure 7. Supplementation with inosine bases, but not with thymine bases, eliminates acid stress response activation. A. Total cell area over time and fitted growth rates of microcolonies in response to high concentrations of TMP (5 µg/mL) in normal M9 medium (gray) and in M9 medium supplemented with inosine and thymine (cyan). Black lines depict regions in which colony growth rate g was fitted. **B.** Growth rate over time in inosine (orange) or thymine (purple) supplemented cultures in response to 0.5 µg/mL TMP, measured with our dilution protocol as in Figure 1 of Chapter 1. **C.** Expression of acid stress and RpoS promoters (*gadB, gadA, wrbA, dps, hdeA*) over time in response to TMP added at time zero as in Figure 1 of Chapter 1 with inosine and thymine supplemented throughout the experiment, compared to medium without supplements. **D.** Expression from chromosomally integrated P_{gadB}-*yfp* over time in response to 1 µg/mL TMP in inosine supplemented medium is not pulsing in single cells (orange, n = 39). Only rarely, individual cells also show an increased expression under these conditions. Black lines are mean and standard deviation of two microcolonies.

To test whether acidification of the cytoplasm causes acid stress induction, we measured the intracellular pH in the deletion mutants after adenine or guanine removal and in the wild type under TMP stress. The intracellular pH clearly dropped in the *ΔpurA* assay while nearly no change in pH occurred in the *ΔguaB* assay (Figure 8D). We also observed an immediate drop in intracellular pH by ~0.65 pH units in response to high concentrations of TMP (Figure 8D); a similar but weaker pH drop also occurred in response to lower TMP concentrations (Figure 8E). The pH dynamics following TMP addition were different from those upon adenine removal in the Δ*purA* mutant, possibly due to the different point of inhibition in the adenine biosynthesis pathway and different dynamics of adenine nucleotide depletion. While ATP and adenosine were suggested to have a protective role in

acid resistance (Sun et al., 2011, 2012), the molecular mechanisms that cause this intracellular acidification upon adenine depletion remain to be further elucidated. Overall, we showed that the depletion of adenine bases leads to an acid stress response. We propose that this is the mechanism which activates the acid stress response under TMP stress. We cannot, however, exclude that other mechanisms, like an imbalance in the turnover of purine and pyrimidine nucleotides, are causal for the acid stress response induction under TMP.

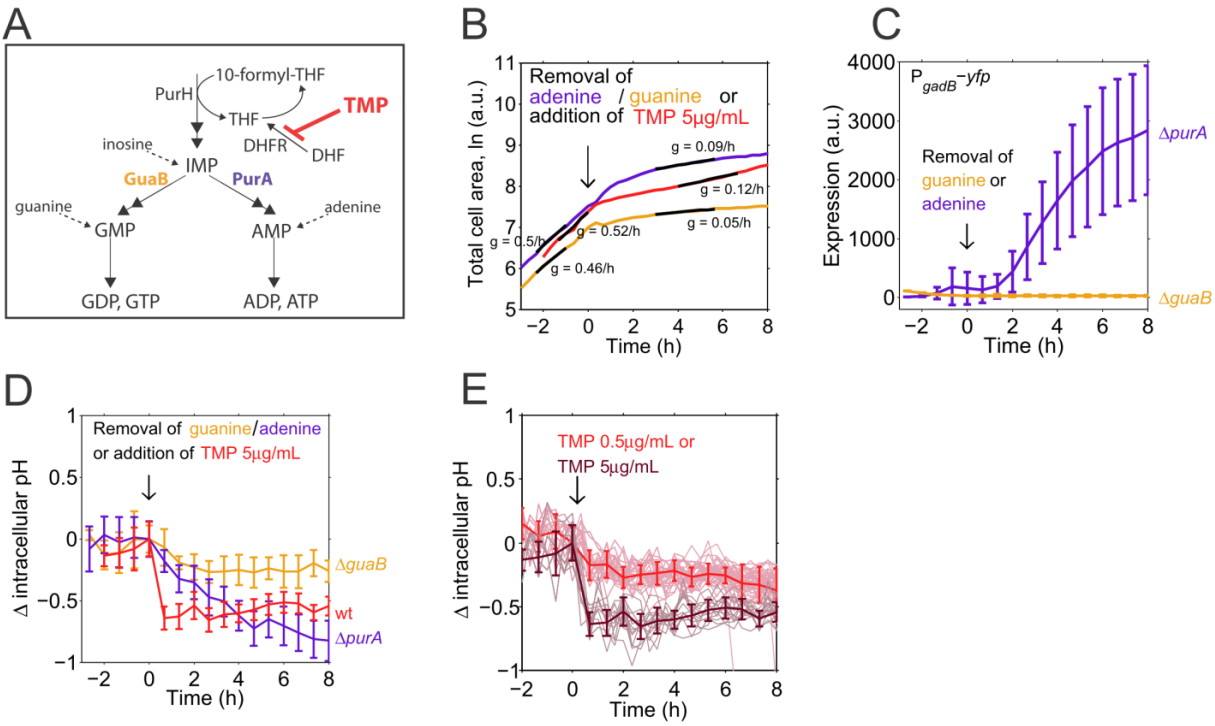

Figure 8. Depletion of adenine nucleotides, a downstream effect of DHFR-inhibition by TMP, causes acid stress response activation and an intracellular pH drop. A. Schematic of the purine biosynthesis pathway. TMP (red) inhibits DHFR (FolA) which catalyzes the production of tetrahydrofolate (THF) from dihydrofolate (DHF). 10-formyl-THF, a derivative of THF, is needed for the production of inosine monophosphate (IMP), the precursor for guanine and adenine nucleotides. Inosine, adenine, and guanine can be supplemented and enter the pathway as indicated (dotted arrows). **B.** Total cell area over time and fitted growth rates of one microcolony each in response to guanine depletion in a Δ*guaB* strain (orange), adenine depletion in a Δ*purA* strain (purple), and addition of 5 µg/mL TMP addition in the wild type. Black lines depict regions in which colony growth rate g was fitted. **C.** P_{gadB}-*yfp* expression over time averaged over single cells in *purA* (n = 58 from one microcolony) and *guaB* (n = 8 from one microcolony) deletion mutants in response to sudden removal of adenine or guanine, respectively, mimicking different downstream effects of TMP. **D.** Change in intracellular pH in Δ*purA* (n = 53 from one microcolony) and Δ*guaB* (n = 7 from one microcolony) mutants in response to sudden removal of adenine or guanine, respectively, and in the wildtype without supplements treated with 5µg/mL TMP (red, n = 14 from one microcolony). Lines are means, errors bars are standard deviations for a microcolony. **E.** Change in intracellular pH of individual cells over time in response to TMP at 0.5 µg/mL (light red, n = 56 from one microcolony) and 5 µg/mL (dark red, n = 14 from one microcolony). The dark red line is the same as the red line in

panel D. Thick lines and error bars are mean and standard deviation across single cells in a microcolony.

2.2.7 Deletion of the NADH dehydrogenase amplifies pH drop, *gadBC* response, and growth rate drop under TMP

To further validate the contribution of the intracellular pH drop to acid stress response induction under TMP, we screened 160 gene deletion mutants (Baba et al., 2006) for changes in growth rate and *gadBC* expression. Mutants were selected to cover genes involved in acid stress response activation and pH homeostasis (Methods). The deletion strains Δ*gadE* and Δ*rcsB* no longer upregulated *gadBC* expression (Figure 9A), consistent with the role of these genes as important regulators of the glutamate-dependent acid resistance system (Foster, 2004; Krin et al., 2010). Like most mutants screened, Δ*gadE* and Δ*rcsB* had only minor fitness disadvantages under TMP, suggesting that the glutamate-dependent acid stress response is dispensable under TMP (Figure 9B). Interestingly, the Δ*nuoC* strain showed an aggravated growth rate drop (Figure 9B) and prolonged and amplified *gadBC* expression (Figure 9A) and pH drop (Figure 9C). NuoC is an essential component for the proper formation of the proton-pumping NADH dehydrogenase I complex (Sinha et al., 2015) which can likely protect from mild acid stress (Kanjee and Houry, 2013; Krulwich et al., 2011). Other respiratory chain mutants did not show a strongly altered response. Thus, amplifying the pH drop via reduced proton pumping in the Δ*nuoC* strain results in an amplified and prolonged acid stress response, further supporting that an intracellular pH drop is a key trigger of the acid stress response to TMP.

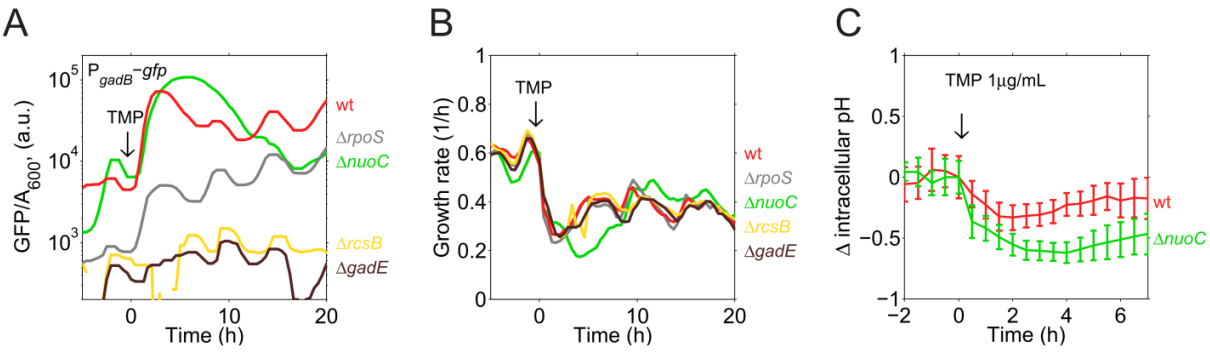

Figure 9. *GadBC* expression, growth rate and intracellular pH drop of single gene deletion mutants in response to TMP. A. P_{gadB}-*gfp* expression over time in the single gene deletion mutants Δ*rpoS*, Δ*nuoC,* Δ*rcsB* and Δ*gadE* compared to the wild type BW25113 (wt). **B.** Growth rate over time in response to 0.5 µg/mL TMP for the same mutants. **C.** Change in intracellular pH over time in response to 1 µg/mL TMP for wild type (red, number of analyzed cells n = 137) and Δ*nuoC* (green, n = 67). Lines and error bars are mean and standard deviation across single cells in a microcolony.

2.3 Discussion

We showed that the antibiotic TMP induces a functional acid stress response. This may happen via the depletion of adenine nucleotides, which leads to an intracellular pH drop and RpoS induction (Figure 10). This acid stress response, including the acid resistance proteins GadB and GadC, cross-protects bacteria from subsequent acid stress. Single-cell survival under acid stress is predictable from the variable expression of *gadBC*, with those cells surviving longer that have a higher intracellular pH (Figure 10). In summary, our results propose the chain of events and molecular mechanisms by which the antibiotic TMP cross-protects from an environmental acid stress. How the depletion of adenine nucleotides leads to intracellular acidification and acid stress induction is not clear yet. We speculate that decreased intracellular ATP levels either impair pH homeostasis or induce other ATP-generating, acidifying mechanisms. We note that, whereas the depletion of adenine nucleotides leads to the activation of an acid stress response, it is not completely clear that this is indeed the mechanism by which TMP induces the acid stress response.

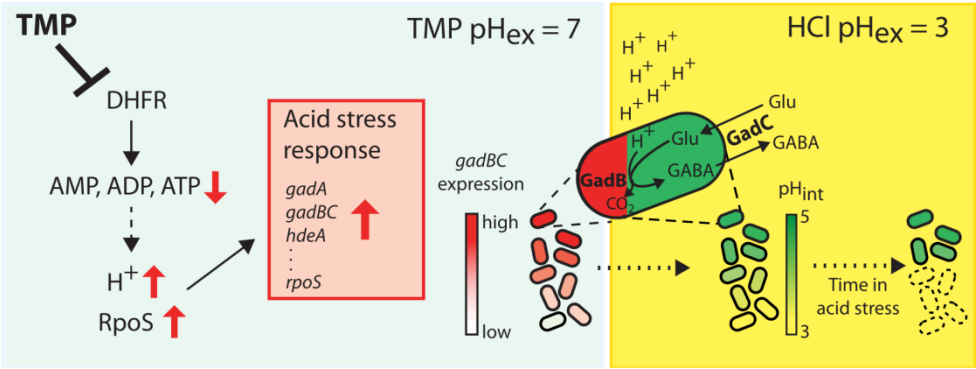

Figure 10. Summary of the proposed molecular mechanisms by which TMP cross-protects from acid stress. See main text for details; every single cell has its distinct *gadBC* level (different intensities of red) which influences its intracellular pH (different intensities of green). Abbreviations: DHFR: dihydrofolate reductase; AMP, ADP, ATP: adenine nucleotides; RpoS: general stress sigma factor; H^+: proton; *gadA, gadBC, hdeA*: acid stress promoters; *rpoS:* RpoS promoter; Glu: glutamate; GABA: gamma-aminobutyric acid; pH_{int}: intracellular pH; pH_{ex}: extracellular pH

Most antibiotics affect the expression of many bacterial genes, with consequences for microbial communities and host-microbe interactions (Hoffman et al., 2005; Justice et al., 2008; Maurice et al., 2013). Some of these regulatory responses are direct downstream effects of drug target inhibition but the cause and functional role of most gene expression changes is rather obscure (Price et al., 2013). In Chapter 1, precise measurements of the genome-wide transcriptional response dynamics to antibiotics empowered us to identify a specific stressor (acid) against which TMP could cross-protect. This approach is generally applicable and will enable the systematic identification of pairs of environmental stressor and cross-protecting or -sensitizing antibiotic, together with the optimal time-window that maximizes these effects. Based on our data (Chapter 1, Figure 5B), we expect specific cross-protection effects between TET or NIT and oxidative stress, which has indeed been shown

before between NIT and H_2O_2 (Basak and Chatterjee, 1994). Further, we would expect cross-protection between NIT and DNA damaging agents, and TET and temperature shock. The RpoS induction under TMP might further cross-protect from various environmental stressors. More generally, our results suggest that the gene expression state induced by an antibiotic can completely change the cell's fitness in a subsequent environment. This finding may lead to new strategies for designing advanced treatments that potentiate the effects of antibiotics (Allison et al., 2011; Morones-Ramirez et al., 2013) and exploit bacterial vulnerabilities by temporally switching between different antibiotics in ways that accelerate the eradication of pathogens.

By focusing on the *gadB* promoter, which controls acid resistance proteins that are well characterized at the population level, we were able to predict and functionally explain single-cell survival and its high variability among cells. Our single-cell study thus exploited natural variability to infer causal chains of molecular events from temporal correlations. This approach can further suggest survival strategies: the high variability in *gadBC* expression observed here may hint at a bet-hedging strategy in which populations can maximize their fitness by keeping a fraction of cells in a less fit state that prepares them for a future environment. The best-known example for this kind of bet-hedging strategy is bacterial persistence (Balaban et al., 2004). It remains to be tested if expression of acid stress genes is costly, i.e. if a bet-hedging strategy underlies the response characteristics of the glutamate-dependent acid resistance system revealed here.

Overall, this work shows how exposure to antibiotics triggers bacterial responses that can subsequently alter cell physiology and directly affect fitness upon a change in environment. Such environmental changes are common in an infected host where bacteria often encounter antibiotics together with environmental stressors like acid, reactive oxygen species, or heat. In particular, immune cells attack bacteria with oxidative bursts in an acidic phagosome (Audia et al., 2001). Cross-protection effects may therefore complicate antimicrobial treatment by impeding the eradication of bacteria that were exposed to antibiotics. An acidic environment can also be found in the mammalian digestive system, and can be caused by gastric acid, food, other drugs or other bacterial species; here, the changed sensitivity of a particular species to acid may have effects on microbiome composition. Future research will show how widespread cross-protection and -sensitivity between antibiotics and environmental stressors are, and how they can be prevented or exploited in treatments.

2.4 Methods

2.4.1 Strains, antibiotics, and culture conditions

We used *E. coli* K-12 strain MG1655 as wild type, unless stated otherwise. Deletion strains, i.e. Δ*guaB*, Δ*purA*, Δ*nuoC,* Δ*rpoS,* and all strains listed below, are from the KEIO collection (Baba et al., 2006) with parent strain BW25113, unless stated otherwise.

All experiments were performed in minimal M9 medium, as described in Chapter 1. Inosine, guanine, adenine and thymine were added at 0.3 mM. Antibiotics for selection and glycerol stocks were dissolved in water; kanamycin was used at 25 µg/mL; ampicillin at 50 µg/mL; spectinomycin at 100 µg/mL. For the acid stress experiment (Figures 3-6), the pH of the M9 medium without TMP was adjusted to pH 3 with hydrochloric acid (HCl). For the formic acid experiment (Figure 2), the pH of the M9 medium was titrated to pH 6.4. All chemicals were obtained from Sigma-Aldrich except when stated otherwise.

For monitoring *gadBC* expression in deletion mutants, KEIO strains were transformed with the plasmid pUA139 P_{gadB}-*gfp* Amp^R (Table S2). Specifically, the following strains were checked:
aceA, aceB, aceF, acnB, acrB, adhE, adiA, aldA, appB, appC, aqpZ, atpB, atpC, atpD, atpE, atpG, atpH, atpI, cadA, cbpA, cfa, clcA, codB, cydB, cydX, cyoA, cyoB, cyoC, cyoD, cyoE, dkgA, dkgB, dld, dnaK, dps, eutD, fdhF, focA, frdA, fre, gabT, gadB, gadC, gadE, gadW, galE, gcvP, gdhA, gldA, gloA, gloB, gltP, gor, gpmM, gshA, gshB, guaB, hchA, hdeA, hmp, hycA, hycB, hycC, hycD, hycE, hycF, hycG, hycH, hycI, icd, ilvA, ilvC, ilvE, kbl, kdpF, kefB, kefC, kefF, kefG, ldcC, ldhA, lldD, ltaE, lysC, maeB, marA, marR, mdh, mgsA, mhpF, miaB, mnmE, mnmG, mscK, nadR, narG, ndh, ndk, nfsB, nrdD, nrdE, nrdF, nuoA, nuoB, nuoC, nuoE, nuoF, nuoG, nuoH, nuoI, nuoJ, nuoK, nuoL, nuoM, nuoN, ompC, ompF, pflB, phoB, phoE, pntA, pntB, potE, pta, ptsG, purC, purM, purT, puuD, puuE, pykF, rcsB, relA, rpoS, rsxA, sdhA, sdhB, sdhC, sdhD, serA, slp, soxS, speF, sthA, talA, tdcB, tdh, thrA, thrB, thrC, tolC, tynA, wrbA, ydbD, yaeE, yeiG, yghZ, yiaY, yqiL, zwf

We sequenced 50 plasmids from our copy of the promoter-GFP library and did not find the indicated promoters in some cases (*pitB, aqpZ, pheL, dps, b1997, yhcF*). Their promoter names were replaced with the correct names of the promoters as found in these plasmids (*gadA, dps, serA, - , aidB, aidB*) throughout the paper.

Gene expression measurements with the robotic systems and the subsequent data normalization were performed as described in Chapter 1.

2.4.2 Plasmid construction

The plasmid pUA139 P_{gadB}-*gfp* Amp^R (Table S2; used in Figures 1 and 9) was constructed by amplifying P_{gadB} from the MG1655 chromosome using the primers CGGGATCCTCCTGCAGCATGGACTGAG and CCGCTCGAGCATTTTCGTCGTCCCAGGTC (underlined bases are restriction sites; all primers are listed in Table S3). Kan^R on pUA139 was exchanged by Amp^R amplified from the plasmid pZS11-*pHluorin* (Table S2) using the primers GCGAGCTCGTAAACTTGGTCTGACAGTTAC and CGGGATCCTCAGGTGGCACTTTTCGG.

The plasmid pZS11-*pHluorin* (Table S2; used in Figures 6, 8D,E, 9C) was constructed by amplifying the ratiometric *pHluorin* (Martinez et al., 2012) with the primers GGCCGAATTCATTAAAGAGGAGAAAGGTACCGCATGAGTAAAGGAGAAGAACTTTTCACTGG and

GGCCAAGCTTTTATTTGTATAGTTCATCCATGCCATG and putting it on a low-copy number plasmid (pSC101 origin) under a constitutive $P_{LtetO-1}$ promoter without the Tet repressor present (Lutz and Bujard, 1997).

The plasmid pZS41-*mCherry* (Table S2; used in Figures 3, 4, 5, 6E, 7A,D, 8B,C), used for segmentation, was cloned from the plasmid containing the constitutive $P_{LTetO-1}$ promoter with absent Tet repressor (Lutz and Bujard, 1997) and the plasmid pZS2-123 (Cox et al., 2010) which contains the fluorophore *mCherry*.

2.4.3 Strain construction and verification

The Δ*guaB* and Δ*purA* strains were verified phenotypically (i.e. dependence on purine base supplementation) and genotypically by PCR using the primers CGCCGGAAAGAATAATGCCG and CAGTCGATAGTAACCCGCCC for Δ*guaB,* and GTTTTGGCGGTGGACTTGTG and TCAGCGCACGTAATCCGTAA for Δ*purA*; the *ΔnuoC* strain was PCR-verified using primers CACCACGGACCATTTGCAATG and CAGTCATAGCCGAATAGCCT (binding inside the kanamycin resistance cassette); the Δ*rpoS* strain was PCR-verified using the primers ATTACCTGGTGCGTATGGGC and GAAATCCGTAAACCCGCTGC; the strain MG1655 Δ*rpoS* was obtained from the respective KEIO strain by P1 transduction (Lennox, 1955) and PCR-verified with the same primers.

To obtain chromosomally integrated promoter-reporter fusions, we devised an efficient method to easily accept various promoters from the set of plasmids used in (Zaslaver et al., 2006); this method is described in detail in Chapter 3. In short, we used lambda-red recombineering as described in (Datsenko and Wanner, 2000) to integrate PCR products derived from the promoter-GFP library (Zaslaver et al., 2006) into the *intS* locus (chromosome positions 2,466,545 -> 2,467,702; (Keseler et al., 2013)) on the *E. coli* chromosome. First, a sequence containing the fluorophore and the biggest part of the kanamyin resistance cassette was integrated into the *intS* locus. Then, PCR products from the promoter-GFP library were amplified using the primers GCGATACCGTAAAGCACGAG (MKan-1) and TTCTTCACCTTTGCTCATATGTATATCTCC and integrated into this sequence. Through our method, the GFPmut2 from the reporter plasmid library was replaced by a YFP variant from the plasmid pZS2-123 (Cox et al., 2010). Since we detected a mutation in the *gadB* library plasmid, this promoter was first amplified from the chromosome with primers CGGGATCCTCCTGCAGCATGGACTGAG and CCGCTCGAGCATTTTCGTCGTCCCAGGTC and cloned into the library backbone (underlined bases are restriction sites). Recombineering was performed with the plasmid pSIM19 (Datta et al., 2006). All integrated constructs were validated by sequencing the PCR product obtained with primers upstream and downstream of *intS*, respectively: GTACTTACCCCGCACTCCAT and TGTTCAGCACACCAATAGAGG on the chromosomal DNA. This protocol yielded the strains Δ*intS*::P_{gadB}-*yfp* (Table S1; used in Figure 4, 5A-C, 7D), Δ*intS*::P_{wrbA}-*yfp,* Δ*intS*::P_{dps}-*yfp,* and Δ*intS*::P_{folA}-*yfp* (Table S1; all used in Figure 4C and 5D).

To obtain the strains BW25113 Δ*guaB*Δ*intS*::P_{gadB}-*yfp* (Table S1; used in Figure 8C), BW25113 Δ*purA*Δ*intS*::P_{gadB}-*yfp* (Table S1; used in in Figure 8C), and MG1655 Δ*rpoS*Δ*intS*::P_{gadB}-*yfp* (Table S1; used in Figure 3D-E) the kanamycin resistance cassette was first deleted as previously described (Datsenko and Wanner, 2000) using plasmid pCP20 (Cherepanov and Wackernagel, 1995) before lambda-red recombineering. P_{gadB}-*yfp* was amplified from the MG1655 Δ*intS*::P_{gadB}-*yfp* strain (Table S1) and integrated using the primers GTACTTACCCCGCACTCCAT and TGTTCAGCACACCAATAGAGG. To obtain the strain Δ*intS*::P_{gadB}-*mCherry* (Table S1; used in Figure 6F), we replaced the sequence of *gfp* in the plasmid with P_{gadB}-*gfp* by *mCherry* amplified from pZS41-*mCherry* using the primers CCGCTCGAGAGATCCTCTAGATTTAAGAAGGAGATATACATATGGTTTCCAAGGGCGAGGAGG and GCGCCTAGGTCTAGGGCGGCGGATTTGTCCTACTC, followed by recombineering with the primers MKan-1 and CTACTCAGGAGAGCGTTCACC. We also validated all strains with respect to their growth rate, gene expression in response to TMP, and dose-response to kanamycin.

2.4.4 Microfluidics and time-lapse microscopy

For all microscopy experiments, we used a microfluidics device in which bacteria grow in microcolonies. This device allows switching between different inlets, and equilibration to the new condition happens within minutes (CellASIC ONIX, Merck Millipore). Bacteria were inoculated from frozen glycerol stocks at a dilution of 1:1000 to 1:5000 and grown to an optical density (OD_{600}) of 0.05 to 0.1. Then they were diluted 1:100 and loaded into the microfluidics chamber which was preheated to 30°C. This normally led to spatially well separated single cells in the microfluidics chamber. All experiments were performed in a heated chamber at 30°C. Data acquisition started 1-2 hours after loading. Images were taken every 10 to 20 minutes using a 100x oil objective with an EMCCD camera (Hamamatsu) on a Nikon Eclipse Ti-E with a LED light engine (Lumencor). Excitation wavelengths for YFP were CWL/FWHM 513/17 nm and emission wavelengths were dichroic LP 520 nm, CWL/BW 542/27 nm, respectively. Maturation times of *gfp* and *yfp* were below 10 minutes in our conditions, measured by fluorophore accumulation after translational inhibition with CHL in Isopropyl β-D-1-thiogalactopyranoside (IPTG)-inducible $P_{LlacO-1}$ -fluorophore strains (Lutz and Bujard, 1997), as described in (Megerle et al., 2008) (see Chapter 3). In contrast, *mCherry* had a longer maturation time (~32 min, see Chapter 3) and was therefore mostly used as a segmentation color.

2.4.5 Measurements of intracellular pH

For all measurements of intracellular pH, the plasmid pZS11-*pHluorin* was transformed into the strain of interest. For calibration, we used a medium that could be buffered to different pH values (which was not possible with the phosphate buffered M9 minimal medium). We used M63 medium (M63 salts, 1 mM $MgSO_4$, 4 g/L glucose, 1 g/L amicase) buffered to different pH values (pH 8.5 with N-Tris(hydroxymethyl)methyl-3-aminopropanesulfonic acid (TAPS), pH 7.5 with 3-(*N*-Morpholino)propanesulfonic acid (MOPS), pH 6.5 with 1,4-

Piperazinediethanesulfonic acid (PIPES), each 50 mM), and supplemented with 40 mM potassium benzoate and 100 mM methylamine hydrochloride for collapsing the intracellular pH (uncoupling) and pH adjusted with hydrochloric acid and potassium hydroxide. Due to the high proton concentrations at low pH values (pH 3 to pH 5), buffering was not necessary and calibration could be done using normal M9 medium titrated to the desired pH with HCl and 40 mM potassium benzoate for uncoupling. Calibration was performed in the microfluidics system by switching between the different inlets (with medium at different pH). After a switch, the new fluorescence ratio was reached after a few minutes and we imaged every 5 min over a period of 20-30 min. Excitation wavelengths for *pHluorin* were 390/18 nm and 438/24 nm and emission LP 495 nm, BP 520/35 nm. Excitation at 438/24 nm yielded the same results as excitation at 475/28 nm, close to the wavelength used in (Martinez et al., 2012). Calibration was done for each experiment separately due to slight day-to-day changes in microscope illumination. Typical absolute pH values in exponentially growing cells varied between experiments (pH 8 to pH 8.5), probably due to slight variations in uncoupling efficiency and decreased sensitivity of *pHluorin* at higher pH values (Figure 6A). After the addition of HCl, repeated measurements of the same cell had a much smaller variability (coefficient of variation ~3%) than measurements of different cells (coefficient of variation ~12%). The coefficient of variation for the ratio (not translated into pH) before and after the addition of HCl was 5% and 12%, respectively. Fluorescence levels right after HCl addition dropped due to the pH dependence of YFP.

2.4.6 Analysis of single-cell data

Time-lapse microscopy movies were segmented and analyzed using an adapted version of the MATLAB program 'SchnitzCells' (Young et al., 2012). Fluorescence background of the surrounding environment was subtracted as the median fluorescence over all pixels outside bacteria. Expression level was determined by dividing the total fluorescence signal from a cell by its total area. When cells lysed, their fluorescence dropped sharply. Survival time was therefore determined as the last time point at which fluorescence intensity of the segmentation color (*mCherry* or *pHluorin*) was still above the detection threshold. Photobleaching was negligible under our conditions (~1% per frame; determined by imaging a microcolony with 10 s time interval). Bootstrap standard error in Figures 4C, 5 and 6E was calculated using Matlab function *bootstrp,* with n = 1000.

2.5 Supplement

Table S1. Strains used in this chapter.

Strain	**Source**
Escherichia coli MG1655	Uri Alon lab
Escherichia coli BW25113	Keio collection (Baba et al., 2006)
MG1655 Δ*intS*::P_{gadB}-*yfp*	This work, with P_{gadB} amplified from the chromosome
MG1655 Δ*intS*::P_{wrbA}-*yfp*	This work, based on P_{wrbA}-*gfp* plasmid from (Zaslaver et al., 2006)

MG1655 Δ*intS*::P_{dps}-*yfp*	This work, based on P_{dps}-*gfp* plasmid from (Zaslaver et al., 2006)
MG1655 Δ*intS*::P_{folA}-*yfp*	This work, based on P_{folA}-*gfp* plasmid from (Zaslaver et al., 2006)
BW25113 single gene deletion strains	Keio collection (Baba et al., 2006)
BW25113 Δ*guaB* Δ*intS*::P_{gadB}-*yfp*	This work, based on strain from the KEIO collection (Baba et al., 2006) and Δ*intS*::P_{gadB}-*yfp*
BW25113 Δ*purA* Δ*intS*::P_{gadB}-*yfp*	This work, based on strain from the KEIO collection (Baba et al., 2006) and MG1655 Δ*intS*::P_{gadB}-*yfp*
MG1655 Δ*intS*::P_{gadB}-*mCherry*	This work, based on P_{gadB}-*gfp* plasmid and *mCherry* from the plasmid pZS2-123 (Cox et al., 2010)
MG1655 Δ*rpoS* Δ*intS*::P_{gadB}-*yfp*	This work, Δ*rpoS* mutation was P1 transduced from the KEIO strain (Baba et al., 2006) and Δ*intS*::P_{gadB}-*yfp* insertion from the strain MG1655 Δ*intS*::P_{gadB}-*yfp*

Table S2. Plasmids used in this chapter.

Plasmid	**Source**
Plasmid-based promoter-GFP library	Uri Alon lab (Zaslaver et al., 2006)
Plasmid pZS11-*pHluorin*	This work, based on plasmids from (Lutz and Bujard, 1997) and (Martinez et al., 2012)
Plasmid pZS41-*mCherry*	This work, based on plasmids from (Lutz and Bujard, 1997) and (Cox et al., 2010)
Plasmid pUA139 P_{gadB}-*gfp* Amp^R	This work, based on pUA139 plasmid from (Zaslaver et al., 2006) and P_{gadB} amplified from the chromosome
Plasmid pSIM19	Donald Court lab (Datta et al., 2006)
Plasmid pCP20	(Cherepanov and Wackernagel, 1995)

Table S3. List of primers used in this chapter. All oligonucleotides were ordered from Integrated DNA Technologies (IDT).

Primers for P_{gadB} amplification from the MG1655 chromosome: CGGGATCCTCCTGCAGCATGGACTGAG and CCGCTCGAGCATTTTCGTCGTCCCAGGTC
Primers for exchanging Kan^R with Amp^R on pUA139: GCGAGCTCGTAAACTTGGTCTGACAGTTAC and CGGGATCCTCAGGTGGCACTTTTCGG
Primers for *pHluorin* amplification: GGCCGAATTCATTAAAGAGGAGAAAGGTACCGCATGAGTAAAGGAGAAGAACTTTTCACTGG and GGCCAAGCTTTTATTTGTATAGTTCATCCATGCCATG
Primers for Δ*guaB* verification: CGCCGGAAAGAATAATGCCG and CAGTCGATAGTAACCCGCCC
Primers for Δ*purA* verification: GTTTTGGCGGTGGACTTGTG and TCAGCGCACGTAATCCGTAA

Primers for Δ*nuoC* verification: CACCACGGACCATTTGCAATG and CAGTCATAGCCGAATAGCCT (binding inside the kanamycin resistance)
Primers for Δ*rpoS* verification: ATTACCTGGTGCGTATGGGC and GAAATCCGTAAACCCGCTGC
Primers for chromosomal integration of library promoters into *intS* locus: GCGATACCGTAAAGCACGAG (MKan-1) and TTCTTCACCTTTGCTCATATGTATATCTCC
Primers for verifications of chromosomal integrations into *intS* locus, and integrations into single gene knockout strains: GTACTTACCCCGCACTCCAT and TGTTCAGCACACCAATAGAGG
Primers for exchanging *gfp* with *mCherry*: CCGCTCGAGAGATCCTCTAGATTTAAGAAGGAGATATACATATGGTTTCCAAGGGCGAGGAGG and GCGCCTAGGTCTAGGGCGGCGGATTTGTCCTACTC
Primers for integration of P_{gadB}-*mCherry* into the *intS* locus: MKan-1 and CTACTCAGGAGAGCGTTCACC

3. Chapter 3: Dual-reporter method enables quantification of temporal single-cell correlations between promoters during stress responses

The method described here was conceptualized and devised by Georg Rieckh, and the construction of the platform strains was done by Georg Rieckh. The construction of all reporter strains and method verification was done by KM. This method was used for the construction of chromosomal integration strains used in Chapter 2 and published in *Cell Systems* (Mitosch et al., 2017) and for the construction of all chromosomal integration strains used in Chapter 4. The alignment of the whole-genome-sequencing data to the reference genome was done by Marta Lukačišinová.

3.1 Introduction

In the third chapter, we report on the development and validation of a cloning method to integrate promoters into the *E. coli* chromosome. This method is particularly useful when studying gene expression of promoters at the single-cell level as shown in Chapter 2, and when investigating the correlation between different promoters in the same cell, which is the topic of Chapter 4. We show here that this method works efficiently and reliably, and that results obtained with single-cell microscopy using chromosomally integrated promoters are comparable to results from population-level measurements.

Individual cells are never identical, even if they have the same genetic background and sense the same environment. They differ in the copy numbers of biomolecules like DNA or proteins, which are involved in all kinds of cellular processes, such as gene expression, transport, and metabolism. These heterogeneities in the copy number of biomolecules among different cells ('noise') are mainly explained by the fact that every physical and chemical reaction is stochastic in its nature: biochemical reactions ultimately rely on random collisions between diffusing molecules. Processes like transcription, depending on molecules present at low copy numbers, are especially susceptible to heterogeneities (McAdams and Arkin, 1999). Such heterogeneities may be attenuated or further amplified by cellular mechanisms (Rao et al., 2002).

In recent years, methods have been developed to measure the level of heterogeneity ('noise') in gene expression. Tagging of promoters or proteins with a fluorescent protein, combined with single-cell methods like flow cytometry or microscopy, has proved particularly useful (Silander et al., 2012; Taniguchi et al., 2010). A method in which two proteins or promoters are tagged with different fluorescent proteins in the same cell ('dual-reporter method') is instrumental in deciphering underlying sources for such heterogeneities. In particular, a seminal experiment observing two copies of the same promoter with YFP and CFP in the same cell quantified the contributions of different cellular systems to noise in gene expression (Elowitz et al., 2002). These contributions were defined as 'intrinsic noise', i.e. the extent to which expression from two identical copies of a promoter fails to correlate; and 'extrinsic noise': the extent to which expression from these

promoters fluctuates together. Other studies using that method showed that proteins with a similar regulation tend to have similar noise levels in yeast (Stewart-Ornstein et al., 2012) and that noise propagates in gene networks (Pedraza and van Oudenaarden, 2005). When tracking dual-reporter strains over time, it has been shown that this method can be used to reveal regulatory links that are active under certain environmental conditions (Dunlop et al., 2008).

Here, we developed such a dual-reporter method with the goal to study the temporal organization of biological processes during complex stress responses. Two biological processes might happen sequentially or in parallel, and they might be coupled by the same variability source or influenced by different variability sources. This will be the theme of Chapter 4. This third chapter describes a cloning strategy to efficiently integrate promoter-fluorescent protein fusions from a promoter-GFP library (Zaslaver et al., 2006) into the *E. coli* chromosome. We also validated that our constructed strains could accurately report the dynamic response of promoter pairs to a change in the environment.

3.2 Results

3.2.1 Maturation times for YFP, CFP and GFP are of the order of minutes

In dynamic experiments using fluorescent reporters, the fluorescent protein should ideally be produced at the same rate as the protein that it reports. Fluorescent proteins, however, have to traverse an oxygen-dependent maturation step (Shaner et al., 2005), which can vary depending on the bacterial strain, the fluorescent protein and the experimental conditions (Hebisch et al., 2013). We therefore determined the maturation times for different fluorescent proteins (FPs): the YFP variant Venus, the CFP variant mCerulean, and the RFP variant mCherry (Cox et al., 2010) under our experimental conditions as described before (Megerle et al., 2008). This was done by inducing the expression of the FP from an Isopropyl β-D-1-thiogalactopyranoside (IPTG)-inducible *lac*-promoter and subsequently halting translation with high concentrations of chloramphenicol (CHL). The following increase in fluorescence must come from the maturation of FPs, as no new FPs can be translated. Expression curves of single cells are then fitted with an exponential function that asymptotically approaches a constant from below (Figure 1A, Methods).

The maturation times of YFP, GFP and CFP were 7, 6, and 7 min, respectively (Figure 1B). The maturation time of RFP was 32 min (Figure 1B). With a measurement interval of 10-20 min in our quantitative experiments, we concluded that the delay introduced by maturation of YFP, GFP and CFP was negligible; the delay introduced by RFP maturation might, however, impair our results and greater caution should be taken whenever it is necessary to use this FP for quantitative measurements.

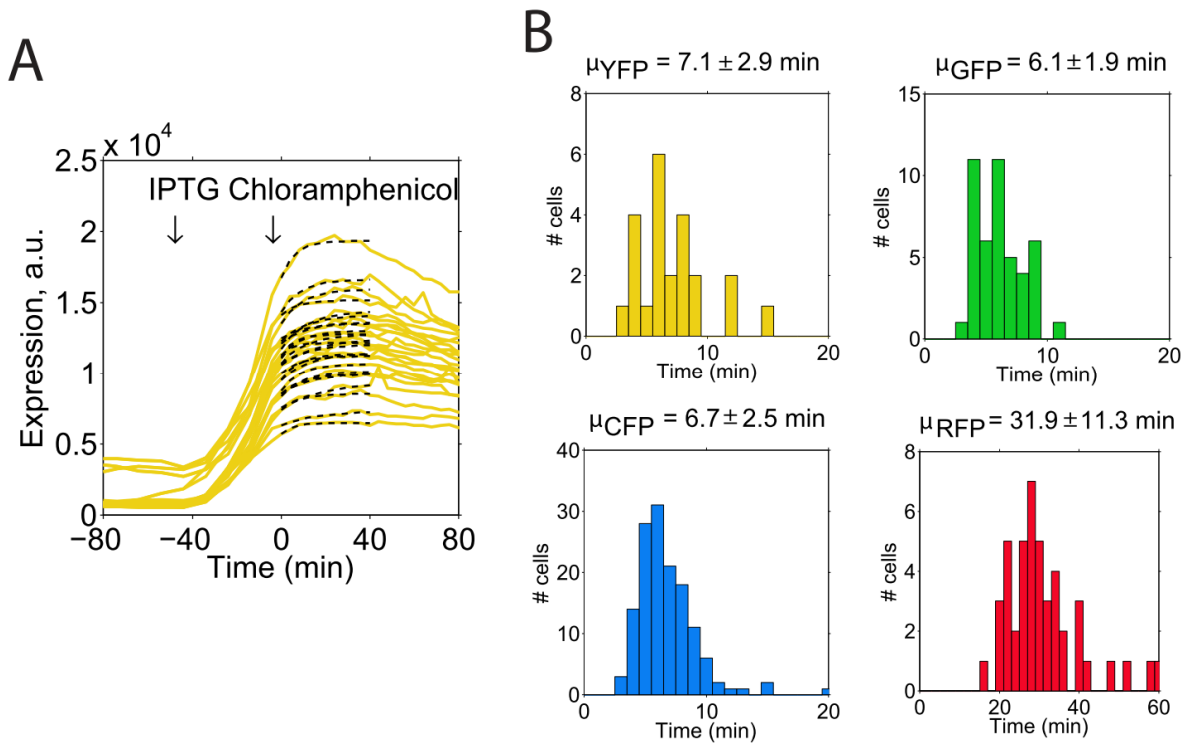

Figure 1. Maturation times of fluorescent proteins. A. YFP expression, determined as total fluorescence/cell area, from the *LlacO-1* promoter in single cells during the induction with 1 mM IPTG and subsequent translation inhibition with 0.7 mg/mL chloramphenicol (CHL, yellow solid lines). The black dashed lines are fits to the single cell time traces (Methods). After 40 min under CHL, expression tended to decrease in single cells, probably due to the physiological stress level induced by high CHL concentrations. Photobleaching was < 0.3% per frame, and therefore not corrected for. **B.** Maturation times of fluorescent proteins in individual cells; mean μ and standard deviation over the measured cells are given (YFP: # of cells n = 23; GFP: n = 45; CFP: n = 116; RFP: n = 46). Note the different time axis for RFP.

3.2.2 Cloning procedure for the integration of promoter-FP pairs into the chromosome

The goal of this method was to measure gene expression from two promoters in the same cell, while minimizing variability stemming from differences in plasmid copy numbers (Dunlop et al., 2008). We therefore devised a method to integrate two promoters from the promoter-GFP library (Zaslaver et al., 2006) into the chromosome, switching fluorescent proteins and antibiotic resistance markers. By dealing with short PCR products, this method additionally circumvents the problem that integration of constructs using recombineering gets more difficult with longer insert size (Kuhlman and Cox, 2010). The PCR reactions were further designed to avoid using long primers (~70nt), which are common for classical recombineering (Datsenko and Wanner, 2000), and which are more expensive, and harder to design and handle.

In brief, we first constructed so called 'platforms' and integrated them into the chromosome (Figure 2A). These platforms can later accept short PCR products from the library promoters

(Figure 2B). The platforms were integrated into two positions opposite and approximately equidistant from the *E. coli* chromosomal origin: *intS* (chromosomal position 2,466,545 -> 2,467,702, (Keseler et al., 2013)) and *galK* (chromosomal position 788,831 <- 789,979, (Keseler et al., 2013), Figure 2A). Expression from these positions has been probed before (Block et al., 2012; Elowitz et al., 2002) and did not influence bacterial fitness under our experimental conditions. We used the YFP variant Venus and the CFP variant Cerulean (Cox et al., 2010; Shaner et al., 2005) for the dual-reporter method due to their similar and short maturation times (Figure 1B) and their good spectral separation that allowed imaging without any corrections for bleedthrough.

To construct the platforms, the promoterless plasmid from (Zaslaver et al., 2006) was used. First, the reporter gene was changed from GFPmut2 to either YFP or a CFP (Cox et al., 2010). The second modification was to provide a selectable marker (CHL or ampicillin (AMP)) for the platform that would be knocked out upon successful integration of the final reporting construct. In a third step, the intact kanamycin (KAN) resistance cassette was replaced by a defunct fragment, starting after the start codon of its protein coding region. In an alternative platform, the KAN resistance cassette was exchanged for a defunct AMP resistance cassette. This yielded plasmids containing the desired platforms which had each a defunct antibiotic resistance cassette (against KAN and AMP, respectively), a functioning resistance cassette (against CHL and KAN, respectively) and a FP (YFP and CFP, respectively). The platforms were subsequently integrated into the two different chromosomal locations (*galK* and *intS*, Figure 2A) using lambda-red-recombineering as described in (Datsenko and Wanner, 2000). Finally, all integrated platforms were checked for mutations by sequencing PCR products from the *intS* and galK regions. Next, promoters of interest (*poi*) were integrated into these platforms. For this, the *poi* and the necessary homology regions were amplified via PCR (Figure 2B) and integrated into the platform using recombineering, removing the functioning resistance cassette and completing the defunct selectable marker upon successful integration.

This method allowed for efficient chromosomal integration of library promoters and most *poi*s could be integrated. We successfully integrated 30 promoter pairs, however, integration of one promoter together with YFP was extremely inefficient (*recA*) and we repeatedly failed to integrate another promoter (*glyA*) together with YFP, possibly due to more efficient recombination of the PCR product at different chromosomal locations. All integrands were checked by sequencing the promoter in a PCR product from the *intS* and *galK* regions. In addition, all newly constructed strains were checked for their growth rate using the dilution protocol described in Chapter 1, fluorescent protein expression and resistance to KAN and AMP, respectively. The ratio between the GFP concentration expressed from the plasmid and the YFP expression expressed from the chromosomally integrated copy, measured at the population level using our robot system, was not exactly the same for all promoters and varied between 2 and 10. As the ratio was not systematically related to the promoter strength, this promoter-specific expression ratio might be explained by the titration of transcription factors by plasmid-borne promoters (Brewster et al., 2014), or might have other yet unidentified reasons. Only strains with consistent results in the previously mentioned checks were used for data acquisition. All strains constructed with this

method and used in quantitative experiments are listed in Table S1. Overall, this method enabled the efficient integration of pairs of promoter-FP constructs into the chromosome, allowing to change antibiotic resistance and FP in one step. With suitable platforms, any pair of resistance marker and reporter protein can be used similarly.

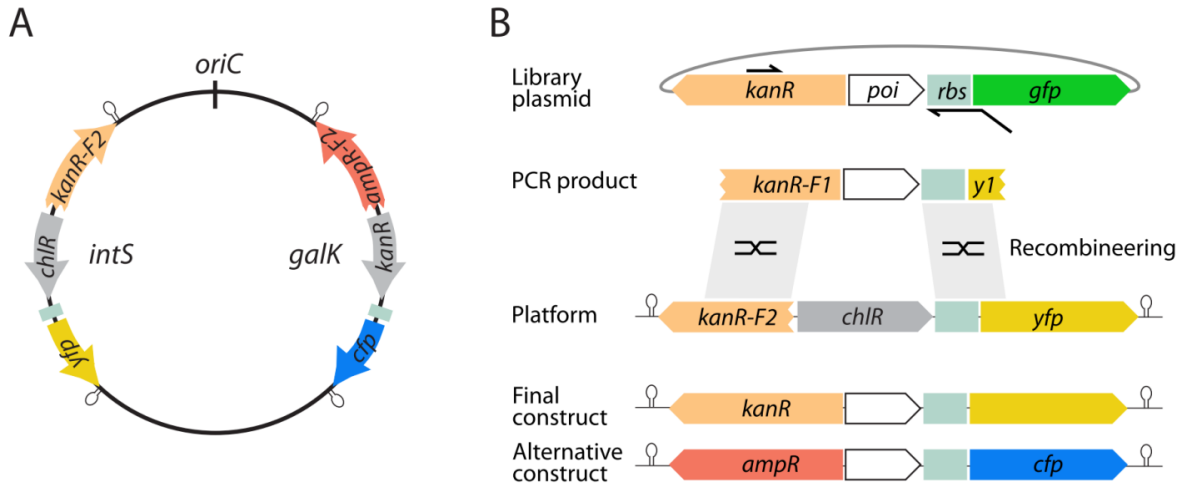

Figure 2. Procedure to integrate pairs of library promoters into the chromosome. A. Schematic showing platforms integrated into the *E. coli* chromosome. Platforms containing a fluorescent protein sequence for *yfp* (yellow) or *cfp* (blue), respectively, a ribosomal binding site (green), a resistance gene for selection on CHL (*chlR*, gray) or KAN (*kanR*, gray), respectively, and a fragment of a second resistance gene against KAN (*kanR-F2,* peach) or AMP (*ampR-F2*, red), respectively, were integrated into the chromosomal positions of *intS* or *galK*, respectively. Each platform is enclosed by terminators (loops). Proportions of the *E. coli* chromosome are not drawn to scale. **B.** Procedure for the integration of promoters from the promoter-GFP library into the platforms. A PCR product was generated from the promoter-GFP library plasmid containing the promoter of interest (*poi*). Primers are depicted as black arrows. The resulting PCR product was then integrated into the chromosome-based platforms using recombineering. This yielded chromosomally integrated *poi-yfp* or *poi-cfp* constructs with *kanR* or *ampR* resistance, respectively. Image 2B by courtesy of Georg Rieckh.

3.2.3 Whole genome sequencing of integrated strains

In order to check whether our developed integration method introduced unwanted sequence changes, we did whole genome sequencing for three strains constructed by recombineering: Δ*rpoS* Δ*intS*::P_{gadB}-*yfp*, Δ*intS*::P_{folA}-*yfp* Δ*galK*::P_{gadB}-*cfp*, and Δ*intS*::P_{ahpC}-*yfp* Δ*galK*::P_{iscR}-*cfp*, and compared them to the used wildtype MG1655, which is the parent of the promoter-GFP library (Zaslaver et al., 2006). We used the sequenced *E. coli* MG1655 (GenBank #NC_000913) as a reference. We noticed that our wildtype had several genomic changes, including a large deletion around the global transcription factor *fnr* which has been described before (see Table 1A, (Soupene et al., 2003)). We further tested three plasmid-containing strains from the promoter-GFP library (*gadB, serA, cspA*) by PCR, and all of them also harbor this large deletion (Methods). We therefore concluded that this deletion is likely present in the whole promoter-GFP library. As this deletion has been shown to impair growth mainly under anaerobic conditions and in certain sugars, we have no reason to

believe that our results are impaired by the deleted genes. In addition, comparisons for the expression of the *gadB* promoter under trimethoprim (TMP) between our MG1655 strain and the KEIO parent strain BW25113 were consistent (Chapter 2, Figure 1 and 2).

Table 1A: Mutations present in the used MG1655 strain compared to the reference sequence (GenBank #NC_000913):

Gene(s)	Mutation	Annotation
ynaJ, uspE, fnr, ogt, abgT, abgB, abgA, abgR, smrA, ydaM, ydaN, dbpA, ttcA	Δ13,756 bp	Deletion of genes
glpR	+1 bp	Insertion into already present insertion
uhpT	A -> C	Nonsynonymous mutation
gltP → / ← *yjcO*	+GC	Insertion into intergenic repeat region
rrfD–rrlD		Possible rearrangement
stfP/stfE		Inversions inside cryptic prophage

Conversely, our MG1655 strain did not contain some of the mutations present in the reference sequence (Table 1B).

Table 1B: Mutations present in the reference sequence (GenBank #NC_000913), but not in the used MG1655 strain:

Gene(s)	Mutation	Annotation
clr	+776 bp	Insertion of mobile element
insB1–insA	+776 bp	Insertion of mobile element
gatC	+2 bp	Insertion into gene
ychE/oppA	+1,199 bp	Insertion of mobile element

The whole genome sequencing of our strains revealed that even the strains that underwent up to four recombineering reactions (sequential integration of both platforms, subsequent integration of two promoters) only had minor genomic changes compared to our wildtype strain (see Table 2). In addition, none of the changes seemed to be systematic rearrangements which might be expected after inducing a recombination reaction in the cell. This is also important to check, as by introducing large regions of homology (the intergenic regions from the promoter-library), one might be worried that this provides templates for homologous recombination. However, we cannot rule out gene amplifications which were hard to detect using our sequence analysis method. We therefore concluded that our method can be used to integrate promoter-FP constructs into the chromosome without introducing major genomic changes.

Table 2. Mutations introduced during strain construction. We could not detect any mutations in the other checked strains.

Strain	Gene	Mutation	Annotation
Δ*rpoS* Δ*intS*::P_{gadB}-*yfp*	*hycG*	G→T	Synonymous point mutation

3.2.4 Expression of CFP and YFP from identical promoters on both chromosomal positions is highly correlated

To test whether expression was independent of the chromosomal position of integration (*intS* and *galK*) and the chosen FPs (YFP and CFP), we integrated several promoters ($P_{LlacO-1}$, P_{gadB}) at both chromosomal positions and also swapped color for one promoter ($P_{LlacO-1}$). As the induced expression of the *LlacO-1* promoter is relatively homogeneous among single cells (see Figure 3B, and (Block et al., 2012)), we also tested the *gadB* promoter, which has very heterogeneous expression and covers a great range of expression levels after induction by TMP (Figure 3B); this tests how well this method works for promoters with varying expression and induction levels. Two identical copies of the same promoter integrated at two different chromosomal positions should behave very similarly if the dominating variability does not come from binding and unbinding events at the promoter and transcription or translation bursts, but rather from fluctuations in transcription and translation regulators, such as transcription factors or ribosomes (Block et al., 2012; Elowitz et al., 2002). We measured maximum expression level, fold-changes and response times, which were determined as the time until half maximum expression was reached after induction with 1 mM IPTG ($P_{LlacO-1}$) and 0.5 µg/mL TMP (P_{gadB}). Maximum expression levels and response times were highly correlated in all these controls ($\rho > 0.77$ for all compared quantities; Figure 3). We therefore concluded that this method can reliably detect correlations in response times and expression levels for promoters that are not dominated by intrinsic noise.

If the fluorescent proteins and chromosomal loci behaved exactly the same, we should also find highly similar absolute response times and fold-changes in expression when averaging over many cells. We found indeed highly similar response times when comparing expression of YFP and CFP (Figure 3A), the fold-changes, however, differed (Figure 3B, insets): Expression of CFP yielded lower fold-changes than expression of YFP. We noticed that cellular autofluorescence was particularly high in the CFP channel, but completely absent in the YFP channel. Such autofluorescence can be measured in bacteria without any recombinant fluorescent protein present, and may come from intracellular flavins, NAD/H or amino acids (Mihalcescu et al., 2015; Monici, 2005). Upon subtracting CFP autofluorescence, measured in a bacterial microcolony without CFP present under the same experimental and imaging conditions, fold-changes in expression became more similar (Figure 3B, inset in 3rd panel). Caution should therefore be taken with respect to the high autofluorescence in the CFP channel: we consequently only combined promoters with CFP that had a mean expression level well above this autofluorescence. Overall, we concluded that our method can be used to reliably detect correlations in expression and response times for promoter pairs. In addition, it can reliably report on absolute response times and fold changes in expression. In the presented controls, the combined promoter pairs were under the exact same regulation. We hypothesized that it should also be possible to detect correlations between promoters that were not identical.

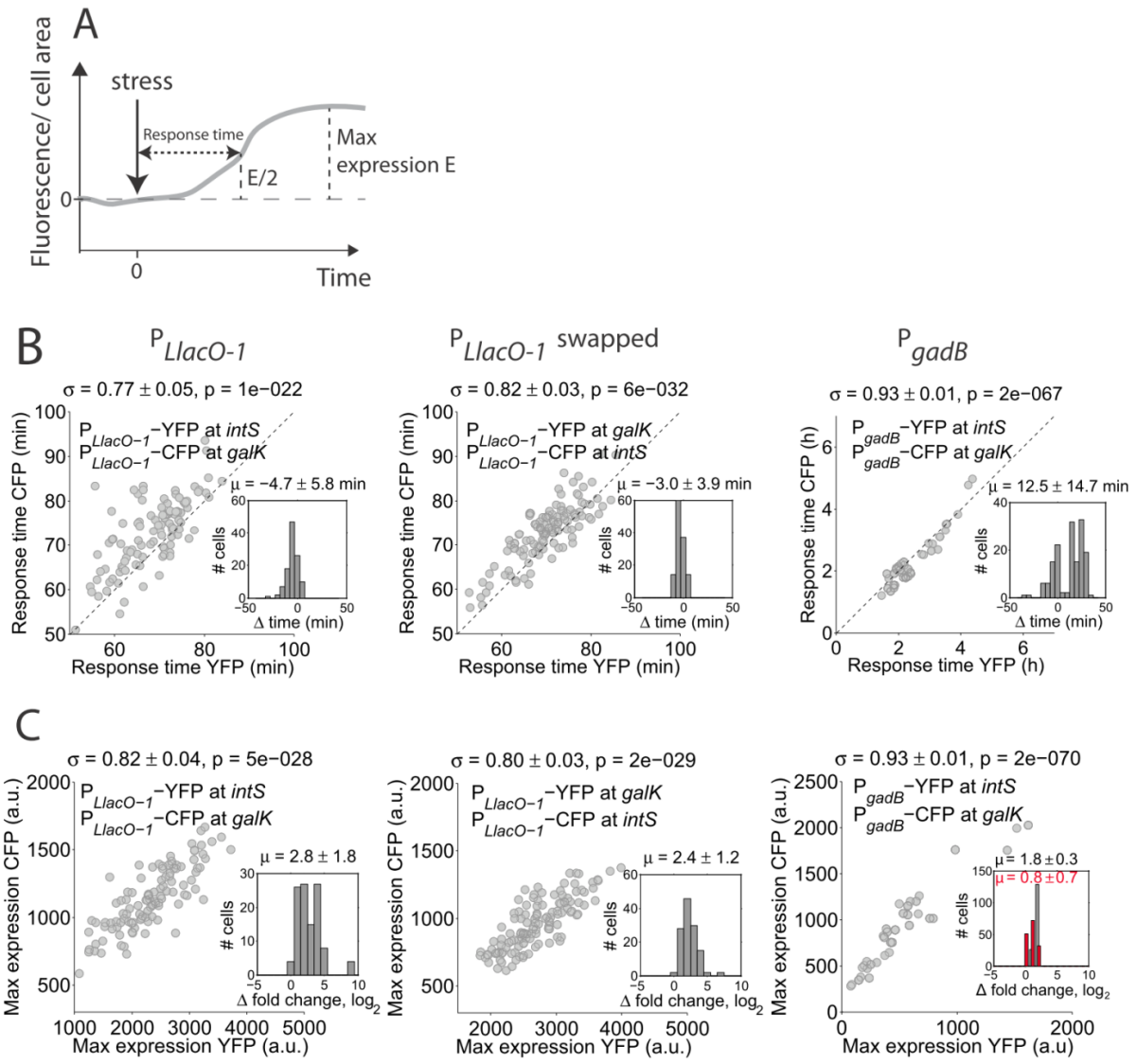

Figure 3. Response times and maximum expression from identical promoters integrated at both chromosomal positions are highly correlated as measured in single cells. A. Scheme showing the maximum expression level and the response time, determined as the time until the half maximum expression level is reached on a linear scale, after stress addition at time point 0. **B.** Correlation of response times measured with YFP and CFP reporters for $P_{LlacO-1}$–FP and P_{gadB}–FP integrated at *intS* and *galK* and with fluorophores swapped for $P_{LlacO-1}$. Every grey dot comes from a single cell. Inset: Histogram of the difference Δ in response times between YFP and CFP. Mean μ and standard deviation are given. **C.** Correlation of maximum expression level measured with YFP and CFP reporters for $P_{LlacO-1}$–FP and P_{gadB}–FP integrated at *intS* and *galK* and with fluorophores swapped for $P_{LlacO-1}$. Inset: Difference Δ in $\log_2$ fold-change between YFP and CFP without autofluorescence subtraction. Red bars in right panel depict the same, but with CFP autofluorescence subtraction. Mean μ and standard deviation are given. Number of analyzed cells n = 111 from one microcolony ($P_{LlacO-1}$), n = 125 from one microcolony ($P_{LlacO-1}$ swapped) and n = 38 from two microcolonies (P_{gadB}). Pearson correlation coefficients ρ, errors from bootstrapping (Methods), and p-values are given for **B** and **C**.

3.2.5 Comparison between population-level data and single-cell data

In order to further validate our single-cell method and detect potential drawbacks of both methods used to measure dynamic gene expression changes, we directly compared the results from our population-level method and our single-cell method. The population-level measurements were done with promoter-GFP constructs on a plasmid-based system using a plate-reader; the single-cell measurements were done with chromosomally integrated promoter-YFP and -CFP strains using time-lapse fluorescence microscopy and microfluidics. As measures of comparison we used fold-changes and the response time (determined as the time until half maximum expression on a linear scale) of individual promoters in response to trimethoprim (TMP), tetracycline (TET) and nitrofurantoin (NIT). To make the single-cell data comparable to the population data, where expression is measured as fluorescence per absorbance, which corresponds to cell mass, we determined the total fluorescence of a microcolony at each time point and divided it by the total cell area at that time point. From this quantity, we determined response times and fold-changes in expression.

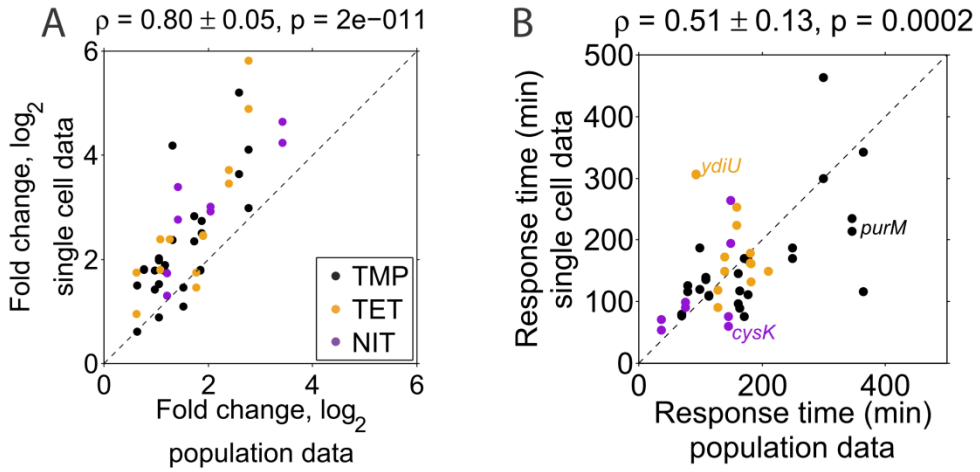

Figure 4. Measures of gene expression dynamics determined from population data and single cell data are well correlated. A. Fold changes from cultures stressed with 0.5 µg/mL TMP (blue), 0.7 µg/mL TET (red), and 4 µg/mL NIT (green), compared between the population-level data and the single-cell data. Every dot is from a microcolony and two microcolonies per promoter have been analyzed. All promoters analyzed for this plot are listed in Table S1. Pearson correlation coefficient is 0.80, error is from bootstrapping (Methods) and the p value is given. **B.** Same as A. but for response times. Pearson correlation coefficient is 0.51.

Fold-changes determined for the population data and the single-cell data determined from individual microcolonies were highly correlated (ρ = 0.80, Figure 4A). However, the single-cell data showed systematically higher fold-changes especially for promoters with high expression changes. We attributed these systematic differences to the autofluorescence properties of the fluorophores: the GFP channel, as well as the CFP channel, has strong autofluorescence (Mihalcescu et al., 2015) which must be subtracted. In contrast, the YFP channel has no detectable autofluorescence and has therefore a higher sensitivity in

reporting fold changes. Response times determined for the population data and the single-cell data were consistent for many promoters, and correlated well (ρ = 0.51, Figure 4B). Some promoters, however, showed greater discrepancies between the population data and the single-cell data. Reasons for these differences could be the fluctuations due to dilutions observed in our population-level protocol (Chapter 1, Figure 3B), or the higher number of binding sites in plasmid-based constructs and a subsequent transcription factor titration effect (Brewster et al., 2014). In addition, discrepancies might come from different cell physiology in the two culturing conditions, i.e. trapped single cells constantly surrounded by fresh medium in the microfluidics device versus batch-culture growth, which has been described for planktonic versus adhered bacteria (Povolotsky and Hengge, 2012).

3.3 Discussion

Here, we devised a cloning method for the efficient integration of pairs of promoters, combined with the fast maturing fluorescent proteins YFP and CFP, into the *E. coli* chromosome and validated its applicability for the detection of correlations in expression and response times between pairs of promoters. The method allowed integration of promoters from a promoter-GFP library (Zaslaver et al., 2006) at two chromosomal loci, roughly equidistant from the origin of replication, with simultaneous switching of resistance and fluorescent proteins. We confirmed that the protocol chosen for the integration of promoters, recombineering, did not introduce chromosomal rearrangements. We noticed that autofluorescence in the CFP channel limits this method in that only promoters with expression above autofluorescence can be analyzed quantitatively; fold-changes determined with CFP are also less reliable compared to YFP. In general, strains constructed with this method and measured using microfluidics and microscopy showed good agreement with population-measurements using plasmid-based promoter-GFP constructs.

As this method is able to report response time and expression correlations between identical promoter pairs, it should also be able to detect correlations between promoter pairs that are not identical. In principle, any kind of promoters can be combined, which makes this method a powerful tool to study the relations between and within biological processes.

3.4 Methods

3.4.1 Culture conditions

Culture conditions were the same as described in Chapters 1 and 2. We used M9 minimal medium for all experiments.

3.4.2 Strain construction and verification

For the construction of IPTG-inducible fluorescent reporter plasmids (pZS12-YFP/ -CFP/ -RFP), we cloned the fluorescent proteins from the plasmid pZS2-123 (Cox et al., 2010) behind the *LlacO-1* promoter (Lutz and Bujard, 1997) on a pSC101 origin. For the maturation time measurements of GFP, we used the P_{lacZ} promoter from the promoter-GFP library (Zaslaver et al., 2006).

To construct the platforms, the origin of replication of the promoterless plasmid from (Zaslaver et al., 2006), was first changed to a pZA origin (Lutz and Bujard, 1997). The exchange of GFPmut2 to either YFP or a CFP (Cox et al., 2010) was achieved by using the primers cYFP-1 and cYFP-2 for YFP, and cCFP-1 and cCFP-2 for CFP (see Table 3 for primer sequences) and the restriction enzymes HindIII and NdeI. In the plasmid with CFP, the KAN resistance cassette was exchanged by an AMP resistance cassette using restriction and ligation. This resulted in the plasmids p-KAN-YFP and p-AMP-CFP. To add a selectable marker for the platform that would be knocked out upon successful integration of the final reporting construct, the CHL resistance cassette from a plasmid library (Lutz and Bujard, 1997) was put between the XhoI and BamHI restriction sites with primers CmR-1 and CmR-2 and cloned into the plasmid p-KAN-YFP, resulting in the plasmid p-KAN-CHL-YFP. Likewise, a KAN resistance cassette was cloned between the XhoI and BamHI restriction sites with primers KanR-1 and KanR-2, resulting in the plasmid p-AMP-KAN-CFP.

To replace the intact KAN resistance cassette in p-KAN-CHL-YFP by a defunct fragment, starting after the start codon of its protein coding region, whole-plasmid PCR was used with primers CmR-1 and KnF, which also contains an XhoI restriction site. Likewise, to replace the intact AMP resistance in p-AMP-KAN-CFP with a defunct fragment, the same procedure was applied using the primers AmpF and CmEnd. The platforms were integrated into two different chromosomal locations (*galK* and *intS*, Figure 2A) using lambda-red-recombineering as described in (Datsenko and Wanner, 2000), with the recombineering plasmid pSIM6 (Datta et al., 2006) and primers intS-1 and intS-2, or galK-1 and galK-2. Finally, all integrated platforms were checked for mutations by sequencing the PCR product obtained by using primers intS-up, intS-dn, galK-up, galK-dn on the chromosomal DNA.

For the integration of promoters of interest into the platforms, promoters and the necessary homology regions were amplified via PCR and the primers MKan-1 and mYFP for the platform with YFP, and the primers AmpF2 and mCFP for the platform with CFP. Integration

was done using recombineering with the recombineering plasmid pSIM19 (Datta et al., 2006) and PCR-checked by sequencing the PCR product obtained by using primers intS-up, intS-dn, galK-up, galK-dn on the chromosomal DNA with the sequencing primers mKanProm_PromSeq and mAmpR_PromSeq (Table 3).

For the construction of dual-reporter strains, first a promoter of interest was integrated at the *galK* locus, combining with *cfp.* Promoters integrated at this location needed to have high expression of fluorescent protein, as the CFP autofluorescence would otherwise mask expression changes. Subsequently, the second promoter of interest was integrated at the *intS* locus, combining with *yfp.* Autofluorescence in the YFP channel was negligible. Therefore, also promoters with lower expression could be integrated at this locus. The fluorescent protein Venus is known to be particularly susceptible to photobleaching (Shaner et al., 2005). In our experiments, we tried to keep photobleaching to a minimum by keeping light intensities and exposure times low. However, photobleaching was not completely unavoidable. The highest detected bleaching for all our conditions was 3% per frame for YFP and 0.5% per frame for CFP, determined by imaging a microcolony with 10s time interval. In an experiment with 40 frames per imaging position and 3% bleaching per frame, the initially present fluorescence would drop to 30% of its value by the end of the experiment. As under all our conditions, expression from promoters in the YFP channel was strongly increasing over time, we considered this bleaching to have a rather minor effect, and did not correct for it.

Table 3. Primers used for the construction of chromosomally integrated promoter-FP strains. Underlined bases are restriction sites.

Primers used to exchange GFPmut2 for YFP: cYFP-1: AGAAAGGATCCGAGAAGAACTTTTCACTGGAG and cYFP-2: ATGACCTCGAGCTGAATGAACTGCAGGAC
Primers used to exchange GFPmut2 for CFP: cCFP-1: GTCCGGGATCCTCTAGATTTAAG and cCFP-2: CTCGAGGGGATCCTCTAGATT
Primers used to integrate a CHL resistance into the plasmid p-KAN-YFP: CmR-1: AGATACTCGAGGTGAAGACGAAAGGG and CmR-2: AGAATCTCGAGTAGACGTCGATATCTGGCG
Primers used to integrate a KAN resistance into the plasmid p-AMP-CFP: KanR-1: AGAATCTCGAGTCGGAATTGCCAGCTGGGGC and KanR-2: ATGACAGGATCCTCGAACCCCAGAGTCCCGCTCAGAAG
Primers used for whole-plasmid PCR to make a defunct KAN resistance: KnF: AGAATCTCGAGGATATCTGGCGAAAATGAGAC and CmR-1
Primers used for whole-plasmid PCR to make defunct AMP resistance: AmpF: ATGACCTCGAGAGTATTCAACATTTCCGTGT CmEnd: CTAGTGCTTGGATTCTCACC
Primers used to integrate platform into *intS* locus: intS-1: CCGTAGATTTACAGTTCGTCATGGTTCGCTTCAGATCGTTGACAGCCGCAGAGTCAGTGAGCGAGGAAGC

and intS-2: ATAGTTGTTAAGGTCGCTCACTCCACCTTCTCATCAAGCCAGTCCGCCCATGAAGTCAGCCCCATACGAT
Primers used to integrate platform into *galK* locus: galK-1: GTTTGCGCGCAGTCAGCGATATCCATTTTCGCGAATCCGGAGTGTAAGAAGAGTCAGTGAGCGAGGAAG C and galK-2: ACCATCGGGTGCCAGTGCGGGAGTTTCGTTCAGCACTGTCCTGCTCCTTGTGAAGTCAGCCCCATACGAT
Check primers for *intS* locus: intS-up: GTACTTACCCCGCACTCCAT intS_dn: TGTTCAGCACACCAATAGAGG
Check primers for *galK* locus: galK-up: GTTAATTATCATTTTGCACCGCGTC and galK-dn: GGAAAGTAAAGTCGCACCCC
Primers for the amplification of *poi* from library plasmids for integration combined with YFP: MKan-1: GCGATACCGTAAAGCACGAG and mYFP: TTCTTCACCTTTGCTCATATGTATATCTCC
Primers for the amplification of *poi* from library plasmids for integration combined with CFP: AmpF2: GACCAGGATAGGAACCACACCAGTAAACAGCTCCTCGCCCTTGCTCATATGTATATCTCCTTCTTAAATCTA GAG and mCFP: CAAAATGCCGCAAAAAAGGGAATAAGGGCGACACGGAAATGTTGAATACTCATACTCTTCCTTTTTCAATA TTAT TGAAGCATTTATCAGGGTTATTGTCTCATGAGCGGATACATATTTGAAGACGTCTAAGAAACCATTATTAT CATG
Primers to verify promoters integrated into platforms: mKanProm_PromSeq: CAACCTTACCAGAGGGCG mAmpR_PromSeq: TTGTCTCATGAGCGGATACA

The deletion around *fnr* in *E- coli* MG1655 strain was checked using the primers CGCAATCAGGGACGTACAGA and TCGCATCATGGTTTGCCTCT, which yielded a 2400 bp long product if the region was deleted.

3.4.3 Determination of maturation times

For determining the maturation time in single cells, we grew bacteria in our microfluidics device and induced the expression of plasmid-based FPs under the $P_{LlacO-1}$ promoter (Lutz and Bujard, 1997) or the or the P_{lacZ} promoter for GFP (Zaslaver et al., 2006) with 1 mM IPTG. After 40min, we inhibited protein production and cell growth by flushing in 0.7 mg/mL CHL. Similarly high concentrations have been used before (Megerle et al., 2008), and we applied such high concentrations (~140 x MIC), as lower concentrations did not result in an instantaneous halt in growth which would impair the precise determination of maturation times. Applying such a high concentration did not result in any visible cell death, but lead to a decrease in fluorescence ~40 min after the addition of the translation inhibitor (Figure 1A).

Applying this protocol, any increase in fluorescence signal after this sudden halt in protein production must consequently stem from initially immature protein that matured during the assay. The maturation time can be determined by fitting a mathematical model to the fluorescent protein concentration curves. The set of differential equations describing change in cell mass (S), in the concentration of total immature protein (I) and mature protein (M) have been described before (Gordon et al., 2007) and are as follows:

$$\frac{dS}{dt} = g \cdot S$$
$$\frac{dI}{dt} = k \cdot S - m \cdot I$$
$$\frac{dM}{dt} = m \cdot I$$

where g is the growth rate, k the protein production rate, and m the maturation rate.
When cell growth and protein production halt, g = 0 and k = 0, which results in:

$$\frac{dI}{dt} = -m \cdot I$$

$$\frac{dM}{dt} = m \cdot I$$

The equations are solved as:

$$I(t) = I_0 \cdot e^{-mt}$$

$$M(t) = M_0 + I_0(1 - e^{-mt})$$

The equation for M(t), the concentration of matured protein was fitted to the trajectories of fluorescence concentration in single cells starting at the time point of CHL addition until curves did not increase in expression any longer, using the MATLAB function 'fit'. Decrease at later time points may be due to damage of the bacterial cells by the high concentrations of CHL used. Only curves with a goodness of fit > 0.8 were included into the analysis.

3.4.4 Whole genome sequencing

Genomic DNA was purified from overnight cultures using the Promega Wizard Genomic DNA Purification Kit (catalogue number A1120). Library preparation, multiplexing, and sequencing were performed at LGC Genomics. The samples were sequenced on an Illumina NextSeq500 (paired-end sequencing, 150 bp read length, mean coverage: 75-115-fold). Sequencing data were analyzed using Breseq (Barrick et al., 2014) (Version 0.25) and Geneious (Kearse et al., 2012) (Version 8, http://www.geneious.com). Reads were aligned to the deposited MG1655 reference (NC_000913) using Bowtie2. The mutations identified by Breseq were manually inspected for false positives; regions with ambiguous evidence were

further examined in Geneious and IGV (Robinson et al., 2011; Thorvaldsdóttir et al., 2013); all validated mutations are listed in Tables 1A, 1B and 2.

3.4.5 Analysis of microscopy data

Microscopy data were analyzed semi-automatically using an adapted version of the MATLAB program 'SchnitzCells' (Young et al., 2012) as described in Chapter 2. Adaptations to the software included the introduction of a fluorescence intensity threshold. Only pixels above this threshold were taken for further image processing, which greatly improved the segmentation procedure. This threshold was adjusted manually for each movie according to the brightness of the segmentation images, making sure that all cells present in a frame were included.

For all data included in this chapter, the plasmid pZS41-*mCherry* was used for segmentation, which was constructed as described in Chapter 2. The autofluorescence background of a certain fluorescent color was subtracted as the mean expression of a microcolony from bacteria without that fluorescent protein present. In cases where the autofluorescence background had an upward trend during our dynamic experiments (which was the case for CFP under NIT), the autofluorescence background at each time point was subtracted as the mean expression of cells without that fluorescent protein present at that time point.

Every cell appearing in the last time frame was included in the analysis and counted as a single trajectory. In cases where microcolony size had an impact on gene expression (as for promoters from the Gad system and RpoS-regulated promoters), data were cropped before this trend became apparent. Response times were determined as the time until half maximum expression was reached on a linear scale. Fold-changes were determined as the maximum value of the $\log_2$ data shifted to 0 for t = 0, max expression was determined as the maximum value of non-normalized, but background and autofluorescence subtracted data. Bootstrap standard error in Figures 3 and 4 was calculated using the Matlab function *bootstrp,* with n = 1000.

3.5 Supplement

Table S1. Dual-reporter strains constructed and used in this work and measured under the indicated condition. Promoters labeled with * were analyzed for Figure 4.

Promoter-CFP at *galK* locus	**Promoter-YFP at *intS* locus**	**Measured under**
gadB	*gadA**	TMP
gadB	*recA**	TMP
gadB	*fpr**	TMP
gadB	*gadW**	TMP
gadB	*folA**	TMP
gadB	*glmU**	TMP
gadB	*guaB**	TMP

gadB	*ldhA**	TMP
gadB	*osmC**	TMP
gadB	*purT**	TMP
gadB	*sdhC**	TMP
gadB	*purM**	TMP
gadB	*wrbA**	TMP
gadB	*dps**	TMP
gadB	*gadB**	TMP
recA	*fpr**	NIT
recA	*cspA**	NIT
*recA**	*ybjC**	NIT
recA	*cysK**	NIT
*cspA**	*dnaK**	TET
cspA	*ahpC**	TET
cspA	*rpsA**	TET
cspA	*rpmE**	TET
iscR	*nrdH**	TET
*iscR**	*ahpC**	TET
iscR	*ydiU**	TET
iscR	*rpsA**	TET
LlacO-1	*LlacO-1*	IPTG
LlacO-1-YFP at *galK* locus	*LlacO-1*-CFP at *intS* locus	IPTG

4. Chapter 4: Temporal organization of gene expression in single cells during complex stress responses

This work uses the dual-reporter method which was conceptualized and devised by Georg Rieckh and which is described in detail in Chapter 3.

4.1 Introduction

In this fourth Chapter, we investigate the temporal organization of gene expression in single cells when stressed with low concentrations of antibiotics. We selected genes based on the population data presented in Chapter 1, and use the dual-reporter method explained in Chapter 3. First, we describe how the variability in the timing of gene expression changes with the response time for individual promoters, and in different stress conditions. Then, we ask if pairs of promoters are expressed with a clear temporal order in single cells and which promoters and biological processes are temporally coupled. This provides new insight into the temporal dependencies of biological processes, and the different sources of variability that affect the expression variability of various genes during complex stress responses.

Environmental changes often entail a longsome adaptation process with substantial changes in bacterial gene expression. These gene expression changes may appear coordinated in time when observed at the population level: certain biological processes, i.e. groups of genes with similar regulation or related function, are expressed at similar time-points and different processes appear to be expressed in a clear temporal order. A group of genes with similar regulation or related function expressed at a similar time-point will be termed a 'response program' here. For example, upon exposure to nutrients, *Bacillus subtilis* spores are revived in a highly coordinated manner: proteins needed for gene expression are activated very early, followed by biosynthesis and metabolic proteins and subsequently, cell division proteins are produced (Sinai et al., 2015). Further, the switch from glycolytic to gluconeogenic carbon sources in yeast entails the temporally coordinated expression of certain transcription factors (Zampar et al., 2013). In addition, clear temporal order has also been suggested based on population-level data for genes within specific pathways like the DNA-damage response (SOS response) (Ronen, 2002) or an amino acid biosynthesis pathway (Zaslaver et al., 2004).

A temporal organization might be 'hard-wired' in the gene regulatory network, meaning that just an initial trigger is needed to start the expression of a cascade of regulatory events. This may be the case for environmental conditions which the cells have experienced before in their evolutionary history and to which they have found a solution that provides a fitness benefit. Alternatively, a clear temporal order could be the consequence of an inevitable sequence of biochemical events. An example for this is the mechanism proposed in Chapter 2: the depletion of adenine nucleotides which leads to an intracellular pH drop and the subsequent activation of acid stress promoters under TMP. In Chapter 1, we have shown that promoters belonging to the same stress response programs tend to be expressed at

similar time-points after the exposure to antibiotics (Chapter 1, Figure 5), and these time-points vary strongly between response programs. In this example, and also the aforementioned ones, it is not clear whether this temporal organization is hard-wired, whether it is the reaction to an inevitable sequence of biochemical events, or whether it contains aspects of both scenarios.

At the population level, where measurements are averaged over many single cells, each biological process appears to be activated at a clearly defined time-point. However, at the single cell level, the activation of these processes may be homogeneous or heterogeneous from cell to cell. For example, bacteriocin expression has been shown to be highly variable in time in response to low concentrations of the DNA-damaging antibiotic mitomycin C (Mader et al., 2015). Similarly, bacteria show heterogeneous timing in the expression of an arabinose promoter in response to low extracellular concentrations of the inducer arabinose (Megerle et al., 2008). When comparing the expression of two genes, such heterogeneous timing may further have the consequence that the temporal order of those two genes in every single cell is not the same as the averaged temporal order determined at the population level. This issue has hardly been addressed before and can provide important information: First, it is highly important for the interpretation of population-level data: the notion that a response program measured at the population-level is adaptive or even optimal should be reflected in a clear temporal order in individual cells (Zaslaver et al., 2004). Second, measuring the timing of several promoters in the same cell can suggest causal links and chains of events that can be tested in targeted follow-up experiments and thus elucidate the molecular mechanisms of complex stress responses in unprecedented detail.

Here, we ask whether response programs are expressed in a clear temporal order, i.e. 'sequentially', or if they run 'in parallel' (Figure 1A-C; (Yurkovsky and Nachman, 2013)). In a strictly sequential activation of the programs X and Y, a gene from program X with promoter P_X is expressed before a gene from program Y with promoter P_Y in every single cell (Figure 1C). If programs run in parallel, there can be cells in a population that first activate P_X, and others which first activate P_Y (Figure 1C). A clear temporal order may hint at biological processes that are dependent on each other, point at processes that evolved for a specific purpose, and can reveal the sequence of molecular events happening during the adaptation to a new environment. We further ask which response programs are temporally independent or coupled (Figure 1D). Here, coupling means that cells which activate program X early, will also activate program Y early; cells that activate program X late will also activate program Y late (Figure 1D). Such coupled programs might be activated in parallel, or sequentially (Figure 1E). Coupling can hint at regulatory links between response programs (Dunlop et al., 2008). However, also genes with no links at the gene regulatory level can be coupled if their activation is either determined by the same specific biochemical event, like an intracellular pH drop, or if global factors acting on many genes, such as the cellular growth rate, determine their variability.

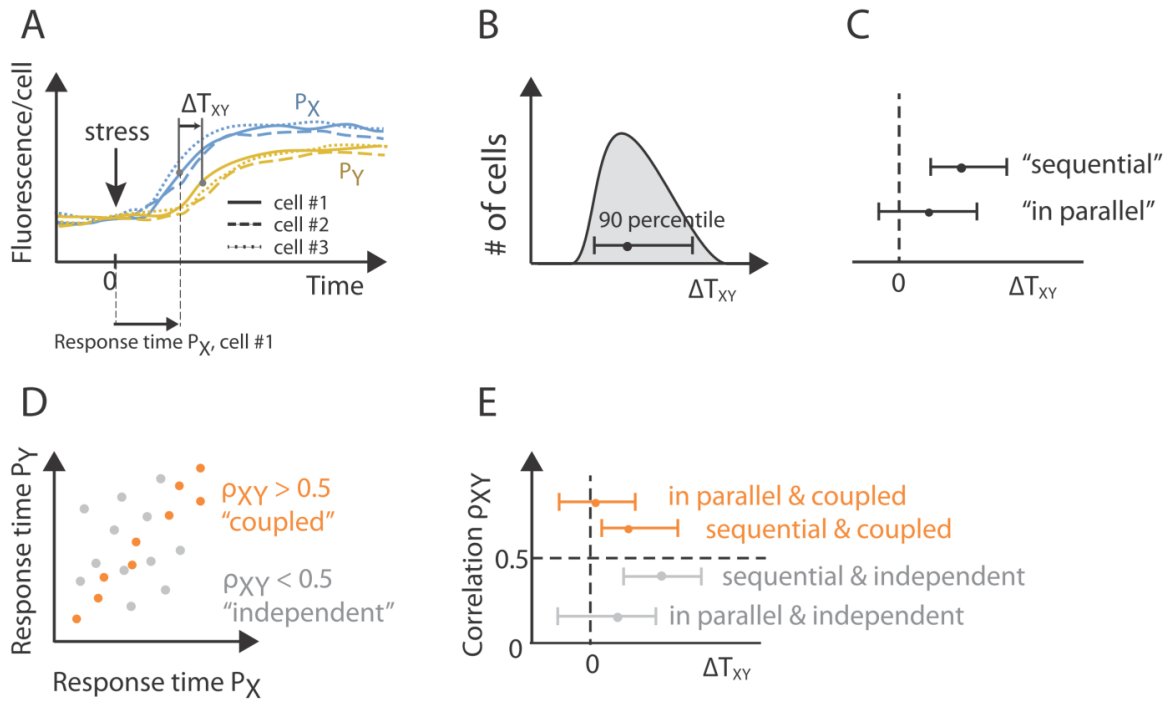

Figure 1. How are response programs temporally coordinated in single cells? A. Schematic depicting the expression of two promoters P_X (blue lines) and P_Y (yellow lines) in three individual cells (solid, dashed and dotted lines). The response time for every single cell is defined as the time until half maximum expression is reached. The interval ΔT_{XY} is defined as the difference between the response time of P_Y and the response time of P_X. **B.** The distribution of intervals ΔT_{XY} is depicted as its mean and its 90 percentile (containing 90% of the data, whereas 5% are below and 5% above the depicted line). These measures capture skewed distributions, but do not capture potentially bimodal distributions. **C.** Definition of sequential and parallel programs. If the range of ΔT_{XY} does not cross 0, meaning that in all single cells, the programs X happens before Y, programs are sequential. In contrast, if the range of ΔT_{XY} crosses 0, meaning that in some cells Y happens before program X and in other cells X happens before program Y, programs run in parallel. **D.** Definition of coupled and independent programs. If the response times of P_X and P_Y correlate strongly, programs are said to be coupled. In contrast, if they do not correlate, they are independent. **E.** Plot combining the two measures described in **C** and **D.** Processes can be 1) in parallel and coupled, 2) sequential and coupled, 3) sequential and independent, and 4) in parallel and independent.

We tackled these questions by using the transcriptional dual-reporter strains from Chapter 3. These strains have pairs of promoters integrated into the chromosome in combination with YFP or CFP. We subjected selected dual-promoter strains, which are strongly up-regulated under the respective condition (based on population-level data from Chapter 1), to sublethal concentrations of diverse antibiotics in a microfluidics device and observed gene expression changes using time-lapse microscopy. We found that a promoter from the SOS response was highly heterogeneous in timing under one condition, trimethoprim (TMP) stress, but very homogeneous under another (nitrofurantoin (NIT) stress). The same SOS promoter was activated with a clear temporal order in combination with the oxidative stress response: in every single cell, the oxidative stress response was activated 1-2 h before the SOS response under NIT stress. Conversely, the acid stress response under TMP ran

independently and in parallel with most other programs in the cells, including the highly heterogeneous SOS response. Overall, this work provides insight into the temporal organization of gene expression changes during complex stress responses, suggests chains of biochemical events that trigger these responses, and highlights the effect of different sources of variability on the observed variability in timing.

4.2 Results

4.2.1 Timing gets more heterogeneous at later response times

To quantify the timing variability, we used microfluidics and time-lapse microscopy and determined the response times for 25 promoters in three complex stress conditions: TMP, tetracycline (TET), and NIT. These antibiotic stress conditions result in massive changes in global gene expression (Chapter 1). We selected promoters with a > 2-fold upregulation in the respective condition and a relatively strong expression in order to achieve high signal-to-noise ratios when using microscopy with chromosomally integrated promoters (Chapter 3). The response time for each single cell was determined as the time until its half maximum expression was reached on a linear scale (Figure 2A). We confirmed that this response time measure was not solely determined by the maximum expression levels: the response times for individual cells were in general not strongly correlated with the maximum expression levels for single cells across all conditions (Figure 2B).

The absolute error of the response time, i.e. its standard deviation, increased with the response time, and correlated strongly with it ($\rho = 0.76$, $p = 8 \times 10^{-6}$); later responding promoters were thus more variable in their timing (Figure 2C), which is consistent with previous reports (Amir et al., 2007; Mader et al., 2015; Megerle et al., 2008). We determined a lower limit to this timing variability from these data, which likely reflects a fundamental limit on how homogeneous in time late-responding promoters can be. This limit of timing variability has a slope of 0.2, meaning that responses that happen for example after 5h inevitably have an uncertainty of ± 1h. The observation that promoters with later response times have higher variability is expected due to the higher mean time intervals between stress addition and response, and may be explained by the fact that later responding promoters accumulate variability in the timing of transcription factors or metabolic reactions from preceding processes (Pedraza and van Oudenaarden, 2005).

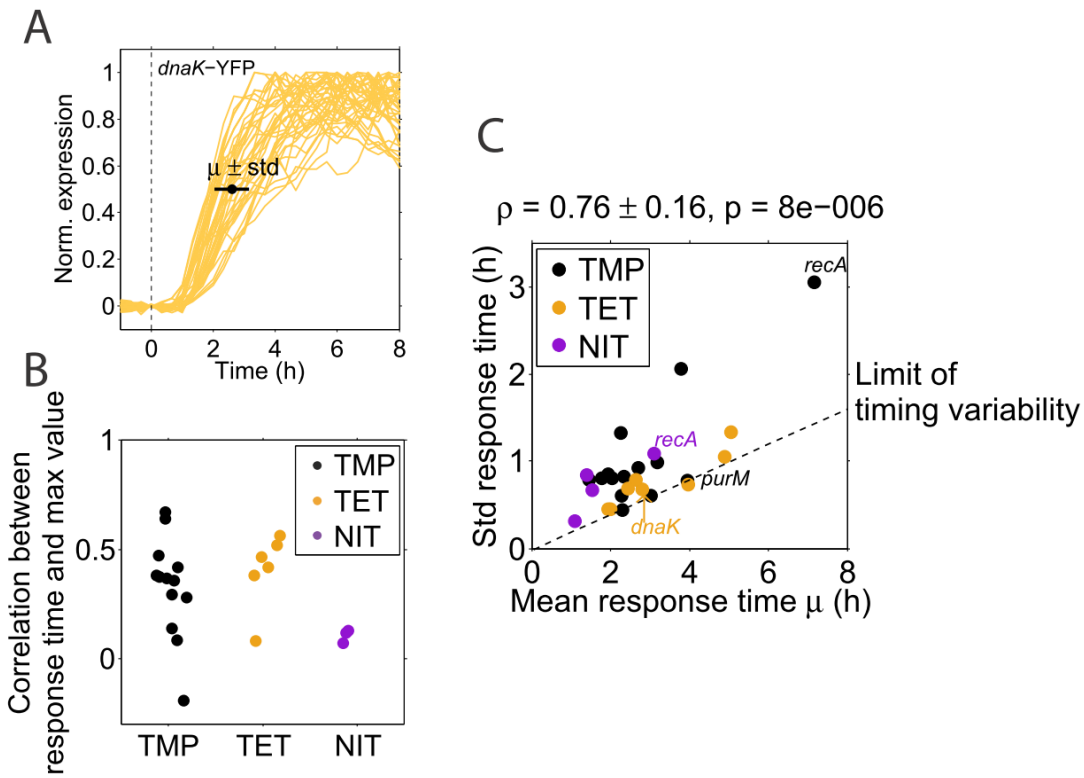

Figure 2. The absolute error of the response times increases with the mean response time. A. The mean μ and the standard deviation 'std' of the response time were determined on normalized single cell data as shown here for the *dnaK* promoter under TET stress. **B.** Pearson correlation coefficient between the maximum expression levels and the response times among single cells across different promoters and different stress conditions (TMP, TET, NIT). The number of analyzed cells was > 17 for each condition, and the correlations were obtained by sampling from the descendants of the single cells present at the time when the stress was added (Methods). **C.** The standard deviation of the response time of different promoters is plotted over the mean of the response time for TMP (blue dots), TET (red dots), and NIT (green dots). Single dots are pooled data from at least two microcolonies for each promoter and condition. The dashed line is a guide to the eye and is a linear fit through the three lowest blue dots. It corresponds to a lower limit to timing variability.

4.2.2 The SOS response can have homogeneous or highly heterogeneous timing

Whereas single cells stressed with TET were close to the lower variability limit for all tested promoters, TMP and NIT activated promoters with high and low heterogeneity in timing (Figure 2C). For example, a promoter with low heterogeneity in response to TMP was *purM* (Figure 2C), an enzyme in *de novo* purine biosynthesis. In contrast, a promoter from the DNA-damage response (SOS response) in *E. coli, recA*, was highly heterogeneous after TMP stress: some cells showed a clear increase in expression already after 3 hours; others only as late as ~9 hours (Figure 3A). This observation suggests that the response is triggered by events involving molecules that are present in low numbers. For example, one of the regulators of *recA* might be present in low copy numbers. This is indeed the case for the response to a certain type of DNA damage, alkylation: as the sensing molecule Ada is on

average present in less than one copy per cell (Uphoff et al., 2016), only cells that have Ada molecules at the time point of damage can react; others can induce the damage response not before the first expression event of Ada occurs, which can delay the response for generations (Uphoff et al., 2016). If a similar situation applies for the SOS response, the activation of *recA* should always be variable in timing, no matter by which stress it is induced.

To address this question, we analyzed the single cell data under another SOS-inducing condition, NIT stress (Figure 3A): here, the timing variability in *recA* expression was much lower, excluding the possibility that the regulators of the SOS response introduce variability by low copy numbers. The prodrug NIT is known to be metabolized into nitro anion radicals which can damage the DNA at any location (Sengupta et al., 1990). Such widespread damage will be quite homogeneous among different cells. This can explain our observation that the SOS response is strong and relatively homogeneous in time and expression level in response to NIT (Figure 3A). With TMP, in contrast, DNA damage is induced by the depletion of thymine bases, and the subsequent stalling of replication forks (Lewin and Amyes, 1991). A reduced growth rate, as the one induced by TMP due to the depletion of purine bases (Kwon et al., 2010), may decrease the number of replication forks per cell (Cooper and Helmstetter, 1968). As the number of replication forks may consequently also be highly variable from cell to cell, stalling and the subsequent SOS response can get very variable in time. These mechanistic differences in the activation of the SOS response are consistent with the differences in timing variability between TMP and NIT.

The SOS response also activates the expression of SulA, a protein that inhibits cell division (Huisman et al., 1984). As cells still grow, but do not divide any longer, this typically results in a filamentous phenotype (Huisman and D'Ari, 1981). SulA expression is expected to be correlated with RecA expression as both proteins are under the control of the SOS regulator regulator LexA (Keseler et al., 2013). We therefore wondered whether the expression of *recA* correlates with cell size under our conditions. Indeed, the strong activation of the SOS response under NIT coincided with the observation that cell sizes can get extremely big for NIT: on average, cell sizes increased by more than 4-fold after 7 hours in NIT stress (Figure 3B,C). Cell sizes also increased with TMP at a similar level of growth inhibition, albeit less strongly. In contrast, cells stressed with TET, which only showed minor activation of the SOS response, kept a constant cell size on average (Figure 3B,C). However, the variability of the cell size did not correspond to the variability in *recA* expression: cells had considerably different sizes under NIT stress, suggesting that also other mechanisms play a role in determining cell size in these conditions.

Measuring the dynamics of single-cell gene expression under three antibiotics, we only observed promoters with highly homogeneous timing for TET (Figure 2C). This might be due to its mechanism of action, inhibition of ribosomes, which are present in high copy numbers (~10,000) per cell (Bremer and Dennis, 2008). In contrast, the DNA damaging antibiotics TMP and NIT both activated homogeneous and heterogeneous timing in different promoters. This included the SOS response which can have great differences in its variability in timing based on the mechanism by which the DNA gets damaged.

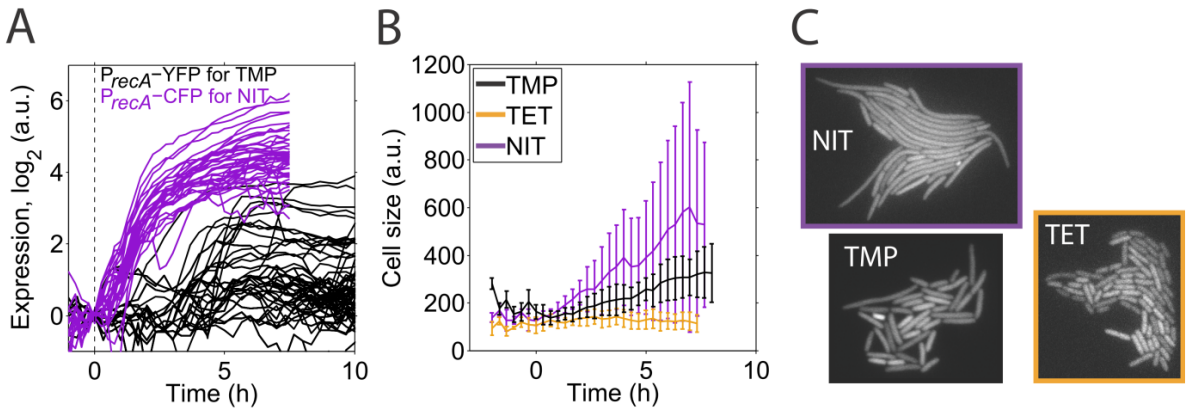

Figure 3. Timing of the SOS response activation is homogeneous under NIT but highly heterogeneous under TMP, with strongly filamenting cells under strong SOS induction. A. Expression of the *recA* promoter in response to TMP (0.5 µg/mL, blue lines) and NIT (4 µg/mL, green lines). The *recA* promoter from the SOS response is fast, and strongly and homogeneously expressed under NIT stress, but later and variably expressed under TMP stress. **B.** Average total cell areas of one microcolony each in response to TMP (0.5 µg/mL, blue line), TET (0.7 µg/mL, red line), or NIT (4 µg/mL, green line) stress. Errors are standard deviations of one microcolony each. **C.** Microscope images of microcolonies stressed for 7 h with TMP, TET, or NIT with the same concentrations as in B.

4.2.3 Temporal order and coupling as a means to identify molecular connections

The variable timing of several promoters, including the *recA* promoter under TMP, raises the question whether variability in timing is related to earlier events, like the early pH drop or the early expression of acid stress genes under TMP. In addition, variable timing in a promoter may also affect the expression of later-responding promoters. To address this question and potentially uncover such molecular connections, we next aimed to identify how prevalent temporal coupling of different responses was during complex stress responses (Figure 1). Several temporal organizations are possible: First, most activated response programs under antibiotic stress could be temporally coupled. This would be the case if there was a global determining factor, for example the growth rate (Tsuru et al., 2009), the cell size (Nachman et al., 2007) or the stage in the cell cycle (Bierbaum and Klumpp, 2015), which would affect the timing of many response programs happening in the cell ('global coupling'), independently of their specific activation. Second, more specific sources of variability could decouple promoters from this global coupling. For example, the master regulator of a pathway might be noisy due to its own low molecule numbers. This would affect the genes within the pathway in a correlated way, but the response times of promoters from different pathways would not correlate with that particular noisy pathway ('pathway-specific noise'; (Stewart-Ornstein et al., 2012)). Pathway-specific noise has previously been identified in the *Bacillus subtilis* cell fate decision upon starvation, where the sporulation and competence pathways run independently from each other (Kuchina et al., 2011). Third, the timing of a certain promoter might be independent from all other promoters in the cell. This would be the case if a promoter has high noise resulting from promoter binding and unbinding by molecules like transcription factors or polymerases ('promoter-specific noise'). Such promoter-specific noise may be more apparent for weakly

expressed promoters whose expression is controlled by low molecule numbers (Taniguchi et al., 2010).

To probe temporal order and coupling, we measured pairs of promoters, combined with the reporters YFP and CFP (Chapter 3), respectively, in the same cells. To compare different responses and environmental conditions, we chose promoters that were strongly up-regulated and part of the enriched biological processes identified in Chapter 1, like the acid stress response combined with the DNA stress response under TMP. Pairs of promoters either shared similar regulation or did not have any obvious or known regulatory connection (Keseler et al., 2013). Due to the selection of strong promoters for our assays, we probably have a bias against detecting promoter-specific noise sources in our data set.

4.2.4 Oxidative stress response precedes DNA stress response during NIT stress in every single cell

First, we wanted to test whether the oxidative stress and the DNA-damage response, which showed a very clear temporal order in response to NIT at the population level (Chapter 1, Figure 5), were also activated clearly sequentially in every single cell, and if these two response programs were coupled. We therefore combined the oxidative stress promoters *fpr* and *ybjC,* both part of the SoxS regulon, with the SOS response promoter *recA*. We found that these promoters were activated strictly sequentially, in that in every single cell the oxidative stress promoter was activated on average 1-2 hours before the DNA damage promoter (Figure 4). This is consistent with the view that NIT increases the amount of reactive species in the cells which is immediately sensed by oxidative stress regulators. The SOS response is, however, only activated after the cell has failed to deal with the oxidative stress and incurred serious DNA damage (Imlay, 2013). Thus, this causal sequence of molecular events is reflected in the temporal sequence of the oxidative stress and SOS response in single cells.

We also tested whether the oxidative stress response and the SOS response were coupled during NIT stress. These two stress responses do not share common transcriptional regulation (Keseler et al., 2013), however, under NIT stress, both systems should be affected by the damaging nitro radicals. We could not reproducibly detect a strong coupling between the oxidative stress promoters and the SOS promoter, meaning that cells that activate the oxidative stress response early did not tend to activate the DNA damage response early. As NIT leads to a strong and heterogeneous increase in the CFP background fluorescence which is hard to correct for, we also measured the expression of *ybjC*-YFP in combination with another fluorescent protein, *recA*-RFP (Methods). This, however, also did also not show a strong coupling between *ybjC* and *recA.* The inability to measure coupling might also be due to the fact that the oxidative stress promoters are not particularly variable in timing, which might prevent us from detecting any correlation. We concluded that the oxidative stress and the DNA damage response are activated strictly sequentially. However, as we could not detect a correlation between their response times, they might either be influenced by different sources of variability, or they might have a common source of variability which is

fluctuating rapidly over time (Pedraza and Paulsson, 2007). Alternatively, our technique may be limited by the small response time variabilities.

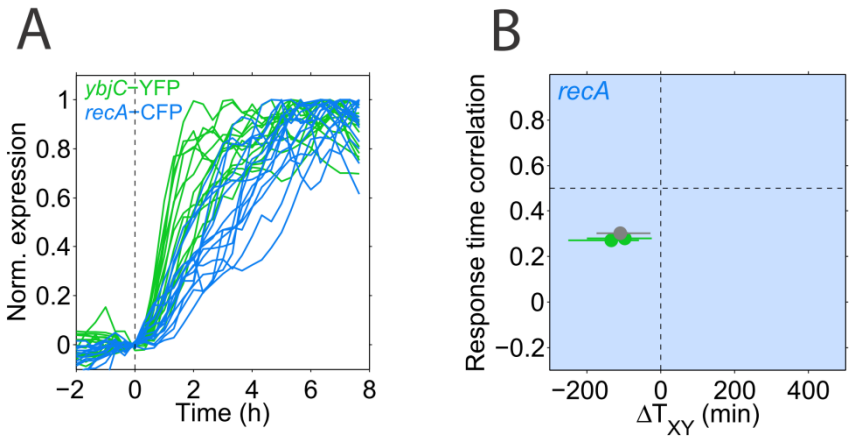

Figure 4. The oxidative stress response precedes the DNA damage response in every single cell. A. Normalized expression of *ybjC*-YFP (green lines) and *recA*-CFP (blue lines) over time in 15 single cells, following one trajectory for each single cell present at the addition of NIT (4 µg/mL) at time-point 0 (Methods). **B.** The response time correlations are plotted over the response time interval of promoters paired with the DNA damage promoter *recA.* Oxidative stress promoters (*fpr, ybjC*) clearly precede the DNA damage response promoter *recA* measured with CFP (green) and RFP (*ybjC,* gray). However, the promoters were not highly correlated, therefore not coupled.

4.2.5 Acid stress response is not coupled to other stress responses under TMP

Next, we asked if the early and striking acid stress response under TMP, as investigated in Chapter 2, influences the timing of other response programs in the bacterial cell. We therefore combined the *gadB* promoter with 13 other promoters from the same and different regulons and biological processes. All those promoters were strongly up-regulated under TMP in the population experiment, and they cover many relevant responses triggered by TMP. We focused on stress response promoters and less on metabolic promoters, except for promoters from the folate acid synthesis pathway which is inhibited by TMP. Biological processes included the general RpoS mediated stress response (*wrbA, dps*), the DNA-damage response (*recA*), folate and guanine biosynthesis (*purM, purT, folA, guaB*), the oxidative stress response (*fpr*), osmotic stress response (*osmC*), a fermentation promoter (*ldhA*), and a cell wall biosynthesis promoter (*glmU*). In addition, we measured promoters from the glutamate-dependent acid stress response (*gadA, gadW*) with similar regulation as *gadB*. As before, we followed the expression of both promoters over time and correlated their response times, expressed as the Pearson correlation coeffient ρ_{XY}. In addition, we determined the response time interval ΔT_{XY} of the two promoters (Figure 1), where *gadB* was P_X and the other promoter was P_Y.

All tested promoters from the glutamate-dependent acid stress response strongly correlated with *gadB*, with Pearson correlation coefficients of 0.76 for *gadA* and 0.51 for

gadW (Figure 5A,C). This excludes the possibility that fluctuations are predominantly generated at the promoter level for the individual promoters of the Gad system (promoter-specific noise). However, few other promoters were strongly correlated in their response times, and therefore coupled with *gadB*; the only exception was *dps* from the RpoS-regulon, confirming the close regulatory linkage between the RpoS response and the acid stress response (Weber et al., 2005). All other measured promoters, including the DNA-damage promoter *recA* (Figure 5B), a promoter from the oxidative stress response (*fpr*), and folate biosynthesis promoters were not coupled with *gadB*. This means that timing variability in these programs is caused by different factors. The strength of coupling was similar to the strength of the correlations between the maximum expression levels for many promoters pairs ($\rho = 0.47$; Figure 5C). Some promoters showed, however, a stronger correlation in their maximum expression levels ($\rho > 0.5$, Figure 5E): the folate biosynthesis pathway (*folA*), the osmotic stress response (*osmC*) and an RpoS-regulated promoter (*wrbA*).

Further, nearly none of the investigated promoters showed a sequential temporal order with *gadB*, even though many promoters appeared several hours later when measured at the population level (Chapter 1, Figure 5B). The glutamate-dependent acid stress promoters *gadA* and *gadW* responded at the same time as *gadB*; many other promoters had their mean interval shifted from $\Delta T_{XY} = 0$, but not all cells responded consistently before or after the *gadB* promoter, respectively. The DNA-damage response promoter *recA* responded hours later than *gadB* (mean $\Delta T_{XY} = 4h$); however, there were still individual cells in which the *recA* promoter responded before the *gadB* promoter (Figure 5B), supporting that under TMP stress, different processes introduce variability into the DNA damage and the acid stress response, respectively. We conclude from these data that promoters within the glutamate-dependent acid response system are activated at the same time, and that this stress response program runs in parallel with most other response programs triggered by TMP. In addition, the acid stress response is not coupled to any other response programs, except to the RpoS response, but the promoters within its own regulon are strongly coupled to each other.

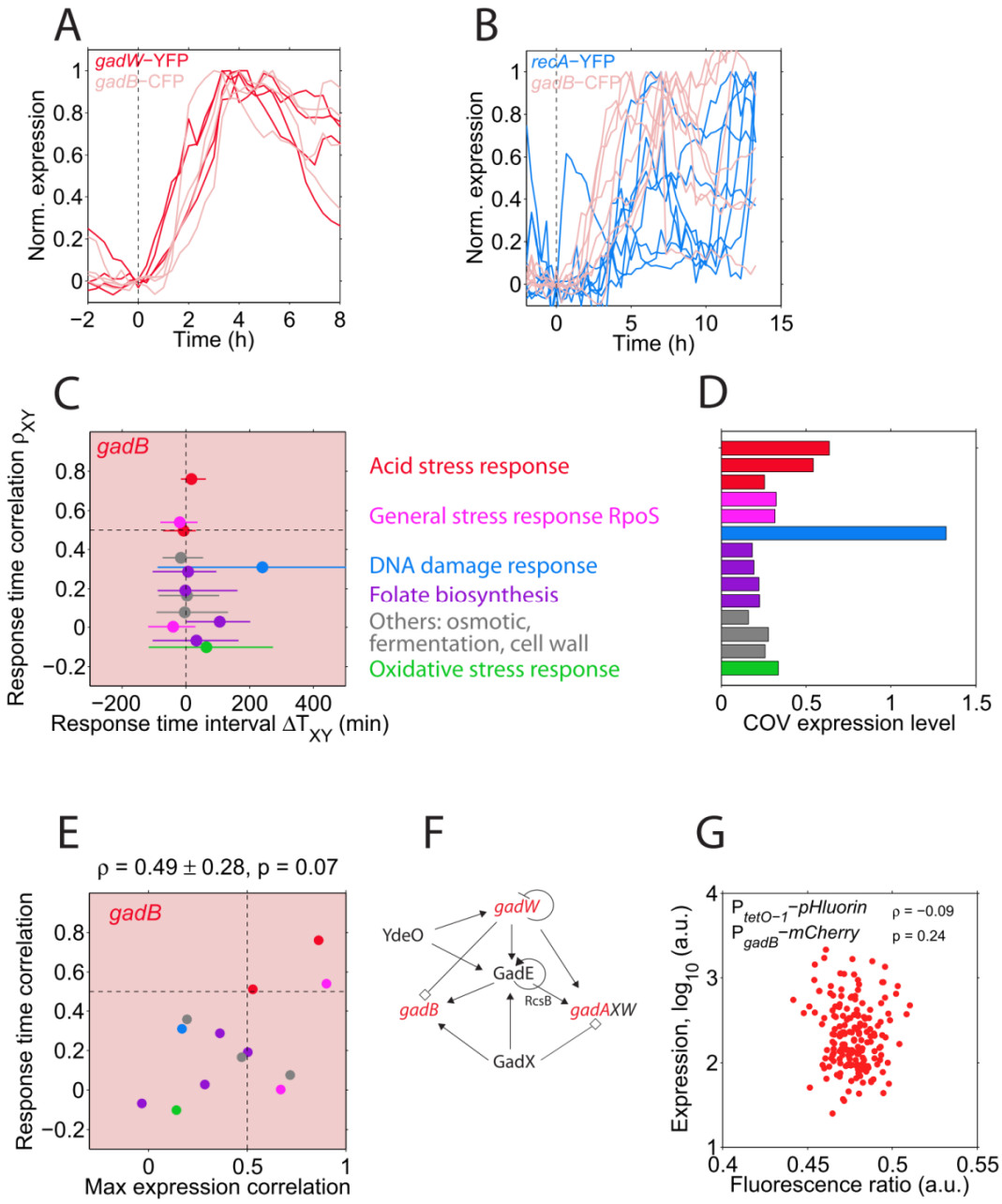

Figure 5. The glutamate-dependent acid stress response program runs in parallel and independently from other response programs, and its variability is induced at the regulatory level. **A.** Normalized expression of *gadW*-YFP (red lines) and *gadB*-CFP (pink lines) over time in 4 single cells, following one trajectory for each single cell present at the addition of TMP (0.5 µg/mL) at time-point 0 (Methods). **B.** Normalized expression of *recA*-YFP (blue lines) and *gadB*-CFP (pink lines) over time in 8 single cells, following one trajectory for each single cell present at the addition of TMP (0.5 µg/mL) at time-point 0. Only cells with a > 2-fold expression change were analyzed. The normalization for the *gadB* data was only done between 0 and 9 hours after TMP addition, as up-regulation at later time-points is likely due to the big microcolony size (Methods). This is why the *gadB* expression levels can go above 1 for later time-points. **C.** Response time correlations are plotted over response time intervals for promoters paired with the acid stress promoter *gadB.* Promoters from the Gad system (red) and the RpoS-regulated promoter *dps* (magenta) are coupled

with the *gadB* promoter. All other tested promoters are independent ($\rho_{XY} < 0.5$). Purple: folate biosynthesis promoters; gray: promoters from the osmotic stress response, fermentation and cell wall biosynthesis; blue: SOS promoter; green: oxidative stress promoter. **D.** The coefficient of variation COV (standard deviation of maximum expression divided by the mean of the maximum expression) for all promoters shown in A. Acid stress promoters (*gadA, gadB*) and the DNA damage promoter *recA* show particularly high expression variability. **E.** The response time correlation for promoter pairs correlates with the correlation between the maximum expression values. **F.** Architecture of the regulatory network controlling the expression from the *gadW, gadA,* and *gadB* promoters. Pointed arrows mean transcriptional activation, blunt arrows inhibition and diamonds at the arrowhead means dual regulation. The transcription factors YdeO, GadE, GadX, and GadW form a closely interlinked network that activates transcription from the *gadB* and *gadA* operons. The proteins GadA and GadB are the effectors that lower intracellular proton levels (see Chapter 2, Figure 4A). Note that each of the depicted promoters has several additional regulators that are not depicted here (Keseler et al., 2013). **G.** The *gadB* expression 3h after TMP addition measured with *gadB*-mCherry is not correlated with the fluorescence ratio measured with the ratiometric *pHluorin* (see Methods Chapter 2), which is a proxy for intracellular pH. Intracellular pH is therefore unlikely to be the source of variability in gene expression.

The *gadA* and the *gadB* promoter from the glutamate-dependent acid response system showed particularly high expression variability (Figure 4B). This extends the results from Chapter 2 where we already showed particularly strong expression variability for the *gadB* promoter. In general, such high variability could come from variability at the level of the stressor itself (protons in this particular case), or could be introduced further downstream, for example by the stress sensing mechanism or the gene expression machinery. To address whether the expression variability is a consequence of intracellular pH or whether it is introduced in a more downstream process, we went back to the data from Chapter 2. There, we measured the fluorescence ratio using the ratiometric sensor *pHluorin* together with *gadB* expression in response to TMP in the same single cells. At these high pH values around pH 8, the fluorescence ratio is linearly related with the intracellular pH (Chapter 2, Figure 6A). We found that the fluorescence ratio in response to TMP was quite homogeneous among single cells (Figure 5G), and not significantly correlated with *gadB* expression measured at 3h after TMP addition, when *gadB* expression was close to maximal. These data suggest that the expression variability of the Gad system is not rooted in the level of the stressors itself, but is rather introduced by further downstream processes of sensing or gene expression. From the closely interconnected regulatory network of *gadA* and *gadB* expression (Figure 4D), and the fact that the master regulator GadE has around 10 different inputs and is positively autoregulated (Keseler et al., 2013), it seems plausible that variability is generated at the level of the master regulator GadE.

4.2.6 Promoters from different responses are coupled under TET

As TET did not trigger high variability in the timing of individual promoters (Figure 2C), we wondered how this feature was reflected in the coupling and temporal order of promoters. We therefore measured different promoters in combination with the iron-sulfur cluster regulator *iscR* and the major cold shock promoter *cspA,* both of which were strongly

upregulated under TET stress. As before, promoters were chosen from the same response programs or from different ones. In contrast to our observation with TMP, we found promoters with and without regulatory connections that were strongly coupled with *iscR* or *cspA* (Figure 6).

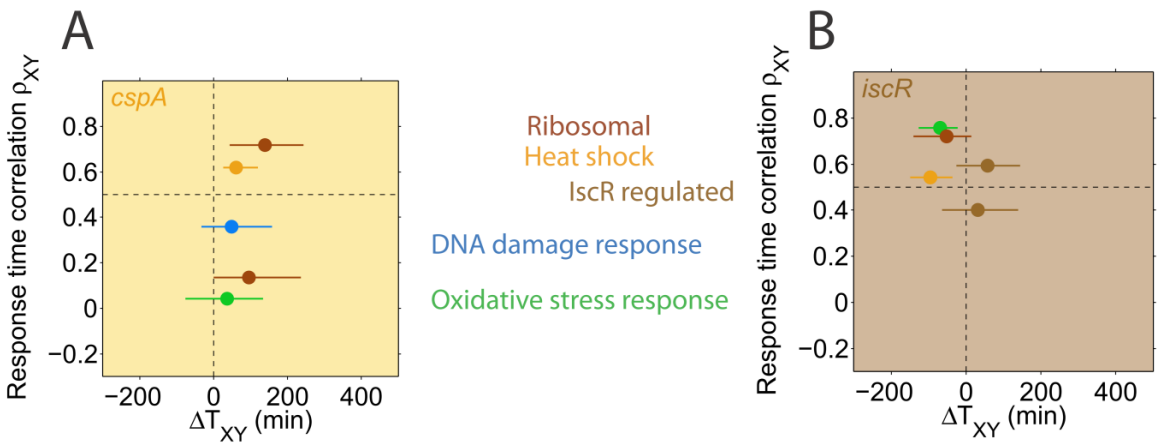

Figure 6. Coupling and temporal order of various responses with the cold shock promoter *cspA* and the iron-sulfur regulator *iscR*. A. The response time correlations are plotted over the response time intervals of promoters paired with the cold shock promoter *cspA*. The heat shock promoter *dnaK* and the ribosomal promoter *rpsA* show a strong correlation and a clear temporal order with the *cspA* promoter. The DNA-damage response promoter *recA,* the ribosomal promoter *rpmE,* and the oxidative stress promoter *ahpC* are not coupled with *cspA*. **B.** The response time correlations are plotted over the response time intervals of promoters paired with the iron-sulfur cluster promoter *iscR.* The oxidative stress promoter *ahpC,* the ribosomal promoter *rpsA,* the heat shock promoter *dnaK,* and the IscR-regulated promoter *ydiU* show a strong correlation and therefore coupling with the *iscR* promoter.

We found a strong coupling (ρ = 0.62) and a clear temporal order between the cold shock promoter *cspA* and the heat shock promoter *dnaK* (Figure 6A): in every single cell, *cspA* was activated before *dnaK,* on average one hour earlier. Both genes act in temperature shock, but have previously been shown to be expressed oppositely (VanBogelen and Neidhardt, 1990) and do not have a known common regulator. In principle, however, both genes can be activated in response to translation inhibition (VanBogelen and Neidhardt, 1990). Similarly, the ribosomal promoter *rpsA* was activated after *cspA* in every single cell and was upregulated on average 2.3 hours later. These two promoters were also strongly coupled (ρ = 0.72; Figure 6A). This is likely because both promoters share a common regulator: both *cspA* (Brandi et al., 2016) and *rpsA* are negatively regulated by ppGpp (Keseler et al., 2013) and the intracellular levels of this alarmone decrease under TET stress (John and Goldberg, 1978), which could explain their strong coupling. In contrast, other promoters without a known regulatory interaction with *cspA*, i.e. the ribosomal promoter *rpmE,* the oxidative stress promoter *ahpC,* and the DNA damage response promoter *recA* did not show coupling nor a clear temporal order with *cspA*. Based on these results, we suggest that *dnaK* and *rpsA* might be coupled to *cspA* because of a common molecular event that triggers their activation: translation inhibition in the case of the heat shock promoter *dnaK,* which leads to

ppGpp depletion that can couple *cspA* to *rpsA*. However, the strong correlations between *cspA* and *dnaK/rpsA* might also be caused by global factors, like the level of ribosomes, which can have an effect on those promoters. The underlying molecular mechanisms for these couplings therefore remain to be identified.

Many promoters were strongly coupled with the *iscR* promoter (Figure 6B): the oxidative stress promoter *ahpC,* the ribosomal promoter *rpsA,* the IscR-regulated promoter *ydiU*, and the heat shock promoter *dnaK.* The oxidative stress promoter *ahpC* and the iron-sulfur promoter *iscR* have a known regulatory connection: both are known to be activated by intracellular hydrogen peroxide (Jang and Imlay, 2010; Lee et al., 2004; Storz et al., 1990). However, if this mechanism is responsible for their strong coupling under TET stress remains to be confirmed. In general, it seems unlikely that all the couplings between the *iscR* promoter and other promoters have a specific meaning. Rather, it is possible that global factors, instead of pathway- or promoter-specific noise, dictate the variability in timing in these promoters. The variability in timing in all the TET-induced promoters is very low (Figure 2B), further suggesting that no specific noise-generating mechanisms act on these promoters. Global factors that couple these promoters with each other could for example be the bacterial growth rate, the cell size, the ribosome levels, or a combination of them and will likely affect many more promoters than the ones measured here.

4.3 Discussion

In this chapter, we described the temporal organization of gene expression during complex stress responses induced by low concentrations of antibiotics. We found that the variability in response times increased at later response times: each extra hour in response delay adds 12 min to the variability of the timing. Certain promoters, like an SOS promoter under TMP stress, had a particularly strong variability under one stress condition (TMP), but not under another condition (NIT). The DNA damage response in bacteria has been described before to react with a precise pulsing in single cells after DNA damage induced by ultraviolet light (Friedman et al., 2005). It therefore seems that this stress response can respond in different ways, depending on the type of stress applied. Our data suggest that it is the amount of DNA damage itself that leads to a stronger and less variable activation, as in the case of NIT, or to a weaker and more variable activation as with TMP. Variability is therefore created predominantly at the level of the damage itself, not further downstream at the level of sensing or the transcription or translation machinery.

We showed that genes that exhibit a clear temporal order in population-level measurements may not have such a clear order in every single cell. However, in certain cases like the oxidative stress response and the DNA stress response under NIT, the temporal order is precisely followed in every single cell. Such a clear temporal order may hint at biological processes that are dependent on each other, and can reveal the sequence of molecular events happening during complex stress situations in bacteria.

The acid stress response under TMP was highly variable and independent from all other promoters, except from the RpoS-regulon. Our measurements of intracellular pH suggest that it is not a variable pH itself that induces this variability in the acid stress promoters. We rather suggest that variability is introduced into this system by its complex regulatory network, making it independent from other cellular processes. Heterogeneity and temporal independence might have possible functions as a bet-hedging mechanism as discussed in Chapter 2.

In stark contrast to our observations with TMP, many promoters with similar regulation and function, but also putatively unrelated promoters were coupled under TET stress. We suggest that many of these correlations are driven by global, yet unidentified factors. It is unclear, whether these global factors are prevalent under TET stress, compared to the other conditions tested. However, it is plausible that the inhibition of the translation machinery leads to fluctuations in certain processes, like the activity of ribosomes. This could in turn result in growth rate fluctuations that could couple the timing of all kinds of response programs. However, it remains to be shown if TET indeed induces more correlated response time fluctuations than other stress conditions and what is the specific cause for these couplings.

It has recently been shown that the strength of single-cell gene-gene correlations can change depending on the environment (Martins et al., 2017). In general, a population in which most biological processes are correlated might have different survival chances than a population in which different biological processes run independently from each other. For example, in a population with independent and therefore uncorrelated processes, every cell is a specialist for another process and might survive in case of an environmental change, as shown for an acid shock in Chapter 2. In contrast, correlated variability in all processes makes the population less diverse, and might comply with other situations in the bacterial lifestyle.

Overall, this study provides new insight into the temporal organization of complex stress responses and widens our understanding of the factors that influence cell-to-cell variability. Our data suggest that these factors can be the underlying damage itself (as for the DNA damage response), variability generated at the level of the regulatory network (as for the acid stress response), or global factors affecting the fluctuations in many genes. In addition, our data suggest new regulatory links, as between the temperature shock genes *cspA* and *dnaK,* by exploiting natural variability. Cell-to-cell fluctuations have been used before to identify new regulatory connections in mammalian cells (Pina et al., 2015) and this approach seems also applicable in bacteria. We suggest that the here presented approach can also be be applied to other environmental changes and experimental systems.

4.4 Methods

4.4.1 Culture conditions

Culture conditions were the same as described in Chapters 1 to 3. We used M9 minimal medium with glucose and amino acids for all experiments.

4.4.2 Strain construction and verification

Dual reporter strains were constructed and verified as described in Chapter 3. Some promoters from the promoter-GFP library were found to have single point mutations. For these promoters, we amplified the promoter region from the MG1655 chromosome with the following primers:

gadB: CGGGATCCTCCTGCAGCATGGACTGAG and CCGCTCGAGCATTTTCGTCGTCCCAGGTC
gadA: CCGCTCGAGACGCAGGTCGATGGCTG and CGGGATCCGCGGTGAAACTGATGCTGCG
osmC: CCGCTCGAGTGCTGTTGAATTTTCTGCCTG and CGGGATCCGGTTCAGCACGCCACTCT
fpr: CCGCTCGAGGGCGTGAACGGTGAGACT and CGGGATCCCAAGTCACGCACCATTCGCC
ahpC: CCGCTCGAGGCAGGAAGCAGAGCCAGT and CGGGATCCCCGTTTTTGAATGCCTGG

The strain MG1655 Δ*intS*::P_{ybjC}-*yfp* Δ*galK*::P_{recA}-*mCherry* (used in Figure 4B) was constructed by first exchanging the sequence for GFP on the library plasmid for *recA* by the sequence for mCherry. The sequence for mCherry was amplified from the plasmid pZS41-*mCherry* (see Chapter 2) using the primers:
CCGCTCGAGAGATCCTCTAGATTTAAGAAGGAGATATACATATGGTTTCCAAGGGCGAGGAGG and GCGCCTAGGTCTAGGGCGGCGGATTTGTCCTACTC
and ligated into the library plasmid. The promoter-*mCherry* sequence was then amplified with the primers CTACTCAGGAGAGCGTTCACC and AmpF2 (see Chapter 3) and integrated into the CFP platform using recombineering.

4.4.3 Analysis of microscopy data

Microscopy data were normalized and analyzed as described in Chapter 3.

For the determination of response times and their standard deviations, and the coefficient of variation in Figure 5D, all cells that were present in the last frame were analyzed. For the determination of response time correlations and maximum expression correlations, we randomly followed individual cell trajectories after the addition of antibiotics. This randomization was repeated 1000 times and we took the mean correlation from these repetitions as our final correlation. On average, we randomly sampled from the trajectories of around 20 cells. In cases where microcolony size had an impact on gene expression (as for promoters from the *gad* system and RpoS-regulated promoters), data for this promoter

were cropped before this trend became apparent. For all the data presented here, measurements from at least two microcolonies were pooled.

Response times were determined as the time until half maximum expression was reached on a linear scale. Fold-changes were determined as the maximum value of the $\log_2$ data shifted to 0 for t = 0, maximum expression was determined as the maximum value of non-normalized, but background and autofluorescence subtracted data.

Throughout the plots in Figures 4B, 5C,E, 6, promoter pairs are defined to be sequential if the 90 percentile of the interval ΔT_{XY} does not cross the 0. Accordingly, promoters are said to be coupled if their correlation coefficient $\rho_{XY} > 0.5$. The p-value in Figure 5G is from bootstrapping using the Matlab function *bootstrp,* with n = 1000.

Chapter 4: Temporal organization of gene expression in single cells during complex stress responses

Discussion and Conclusion

With the rise of antibiotic resistance (Clatworthy et al., 2007) and the resulting failures to treat infectious diseases (Levy and Marshall, 2004), it is crucial to investigate the many effects that antibiotics can have on bacteria. The aim of this thesis was to progress our understanding of bacterial stress responses based on measuring dynamic gene expression changes in *E. coli*. Thereby, we got insight into the temporal sequence of these changes, their relation with the bacterial growth rate, their underlying mechanisms, their variability in expression and timing, and their consequences for bacterial fitness in constant and changing environments. We investigated in detail the temporal gene expression changes in response to antibiotics with diverse mechanisms of action. We chose sublethal concentrations of antibiotics, which often occur during treatments and in the environment (Andersson and Hughes, 2014), and compared the induced changes between different antibiotics at the same growth rate inhibition. Taken together, the results presented in this thesis are summarized in the following paragraph and discussed below.

The sudden exposure to antibiotics induces an adaptation process that takes several hours, in which massive and temporally structured gene expression changes are induced. This includes the differential expression of numerous stress response genes. The induction of the acid stress response under TMP induced by the depletion of purine nucleotides and an intracellular pH drop, protected bacteria from a subsequent exposure to lethal acid stress. Expression of the acid stress response was highly variable among single cells, and cells with higher expression survived longer in the acidic environment. Our results show that sublethal concentrations of antibiotics can completely change the gene expression state of bacteria, thereby affecting bacterial fitness in different environments. We further investigated the temporal organization and variability of gene expression changes at the single-cell level. Genes that were induced later tended to have a higher variability in their response time among single cells. The SOS response was particularly variable in its timing under TMP, but not under NIT, which suggests that variability is induced at the level of the damage itself. We detected a clear temporal order between oxidative stress genes and an SOS response gene under NIT, suggesting a temporal dependence of these response programs. In contrast, temporal independence was found between the acid stress and all other cellular responses, including the SOS response. Overall, these results provide insight into the timing, variability and cross-protection in bacteria during complex stress responses.

i. Global and specific factors affect bacterial gene expression under antibiotic stress

In Chapter 1, we found that the initial growth rate drop determines the overall rate of gene expression changes, in that slower inhibition leads to a faster overall gene expression response (Chapter 1, Figure 3C,D). The rate at which an antibiotic can inhibit growth after its application probably depends on physical and biochemical properties of the antibiotic, the rate at which essential molecules get depleted, and the environment. All of the antibiotics chosen for this study have a relatively fast effect on bacterial growth, compared to other

antibiotics like ampicillin or sulfonamides, which only show an effect on growth rate after several hours (Greenwood and O'Grady, 1976; Rolinson, 1980). It remains to be seen whether such antibiotics already induce gene expression changes early on, i.e. if bacteria sense the effects of these antibiotics before they have an effect on growth. This could allow them to activate protective genes, and to possibly tolerate higher concentrations of antibiotics, compared to a situation in which the antibiotic has an almost immediate effect on bacterial growth rate. Investigating the mechanisms that determine the rate of the initial growth rate drop, and interfering with them might therefore allow a more effective eradication of bacteria.

In our genome-wide gene expression data in response to antibiotics, we saw that many promoters from specific stress response systems were differentially regulated, many of them unrelated to the antibiotic target, like the acid stress under TMP, or the oxidative stress under TET. This raised the question whether the cells really experience this stress, i.e. acid stress under TMP, or oxidative stress under TET. Alternatively, these stress responses could be activated less specifically (Price et al., 2013), due to the indirect activation via connected regulatory systems. For example, it is known that the RpoS response, which can be induced by a plethora of different inputs, can activate acid stress promoters (Battesti et al., 2011). In addition, transcription factors from the Mar system can also activate oxidative stress promoters (Keseler et al., 2013). Last, the SOS response cannot only be activated by DNA damage, but also via signaling from membrane damage (Aertsen and Michiels, 2006). In this study, we showed that bacteria indeed experience an intracellular pH drop before they activate the acid stress response under TMP (Chapter 2, Figure 8). Further, the fact that TET induces OxyR-regulated promoters and the *iscR* promoter, both of which can be activated by hydrogen peroxide, suggests that TET-stressed cells also experience oxidative stress (Chapter 4, Figure 6). Here, however, due to the low fluorescence signal of a ratiometric oxidative stress sensor, we were unable to measure intracellular reactive oxygen species over time. Such measurements could provide valuable information on the induction of these gene expression changes. Our study underlines the importance of combining data from different levels of physiology, i.e. bacterial metabolism with gene expression, if we want to advance our understanding of bacterial responses (Ray et al., 2011). Recent research has picked up on this topic approaching bacterial responses to antibiotics from the side of metabolism (Zampieri et al., 2017).

ii. Specific cross-protection by an acid response system with anticipatory features

In Chapter 2, we showed a clear and specific case for cross-protection between the antibiotic TMP and acid stress (Chapter 2, Figure 3), and identified the underlying mechanism (Chapter 2, Figure 8). Recently, also other cross-protection effects between the antibiotic ampicillin and heat shock / oxidative stress have been shown (Mathieu et al., 2016). In this case, however, the effect was attributed to a general, ppGpp and RpoS-induced stress response, possibly common to many antibiotics. While ppGpp and RpoS-induced gene expression is also increased under TMP (Sangurdekar et al., 2011), we showed that the acid stress response is induced via a specific mechanism in our case. The main

evidence for that is that the acid stress response was was also activated in an RpoS knockout mutant (Chapter 2, Figure 1). In addition, based on the induced gene expression changes (Chapter 1, Figure 5), our data suggest various additional cross-protection effects, specific to each antibiotic: TET may specifically protect against heat stress, TET and NIT against oxidative stress, and TMP and NIT against DNA stress. The cross-protection between NIT and oxidative DNA stress has indeed been shown before (Basak and Chatterjee, 1994), which further supports the applicability of our approach. Besides cross-protection, we also identified a case of cross-sensitization: cells pretreated with NIT die faster during extreme acid stress (Chapter 2, Figure 3C). Such cross-sensitization effects may be relevant for antibiotic therapy: application of a second stressor in the right time-window after the antibiotic may improve the eradication of bacteria. Our method is well applicable for the detection of temporal gene expression changes in response to other antibiotics as well, and to identify environmental stressors and the right time-windows when antibiotics-pretreated bacteria are particularly sensitive.

While we do not suggest that bacteria anticipate acid stress in response to TMP, the glutamate-dependent acid stress response has features common for an anticipatory response by itself: it is induced by mild acid stress (Arnold et al., 2001; Leyer and Johnson, 1993; Ryu and Beuchat, 1998), but has its strongest activity for severe acid stress at pH values around 4 (Pennacchietti et al., 2009). This seems a very plausible strategy for surviving lethal acid stress: as an immediate growth halt and acidification makes the accumulation of new proteins difficult, cells already strongly produce the necessary enzymes as soon as they sense mild acid stress. The high heterogeneity in expression levels in the system, even during exponential growth conditions (Silander et al., 2012), additionally ensures that there are always some cells in the population that would survive an extreme acid shock. Such high heterogeneity might have a fitness benefit in changing environments (Blake et al., 2006), but whether the expression of these acid stress promoters also has a fitness cost under certain conditions, and can therefore be seen as a bet-hedging mechanism (de Jong et al., 2011), still needs to be investigated.

Overall, the fact that TMP can protect from acid stress might have implications for bacterial infections. For example, if pathogens like *Salmonella* get exposed to TMP before their passage through the stomach, they might be less sensitive to this natural barrier to infection (Audia et al., 2001). In addition, immune cells attack intracellular pathogens by oxidative stress and a low pH inside phagosomes. If pathogens are already protected from acid stress at the time when they get engulfed due to prior exposure to TMP, immune cells may fail to harm them by low pH. However, if these cross-protection effects play any role in the clinic needs to be investigated using different experimental systems like cell culture assays or animal models. A further interesting aspect is that drugs with the same mechanism of action as TMP, the inhibition of folic acid synthesis, are used to inhibit the growth of mammalian cells. Mammalian cells cannot synthesize and need to import folate, and these drugs inhibit the metabolization into folate derivates (Huennekens, 1994). It is tempting to speculate that the here identified mechanism of intracellular pH drop in response to folate inhibition in *E. coli* also applies for other bacterial species or mammalian cells; this possibility needs to be checked in future work.

We show that the acid stress response under TMP is dispensable, as a mutant of the master regulator GadE did not show any decrease in bacterial growth rate. We speculate that this is the case because the intracellular pH drop is likely not the problem that leads to a sustained growth rate inhibition. Bacteria can deal well with such a relatively low drop in intracellular pH, as we also showed in an experiment (Chapter 2, Figure 2). Their main problem under TMP is the inhibition of the folate biosynthesis pathway with many downstream effects, above all the depletion of amino acids and nucleotides (Kwon et al., 2010). The bacterial gene expression responses to antibiotics therefore appear to be an attempt to deal with all the downstream effects that the antibiotic causes; however, bacteria do not have a solution that would relieve their main problem. Bacteria could tolerate high concentrations of TMP if they found a way to massively overproduce the inhibited enzyme, DHFR (Palmer and Kishony, 2014). This is a common resistance mechanism to TMP (Flensburg and Sköld, 1987; Toprak et al., 2012).

iii. Variability in timing and expression level of stress response genes

With respect to timing of gene expression in single cells in response to stress, we found that promoters cannot be less variable in timing than a certain limit. This limit increases at later response times, and probably exists due to the fundamental constraints that later processes accumulate more variability from earlier processes (Pedraza and van Oudenaarden, 2005). Later responses will therefore tend to have a higher absolute variability in timing (Amir et al., 2007; Mader et al., 2015). It will be interesting to quantify how this limit changes at different growth rates, and whether growth rate fluctuations of individual cells, which can also vary for different stress conditions, increase this limit.

Our experiments show two highly variable stress response systems, and suggest that variability is introduced at a different level for each system: for the SOS response, we suggest that heterogeneity in timing and expression level stems from variability in the amount of damage itself (see Chapter 4, Figure 3); in contrast, for the acid stress response, variability in expression level is likely introduced by its gene regulatory network (see Chapter 4, Figure 5F,G). Many other stress response genes did, however, not show high variability in timing nor expression level (Chapter 4, Figure 2C, 4A, 5D). Even though some stress response genes have been shown to be variable from cell-to-cell (Silander et al., 2012), caution should be taken not to assume high variability and underlying diversification strategies for all stress response genes: some stress response systems probably just follow the damage that they sense closely. As for the case of the acid stress response, it will be highly interesting to identify the properties of the underlying genetic circuit that leads to the observed fast and pulse-like dynamics.

iv. Multidimensional variability may have fitness advantages and disadvantages

The acid stress system was highly variable in expression levels, and runs independently from most other response programs in response to TMP, including the SOS response. This was found in an experiment in which we combined many promoters with the acid stress promoter *gadB* and measured the single-cell dynamics of both promoters (Chapter 4, Figure 5). Some cells may therefore be well protected against environmental acid stress, but these cells are likely not the same ones that have the SOS response up-regulated and are well-prepared for the appearance of another DNA stressor. If each stress response also comes with a fitness cost, this 'multidimensional variability' in the population should be beneficial for a population, as every cell carries the cost of a different stress response. However, such a multi-dimensional variability may be detrimental for environmental stressors that tend to appear together; here, a coupled response seems to be the better option. Using our response time measure, we failed to detect coupling between oxidative stress promoters and an SOS promoter under NIT stress, even though both systems are likely induced by reactive nitro radicals and showed a clear temporal order. This observation supports the notion from above that the dynamics of the SOS response, and possibly also the oxidative stress response, do not reflect an evolved population strategy, but are rather precise sensors of the actually occurring damage. For other, metabolic systems in bacteria, the evolved population strategy of anticipation has been described (Mitchell et al., 2009; Tagkopoulos et al., 2008). These measurements were done at the population level and it would be highly interesting to revisit the effects described in these studies at the single-cell.

Our dual-color method, described in Chapter 3, allows the detection of the temporal sequence of events occurring during complex stress responses, and possible dependencies between different response programs. Whereas we could not detect dependencies among different response programs under TMP and NIT stress (Chapter 4, Figures 4B and 5C), promoters from different response programs were coupled under TET. This coupling may be the result of specific interactions via the gene regulatory network or metabolism. However, as all tested promoters showed similarly low variability in timing, we cannot exclude that these couplings are unspecific, and mediated via global factors like the bacterial growth rate or the cellular ribosome content. Ideally, we can identify such a global factor and quantify its contribution to the coupling of promoter pairs under TET in future work.

v. A sequence of biochemical events determines temporal organization of gene expression under antibiotic stress

Our single-cell data on the temporal gene expression to TMP and NIT suggest that the cell does not have a response that is hard-wired in the gene regulatory network to these stressors; rather, the temporal order of gene expression seems to be the consequence of an inevitable sequence of biochemical events: for example, nitro radicals under NIT stress activate an oxidative stress response and lead to DNA damage, which further activates the DNA damage response. This may be in contrast to other timed responses like cellular differentiation or nutrient shifts (Sinai et al., 2015; Zampar et al., 2013), which probably

comprise strategies evolved to be nearly optimal for these environmental shifts. In general, it is an intriguing question which response programs should be coupled by hard-wiring (as for example known for the multiple antibiotic resistance regulon with the oxidative stress regulon), and which ones should be independent at the gene-regulatory level and based on cellular sensing (as for the oxidative stress regulon and the SOS regulon). This distinction surely depends on the costs for sensing (Kussell and Leibler, 2005), and the dynamics and statistics of the environment.

vi. Challenges for the future

Overall, this thesis makes a contribution to our fundamental understanding of cell-to-cell variability, cellular strategies, and the physiological mechanisms underlying gene expression changes in response to antibiotics. This was possible by studying antibiotics with diverse mechanisms of action and downstream effects, and comparing them to each other and to other environmental stressors. Yet, we understand very little about the plethora of physiological changes happening in response to antibiotics. We suggest that investigating further antibiotics with different mechanisms of action using the here presented methods, will uncover additional mechanisms and principles. The combination of gene expression reporters with a metabolite sensor for intracellular pH allowed a deeper insight into the physiological changes happening in response to antibiotics. The development of further good metabolite sensors, like one for oxidative stress, could help to reveal additional mechanisms underlying antibiotics-induced gene expression changes. Further, high-throughput methods for single-cell time-lapse imaging, in which we could use our dual-reporter strains and measure many more promoter pairs and environmental conditions, would be a great advancement.

In recent years, our knowledge on the complex interactions between drugs, bacteria and the host has progressed substantially. Some findings like the potentiation of antibiotics by adjuvants were implemented in clinical therapies (Kalan and Wright, 2011). However, it is still a big step to translate basic research findings into clinical applications. Understanding bacterial responses and strategies will hopefully allow us to minimize the negative effects of bacteria on our health in the future.

References

Adams, K.N., Takaki, K., Connolly, L.E., Wiedenhoft, H., Winglee, K., Humbert, O., Edelstein, P.H., Cosma, C.L., and Ramakrishnan, L. (2011). Drug tolerance in replicating Mycobacteria mediated by a macrophage-induced efflux mechanism. Cell *145*, 39–53.

Aertsen, A., and Michiels, C.W. (2006). Upstream of the SOS response: figure out the trigger. Trends Microbiol. *14*, 421–423.

Allison, K.R., Brynildsen, M.P., and Collins, J.J. (2011). Metabolite-enabled eradication of bacterial persisters by aminoglycosides. Nature *473*, 216–220.

Al-Nabulsi, A.A., Osaili, T.M., Shaker, R.R., Olaimat, A.N., Jaradat, Z.W., Zain Elabedeen, N.A., and Holley, R.A. (2015). Effects of osmotic pressure, acid, or cold stresses on antibiotic susceptibility of Listeria monocytogenes. Food Microbiol. *46*, 154–160.

Amir, A., Kobiler, O., Rokney, A., Oppenheim, A.B., and Stavans, J. (2007). Noise in timing and precision of gene activities in a genetic cascade. Mol. Syst. Biol. *3*.

Amyes, S.G.B., and Smith, J.T. (1974). Trimethoprim action and its analogy with thymine starvation. Antimicrob. Agents Chemother. *5*, 169–178.

Andersson, D.I., and Hughes, D. (2014). Microbiological effects of sublethal levels of antibiotics. Nat. Rev. Microbiol. *12*, 465–478.

Andrews, J.M. (2001). Determination of minimum inhibitory concentrations. J. Antimicrob. Chemother. *48*, 5–16.

Ankomah, P., and Levin, B.R. (2012). Two-drug antimicrobial chemotherapy: a mathematical model and experiments with Mycobacterium marinum. PLoS Pathog. *8*, e1002487.

Arnold, C.N., McElhanon, J., Lee, A., Leonhart, R., and Siegele, D.A. (2001). Global analysis of Escherichia coli gene expression during the acetate-induced acid tolerance response. J. Bacteriol. *183*, 2178–2186.

Arnoldini, M., Vizcarra, I.A., Peña-Miller, R., Stocker, N., Diard, M., Vogel, V., Beardmore, R.E., Hardt, W.-D., and Ackermann, M. (2014). Bistable expression of virulence genes in Salmonella leads to the formation of an antibiotic-tolerant subpopulation. PLoS Biol. *12*, e1001928.

Audia, J.P., Webb, C.C., and Foster, J.W. (2001). Breaking through the acid barrier: An orchestrated response to proton stress by enteric bacteria. Int. J. Med. Microbiol. *291*, 97–106.

Avraham, R., Haseley, N., Brown, D., Penaranda, C., Jijon, H.B., Trombetta, J.J., Satija, R., Shalek, A.K., Xavier, R.J., Regev, A., et al. (2015). Pathogen cell-to-cell variability drives heterogeneity in host immune responses. Cell *162*, 1309–1321.

Baba, T., Ara, T., Hasegawa, M., Takai, Y., Okumura, Y., Baba, M., Datsenko, K.A., Tomita, M., Wanner, B.L., and Mori, H. (2006). Construction of Escherichia coli K-12 in-frame, single-gene knockout mutants: the Keio collection. Mol. Syst. Biol. *2*, 2006.0008.

Balaban, N.Q., Merrin, J., Chait, R., Kowalik, L., and Leibler, S. (2004). Bacterial persistence as a phenotypic switch. Science *305*, 1622–1625.

Bandow, J.E., Brötz, H., Leichert, L.I.O., Labischinski, H., and Hecker, M. (2003). Proteomic approach to understanding antibiotic action. Antimicrob. Agents Chemother. *47*, 948–955.

Bar-Joseph, Z., Gitter, A., and Simon, I. (2012). Studying and modelling dynamic biological processes using time-series gene expression data. Nat. Rev. Genet. *13*, 552–564.

Barrick, J.E., Colburn, G., Deatherage, D.E., Traverse, C.C., Strand, M.D., Borges, J.J., Knoester, D.B., Reba, A., and Meyer, A.G. (2014). Identifying structural variation in haploid microbial genomes from short-read resequencing data using breseq. BMC Genomics *15*, 1039.

Basak, J., and Chatterjee, S.N. (1994). Induction of adaptive response by nitrofurantoin against oxidative DNA damage in some bacterial cells. Mutat. Res. Toxicol. *321*, 127–132.

Basan, M., Zhu, M., Dai, X., Warren, M., Sévin, D., Wang, Y.-P., and Hwa, T. (2015). Inflating bacterial cells by increased protein synthesis. Mol. Syst. Biol. *11*, 836.

Battesti, A., Majdalani, N., and Gottesman, S. (2011). The RpoS-mediated general stress response in Escherichia coli. Annu. Rev. Microbiol. *65*, 189–213.

Beck, J.M., Young, V.B., and Huffnagle, G.B. (2012). The microbiome of the lung. Transl. Res. *160*, 258–266.

Begley, M., Gahan, C.G.M., and Hill, C. (2002). Bile stress response in Listeria monocytogenes LO28: Adaptation, cross-protection, and identification of genetic loci involved in bile resistance. Appl. Environ. Microbiol. *68*, 6005–6012.

Belenky, P., Ye, J.D., Porter, C.B.M., Cohen, N.R., Lobritz, M.A., Ferrante, T., Jain, S., Korry, B.J., Schwarz, E.G., Walker, G.C., et al. (2015). Bactericidal antibiotics induce toxic metabolic perturbations that lead to cellular damage. Cell Rep. *13*, 968–980.

Bergmiller, T., Andersson, A.M.C., Tomasek, K., Balleza, E., Kiviet, D.J., Hauschild, R., Tkačik, G., and Guet, C.C. (2017). Biased partitioning of the multidrug efflux pump AcrAB-TolC underlies long-lived phenotypic heterogeneity. Science *356*, 311–315.

Berry, D.B., and Gasch, A.P. (2008). Stress-activated genomic expression changes serve a preparative role for impending stress in yeast. Mol. Biol. Cell *19*, 4580–4587.

Bierbaum, V., and Klumpp, S. (2015). Impact of the cell division cycle on gene circuits. Phys. Biol. *12*, 066003.

Blake, W.J., Balázsi, G., Kohanski, M.A., Isaacs, F.J., Murphy, K.F., Kuang, Y., Cantor, C.R., Walt, D.R., and Collins, J.J. (2006). Phenotypic consequences of promoter-mediated transcriptional noise. Mol. Cell *24*, 853–865.

Block, D.H.S., Hussein, R., Liang, L.W., and Lim, H.N. (2012). Regulatory consequences of gene translocation in bacteria. Nucleic Acids Res. *40*, 8979–8992.

Bollenbach, T., and Kishony, R. (2011). Resolution of gene regulatory conflicts caused by combinations of antibiotics. Mol. Cell *42*, 413–425.

Bollenbach, T., Quan, S., Chait, R., and Kishony, R. (2009). Nonoptimal microbial response to antibiotics underlies suppressive drug interactions. Cell *139*, 707–718.

Boulineau, S., Tostevin, F., Kiviet, D.J., ten Wolde, P.R., Nghe, P., and Tans, S.J. (2013). Single-cell dynamics reveals sustained growth during diauxic shifts. PLoS ONE *8*, e61686.

Brandi, A., Giangrossi, M., Giuliodori, A.M., and Falconi, M. (2016). An interplay among FIS, H-NS, and guanosine tetraphosphate modulates transcription of the Escherichia coli cspA gene under physiological growth conditions. Front. Mol. Biosci. *3*.

Brazas, M.D., and Hancock, R.E.W. (2005). Using microarray gene signatures to elucidate mechanisms of antibiotic action and resistance. Drug. Discov. Today. *10*, 1245–1252.

Brehm-Stecher, B.F., and Johnson, E.A. (2004). Single-Cell Microbiology: Tools, Technologies, and Applications. Microbiol. Mol. Biol. Rev. *68*, 538–559.

Bremer, H., and Dennis, P.P. (2008). Modulation of chemical composition and other parameters of the cell at different exponential growth rates. EcoSal Plus 2008.

Brewster, R.C., Weinert, F.M., Garcia, H.G., Song, D., Rydenfelt, M., and Phillips, R. (2014). The transcription factor titration effect dictates level of gene expression. Cell *156*, 1312–1323.

Bryant, D.W., and McCalla, D.R. (1980). Nitrofuran induced mutagenesis and error prone repair in Escherichia coli. Chem. Biol. Interact. *31*, 151–166.

Bryant, J.A., Sellars, L.E., Busby, S.J.W., and Lee, D.J. (2014). Chromosome position effects on gene expression in Escherichia coli K-12. Nucleic Acids Res. *42*, 11383–11392.

Burton, N.A., Johnson, M.D., Antczak, P., Robinson, A., and Lund, P.A. (2010). Novel aspects of the acid response network of E. coli K-12 are revealed by a study of transcriptional dynamics. J. Mol. Biol. *401*, 726–742.

Busse, H.J., Wöstmann, C., and Bakker, E.P. (1992). The bactericidal action of streptomycin: membrane permeabilization caused by the insertion of mistranslated proteins into the cytoplasmic membrane of Escherichia coli and subsequent caging of the antibiotic inside the cells due to degradation of these proteins. J. Gen. Microbiol. *138*, 551–561.

Castanie-Cornet, M.-P., Penfound, T.A., Smith, D., Elliott, J.F., and Foster, J.W. (1999). Control of acid resistance in Escherichia coli. J. Bacteriol. *181*, 3525–3535.

Cherepanov, P.P., and Wackernagel, W. (1995). Gene disruption in Escherichia coli: TcR and KmR cassettes with the option of Flp-catalyzed excision of the antibiotic-resistance determinant. Gene *158*, 9–14.

Chevereau, G., and Bollenbach, T. (2015). Systematic discovery of drug interaction mechanisms. Mol. Syst. Biol. *11*, 807.

Chevereau, G., Dravecká, M., Batur, T., Guvenek, A., Ayhan, D.H., Toprak, E., and Bollenbach, T. (2015). Quantifying the determinants of evolutionary dynamics leading to drug resistance. PLoS Biol. *13*, e1002299.

Cho, S., Cho, Y., Lee, S., Kim, J., Yum, H., Kim, S.C., and Cho, B.-K. (2013). Current challenges in bacterial transcriptomics. Genomics Inform. *11*, 76–82.

Cirz, R.T., Chin, J.K., Andes, D.R., Crécy-Lagard, V. de, Craig, W.A., and Romesberg, F.E. (2005). Inhibition of mutation and combating the evolution of antibiotic resistance. PLoS Biol. *3*, e176.

Clatworthy, A.E., Pierson, E., and Hung, D.T. (2007). Targeting virulence: a new paradigm for antimicrobial therapy. Nat. Chem. Biol. *3*, 541–548.

Claudi, B., Spröte, P., Chirkova, A., Personnic, N., Zankl, J., Schürmann, N., Schmidt, A., and Bumann, D. (2014). Phenotypic variation of Salmonella in host tissues delays eradication by antimicrobial chemotherapy. Cell *158*, 722–733.

Conway, T., Creecy, J.P., Maddox, S.M., Grissom, J.E., Conkle, T.L., Shadid, T.M., Teramoto, J., Miguel, P.S., Shimada, T., Ishihama, A., et al. (2014). Unprecedented high-resolution view of bacterial operon architecture revealed by RNA sequencing. MBio *5*, e01442-14.

Cooper, S., and Helmstetter, C.E. (1968). Chromosome replication and the division cycle of Escherichia coli Br. J. Mol. Biol. *31*, 519–540.

Costello, E.K., Lauber, C.L., Hamady, M., Fierer, N., Gordon, J.I., and Knight, R. (2009). Bacterial community variation in human body habitats across space and time. Science *326*, 1694–1697.

Costerton, J.W., and Cheng, K.J. (1975). The role of the bacterial cell envelope in antibiotic resistance. J. Antimicrob. Chemother. *1*, 363–377.

Costerton, J.W., Stewart, P.S., and Greenberg, E.P. (1999). Bacterial biofilms: a common cause of persistent infections. Science *284*, 1318–1322.

Cox, R.S., Dunlop, M.J., and Elowitz, M.B. (2010). A synthetic three-color scaffold for monitoring genetic regulation and noise. J. Biol. Eng. *4*, 10.

Dantas, G., Sommer, M.O.A., Oluwasegun, R.D., and Church, G.M. (2008). Bacteria subsisting on antibiotics. Science *320*, 100–103.

Datsenko, K.A., and Wanner, B.L. (2000). One-step inactivation of chromosomal genes in Escherichia coli K-12 using PCR products. Proc. Natl. Acad. Sci. USA *97*, 6640–6645.

Datta, S., Costantino, N., and Court, D.L. (2006). A set of recombineering plasmids for gram-negative bacteria. Gene *379*, 109–115.

Delacher, S., Derendorf, H., Hollenstein, U., Brunner, M., Joukhadar, C., Hofmann, S., Georgopoulos, A., Eichler, H.G., and Müller, M. (2000). A combined in vivo pharmacokinetic–in vitro pharmacodynamic approach to simulate target site pharmacodynamics of antibiotics in humans. J. Antimicrob. Chemother. *46*, 733–739.

Demple, B. (1991). Regulation of bacterial oxidative stress genes. Annu. Rev. Genet. *25*, 315–337.

Dethlefsen, L., McFall-Ngai, M., and Relman, D.A. (2007). An ecological and evolutionary perspective on human–microbe mutualism and disease. Nature *449*, 811–818.

Dörr, T., Vulić, M., and Lewis, K. (2010). Ciprofloxacin causes persister formation by inducing the TisB toxin in Escherichia coli. PLoS Biol. *8*, e1000317.

Dridi, B., Lupien, A., Bergeron, M.G., Leprohon, P., and Ouellette, M. (2015). Differences in antibiotic-induced oxidative stress responses between laboratory and clinical isolates of Streptococcus pneumoniae. Antimicrob. Agents Chemother. *59*, 5420–5426.

Dunlop, M.J., Cox, R.S., Levine, J.H., Murray, R.M., and Elowitz, M.B. (2008). Regulatory activity revealed by dynamic correlations in gene expression noise. Nat. Genet. *40*, 1493–1498.

El Meouche, I., Siu, Y., and Dunlop, M.J. (2016). Stochastic expression of a multiple antibiotic resistance activator confers transient resistance in single cells. Sci. Rep. *6*, 19538.

Eldar, A., and Elowitz, M.B. (2010). Functional roles for noise in genetic circuits. Nature *467*, 167–173.

Elf, J., Nilsson, K., Tenson, T., and Ehrenberg, M. (2006). Bistable bacterial growth rate in response to antibiotics with low membrane permeability. Phys. Rev. Lett. *97*, 258104.

Elowitz, M.B., Levine, A.J., Siggia, E.D., and Swain, P.S. (2002). Stochastic gene expression in a single cell. Science *297*, 1183–1186.

Esquerré, T., Laguerre, S., Turlan, C., Carpousis, A.J., Girbal, L., and Cocaign-Bousquet, M. (2013). Dual role of transcription and transcript stability in the regulation of gene expression in Escherichia coli cells cultured on glucose at different growth rates. Nucleic Acids Res. *42(4)*, 2460–2472.

Evans, D.J., Brown, M.R.W., Allison, D.G., and Gilbert, P. (1990). Susceptibility of bacterial biofilms to tobramycin: role of specific growth rate and phase in the division cycle. J. Antimicrob. Chemother. *25*, 585–591.

Falconer, S.B., Czarny, T.L., and Brown, E.D. (2011). Antibiotics as probes of biological complexity. Nat. Chem. Biol. *7*, 415–423.

Fleming, A. (1929). On the antibacterial action of cultures of a penicillium, with special reference to their use in the isolation of B. influenzæ. Br. J. Exp. Pathol. *10*, 226–236.

Flensburg, J., and Sköld, O. (1987). Massive overproduction of dihydrofolate reductase in bacteria as a response to the use of trimethoprim. Eur. J. Biochem. *162*, 473–476.

Foster, J.W. (2004). Escherichia coli acid resistance: tales of an amateur acidophile. Nat. Rev. Microbiol. *2*, 898–907.

Fridman, O., Goldberg, A., Ronin, I., Shoresh, N., and Balaban, N.Q. (2014). Optimization of lag time underlies antibiotic tolerance in evolved bacterial populations. Nature *513*, 418–421.

Friedman, N., Vardi, S., Ronen, M., Alon, U., and Stavans, J. (2005). Precise temporal modulation in the response of the SOS DNA repair network in individual bacteria. PLoS Biol. *3*, e238.

Gama-Castro, S., Salgado, H., Peralta-Gil, M., Santos-Zavaleta, A., Muñiz-Rascado, L., Solano-Lira, H., Jimenez-Jacinto, V., Weiss, V., García-Sotelo, J.S., López-Fuentes, A., et al. (2011). RegulonDB version 7.0: transcriptional regulation of Escherichia coli K-12 integrated within genetic sensory response units (Gensor Units). Nucleic Acids Res. *39*, D98–D105.

Gefen, O., Gabay, C., Mumcuoglu, M., Engel, G., and Balaban, N.Q. (2008). Single-cell protein induction dynamics reveals a period of vulnerability to antibiotics in persister bacteria. Proc. Natl. Acad. Sci. USA *105*, 6145–6149.

Gog, J.R., Murcia, A., Osterman, N., Restif, O., McKinley, T.J., Sheppard, M., Achouri, S., Wei, B., Mastroeni, P., Wood, J.L.N., et al. (2012). Dynamics of Salmonella infection of macrophages at the single cell level. J. R. Soc. Interface *9*, 2696–2707.

Goh, E.B., Yim, G., Tsui, W., McClure, J., Surette, M.G., and Davies, J. (2002). Transcriptional modulation of bacterial gene expression by subinhibitory concentrations of antibiotics. Proc. Natl. Acad. Sci. USA *99*, 17025–17030.

Goodson, M., and Rowbury, R.J. (1989). Habituation to normally lethal acidity by prior growth of Escherichia coli at a sub-lethal acid pH value. Lett. Appl. Microbiol. *8*, 77–79.

Gordon, A., Colman-Lerner, A., Chin, T.E., Benjamin, K.R., Yu, R.C., and Brent, R. (2007). Single-cell quantification of molecules and rates using open-source microscope-based cytometry. Nat. Methods *4*, 175–181.

Greco, W.R., Bravo, G., and Parsons, J.C. (1995). The search for synergy: a critical review from a response surface perspective. Pharmacol. Rev. *47*, 331–385.

Greenwood, D., and O'Grady, F. (1976). Activity and interaction of trimethoprim and sulphamethoxazole against Escherichia coli. J. Clin. Pathol. *29*, 162–166.

Greulich, P., Scott, M., Evans, M.R., and Allen, R.J. (2015). Growth-dependent bacterial susceptibility to ribosome-targeting antibiotics. Mol. Syst. Biol. *11*, 796.

Greulich, P., Dolezal, J., Scott, M., Evans, M.R., and Allen, R.J. (2017). Predicting the dynamics of bacterial growth inhibition by ribosome-targeting antibiotics. ArXiv170103702 Q-Bio.

Gupta, R.S. (2011). Origin of diderm (gram-negative) bacteria: antibiotic selection pressure rather than endosymbiosis likely led to the evolution of bacterial cells with two membranes. Antonie Van Leeuwenhoek *100*, 171–182.

Harvey, R.J. (1973). Growth and initiation of protein synthesis in Escherichia coli in the presence of trimethoprim. J. Bacteriol. *114*, 309–322.

Hebisch, E., Knebel, J., Landsberg, J., Frey, E., and Leisner, M. (2013). High variation of fluorescence protein maturation times in closely related Escherichia coli strains. PLoS ONE *8*, e75991.

Helaine, S., Cheverton, A.M., Watson, K.G., Faure, L.M., Matthews, S.A., and Holden, D.W. (2014). Internalization of Salmonella by macrophages induces formation of nonreplicating persisters. Science *343*, 204–208.

Henderson, I.R., Owen, P., and Nataro, J.P. (1999). Molecular switches — the ON and OFF of bacterial phase variation. Mol. Microbiol. *33*, 919–932.

Henry, R.J. (1943). The mode of action of sulfonamides. Bacteriol. Rev. *7*, 175–262.

Hersh, B.M., Farooq, F.T., Barstad, D.N., Blankenhorn, D.L., and Slonczewski, J.L. (1996). A glutamate-dependent acid resistance gene in Escherichia coli. J. Bacteriol. *178*, 3978–3981.

Heuveling, J., Possling, A., and Hengge, R. (2008). A role for Lon protease in the control of the acid resistance genes of Escherichia coli. Mol. Microbiol. *69*, 534–547.

Hinman, A.R. (1990). 1889 to 1989: a century of health and disease. Public Health Rep. *105*, 374–380.

Hoffman, L.R., D'Argenio, D.A., MacCoss, M.J., Zhang, Z., Jones, R.A., and Miller, S.I. (2005). Aminoglycoside antibiotics induce bacterial biofilm formation. Nature *436*, 1171–1175.

Hommais, F., Krin, E., Coppée, J.-Y., Lacroix, C., Yeramian, E., Danchin, A., and Bertin, P. (2004). GadE (YhiE): a novel activator involved in the response to acid environment in Escherichia coli. Microbiology *150*, 61–72.

Hu, J.C., Sherlock, G., Siegele, D.A., Aleksander, S.A., Ball, C.A., Demeter, J., Gouni, S., Holland, T.A., Karp, P.D., Lewis, J.E., et al. (2014). PortEco: a resource for exploring bacterial biology through high-throughput data and analysis tools. Nucleic Acids Res. *42*, D677-684.

Hua, Q., Yang, C., Oshima, T., Mori, H., and Shimizu, K. (2004). Analysis of gene expression in Escherichia coli in response to changes of growth-limiting nutrient in chemostat cultures. Appl. Environ. Microbiol. *70*, 2354–2366.

Huennekens, F.M. (1994). The methotrexate story: A paradigm for development of cancer chemotherapeutic agents. Adv. Enzyme Regul. *34*, 397–419.

Huisman, O., and D'Ari, R. (1981). An inducible DNA replication-cell division coupling mechanism in E. coli. Nature *290*, 797–799.

Huisman, O., D'Ari, R., and Gottesman, S. (1984). Cell-division control in Escherichia coli: specific induction of the SOS function SfiA protein is sufficient to block septation. Proc. Natl. Acad. Sci. USA *81*, 4490–4494.

Imlay, J.A. (2013). The molecular mechanisms and physiological consequences of oxidative stress: lessons from a model bacterium. Nat. Rev. Microbiol. *11*, 443–454.

Inoue, M., Hashimoto, H., and Mitsuhashi, S. (1970). Mechanism of tetracycline resistance in Staphylococcus aureus. I. Inducible resistance to tetracycline. J. Antibiot. (Tokyo) *23*, 68–74.

Jakobsson, H.E., Jernberg, C., Andersson, A.F., Sjölund-Karlsson, M., Jansson, J.K., and Engstrand, L. (2010). Short-term antibiotic treatment has differing long-term impacts on the human throat and gut microbiome. PLoS ONE *5*, e9836.

Jang, S., and Imlay, J.A. (2010). Hydrogen peroxide inactivates the Escherichia coli Isc iron-sulphur assembly system, and OxyR induces the Suf system to compensate. Mol. Microbiol. *78*, 1448–1467.

Jenkins, D.E., Schultz, J.E., and Matin, A. (1988). Starvation-induced cross protection against heat or H2O2 challenge in Escherichia coli. J. Bacteriol. *170*, 3910–3914.

John, A.C.S., and Goldberg, A.L. (1978). Effects of reduced energy production on protein degradation, guanosine tetraphosphate, and RNA synthesis in Escherichia coli. J. Biol. Chem. *253*, 2705–2711.

de Jong, I.G., Haccou, P., and Kuipers, O.P. (2011). Bet hedging or not? A guide to proper classification of microbial survival strategies. BioEssays *33*, 215–223.

Justice, S.S., Hunstad, D.A., Cegelski, L., and Hultgren, S.J. (2008). Morphological plasticity as a bacterial survival strategy. Nat. Rev. Microbiol. *6*, 162–168.

Kalan, L., and Wright, G.D. (2011). Antibiotic adjuvants: multicomponent anti-infective strategies. Expert Rev. Mol. Med. *13*.

Kanjee, U., and Houry, W.A. (2013). Mechanisms of acid resistance in Escherichia coli. Annu. Rev. Microbiol. *67*, 65–81.

Kaper, J.B., Nataro, J.P., and Mobley, H.L.T. (2004). Pathogenic Escherichia coli. Nat. Rev. Microbiol. *2*, 123–140.

Kearse, M., Moir, R., Wilson, A., Stones-Havas, S., Cheung, M., Sturrock, S., Buxton, S., Cooper, A., Markowitz, S., Duran, C., et al. (2012). Geneious Basic: An integrated and extendable desktop software platform for the organization and analysis of sequence data. Bioinformatics *28*, 1647–1649.

Keseler, I.M., Mackie, A., Peralta-Gil, M., Santos-Zavaleta, A., Gama-Castro, S., Bonavides-Martínez, C., Fulcher, C., Huerta, A.M., Kothari, A., Krummenacker, M., et al. (2013). EcoCyc: fusing model organism databases with systems biology. Nucleic Acids Res. *41*, D605–D612.

Klumpp, S., Zhang, Z., and Hwa, T. (2009). Growth rate-dependent global effects on gene expression in bacteria. Cell *139*, 1366–1375.

Kohanski, M.A., Dwyer, D.J., Hayete, B., Lawrence, C.A., and Collins, J.J. (2007). A common mechanism of cellular death induced by bactericidal antibiotics. Cell *130*, 797–810.

Kohanski, M.A., Dwyer, D.J., and Collins, J.J. (2010). How antibiotics kill bacteria: from targets to networks. Nat. Rev. Micro. *8*, 423–435.

Kong, H.H. (2011). Skin microbiome: genomics-based insights into the diversity and role of skin microbes. Trends Mol. Med. *17*, 320–328.

Krin, E., Danchin, A., and Soutourina, O. (2010). RcsB plays a central role in H-NS-dependent regulation of motility and acid stress resistance in Escherichia coli. Res. Microbiol. *161*, 363–371.

Krulwich, T.A., Sachs, G., and Padan, E. (2011). Molecular aspects of bacterial pH sensing and homeostasis. Nat. Rev. Microbiol. *9*, 330–343.

Kuchina, A., Espinar, L., Çağatay, T., Balbin, A.O., Zhang, F., Alvarado, A., Garcia-Ojalvo, J., and Süel, G.M. (2011). Temporal competition between differentiation programs determines cell fate choice. Mol. Syst. Biol. *7*, 557.

Kuhlman, T.E., and Cox, E.C. (2010). Site-specific chromosomal integration of large synthetic constructs. Nucleic Acids Res. *38*, e92–e92.

Kussell, E., and Leibler, S. (2005). Phenotypic diversity, population growth, and information in fluctuating environments. Science *309*, 2075–2078.

Kwon, Y.K., Higgins, M.B., and Rabinowitz, J.D. (2010). Antifolate-induced depletion of intracellular glycine and purines inhibits thymineless death in E. coli. ACS Chem. Biol. *5*, 787–795.

Lázár, V., Pal Singh, G., Spohn, R., Nagy, I., Horváth, B., Hrtyan, M., Busa-Fekete, R., Bogos, B., Méhi, O., Csörgő, B., et al. (2013). Bacterial evolution of antibiotic hypersensitivity. Mol. Syst. Biol. *9*, 700.

Lee, C., Lee, S.M., Mukhopadhyay, P., Kim, S.J., Lee, S.C., Ahn, W.-S., Yu, M.-H., Storz, G., and Ryu, S.E. (2004). Redox regulation of OxyR requires specific disulfide bond formation involving a rapid kinetic reaction path. Nat. Struct. Mol. Biol. *11*, 1179–1185.

Lennox, E.S. (1955). Transduction of linked genetic characters of the host by bacteriophage P1. Virology *1*, 190–206.

Levy, S.B., and Marshall, B. (2004). Antibacterial resistance worldwide: causes, challenges and responses. Nat. Med. *10*, S122–S129.

Lewin, C.S., and Amyes, S.G.B. (1991). The role of the SOS response in bacteria exposed to zidovudine or trimethoprim. J. Med. Microbiol. *34*, 329–332.

Lewis, K. (2010). Persister Cells. Annu. Rev. Microbiol. *64*, 357–372.

Leyer, G.J., and Johnson, E.A. (1993). Acid adaptation induces cross-protection against environmental stresses in Salmonella typhimurium. Appl. Environ. Microbiol. *59*, 1842–1847.

Lin, J., Smith, M.P., Chapin, K.C., Baik, H.S., Bennett, G.N., and Foster, J.W. (1996). Mechanisms of acid resistance in enterohemorrhagic Escherichia coli. Appl. Environ. Microbiol. *62*, 3094–3100.

Lin, J.T., Connelly, M.B., Amolo, C., Otani, S., and Yaver, D.S. (2005). Global transcriptional response of Bacillus subtilis to treatment with subinhibitory concentrations of antibiotics that inhibit protein synthesis. Antimicrob. Agents Chemother. *49*, 1915–1926.

Locke, J.C.W., Young, J.W., Fontes, M., Jiménez, M.J.H., and Elowitz, M.B. (2011). Stochastic pulse regulation in bacterial stress response. Science *334*, 366–369.

Lorian, V. (1975). Some effects of subinhibitory concentrations of antibiotics on bacteria. Bull. N. Y. Acad. Med. *51*, 1046–1055.

Lowder, M., Unge, A., Maraha, N., Jansson, J.K., Swiggett, J., and Oliver, J.D. (2000). Effect of starvation and the viable-but-nonculturable state on green fluorescent protein (GFP) fluorescence in GFP-tagged Pseudomonas fluorescens A506. Appl. Environ. Microbiol. *66*, 3160–3165.

Lutz, R., and Bujard, H. (1997). Independent and tight regulation of transcriptional units in Escherichia coli via the LacR/O, the TetR/O and AraC/I1-I2 regulatory elements. Nucleic Acids Res. *25*, 1203–1210.

Ma, Z., Masuda, N., and Foster, J.W. (2004). Characterization of EvgAS-YdeO-GadE branched regulatory circuit governing glutamate-dependent acid resistance in Escherichia coli. J. Bacteriol. *186*, 7378–7389.

MacKenzie, F.M., and Gould, I.M. (1993). The post-antibiotic effect. J. Antimicrob. Chemother. *32*, 519–537.

Mader, A., Bronk, B. von, Ewald, B., Kesel, S., Schnetz, K., Frey, E., and Opitz, M. (2015). Amount of colicin release in Escherichia coli is regulated by lysis gene expression of the colicin E2 operon. PLoS ONE *10*, e0119124.

Maier, T., Schmidt, A., Güell, M., Kühner, S., Gavin, A.C., Aebersold, R., and Serrano, L. (2011). Quantification of mRNA and protein and integration with protein turnover in a bacterium. Mol. Syst. Biol. *7*, 511.

Maiques, E., Úbeda, C., Campoy, S., Salvador, N., Lasa, Í., Novick, R.P., Barbé, J., and Penadés, J.R. (2006). β-lactam antibiotics induce the SOS response and horizontal transfer of virulence factors in Staphylococcus aureus. J. Bacteriol. *188*, 2726–2729.

Martín, J.F., and Liras, P. (1989). Organization and expression of genes involved in the biosynthesis of antibiotics and other secondary metabolites. Annu. Rev. Microbiol. *43*, 173–206.

Martinez, K.A., Kitko, R.D., Mershon, J.P., Adcox, H.E., Malek, K.A., Berkmen, M.B., and Slonczewski, J.L. (2012). Cytoplasmic pH response to acid stress in individual cells of Escherichia coli and Bacillus subtilis observed by fluorescence ratio imaging microscopy. Appl. Env. Microbiol. *78*, 3706–3714.

Martins, A.J., Narayanan, M., Prüstel, T., Fixsen, B., Park, K., Gottschalk, R.A., Lu, Y., Andrews-Pfannkoch, C., Lau, W.W., Wendelsdorf, K.V., et al. (2017). Environment tunes propagation of cell-to-cell variation in the human macrophage gene network. Cell Syst. *4*, 379–392.e12.

Mathieu, A., Fleurier, S., Frénoy, A., Dairou, J., Bredeche, M.-F., Sanchez-Vizuete, P., Song, X., and Matic, I. (2016). Discovery and function of a general core hormetic stress response in E. coli induced by sublethal concentrations of antibiotics. Cell Rep. *17*, 46–57.

Mathis, R., and Ackermann, M. (2016). Response of single bacterial cells to stress gives rise to complex history dependence at the population level. Proc. Natl. Acad. Sci. USA *113*, 4224–4229.

Maurice, C.F., Haiser, H.J., and Turnbaugh, P.J. (2013). Xenobiotics shape the physiology and gene expression of the active human gut microbiome. Cell *152*, 39–50.

Mazmanian, S.K., Liu, C.H., Tzianabos, A.O., and Kasper, D.L. (2005). An immunomodulatory molecule of symbiotic bacteria directs maturation of the host immune system. Cell *122*, 107–118.

McAdams, H.H., and Arkin, A. (1999). It's a noisy business! Genetic regulation at the nanomolar scale. Trends Genet. *15*, 65–69.

McCormick, S.J., and Tunnicliff, G. (2001). Kinetics of inactivation of glutamate decarboxylase by cysteine-specific reagents. Acta Biochim. Pol. *48*, 573–578.

McMahon, M.A.S., Xu, J., Moore, J.E., Blair, I.S., and McDowell, D.A. (2007). Environmental stress and antibiotic resistance in food-related pathogens. Appl. Env. Microbiol. *73*, 211–217.

McNulty, C.A.M., Boyle, P., Nichols, T., Clappison, P., and Davey, P. (2007). The public's attitudes to and compliance with antibiotics. J. Antimicrob. Chemother. *60*, i63–i68.

Megerle, J.A., Fritz, G., Gerland, U., Jung, K., and Rädler, J.O. (2008). Timing and dynamics of single cell gene expression in the arabinose utilization system. Biophys. J. *95*, 2103–2115.

Mégraud, F. (2004). H pylori antibiotic resistance: prevalence, importance, and advances in testing. Gut *53*, 1374–1384.

Meredith, H.R., Lopatkin, A.J., Anderson, D.J., and You, L. (2015). Bacterial temporal dynamics enable optimal design of antibiotic treatment. PLoS Comput. Biol. *11*, e1004201.

Miesenböck, G., De Angelis, D.A., and Rothman, J.E. (1998). Visualizing secretion and synaptic transmission with pH-sensitive green fluorescent proteins. Nature *394*, 192–195.

Mihalcescu, I., Gateau, M.V.-M., Chelli, B., Pinel, C., and Ravanat, J.-L. (2015). Green autofluorescence, a double edged monitoring tool for bacterial growth and activity in micro-plates. Phys. Biol. *12*, 066016.

Miller, C., Thomsen, L.E., Gaggero, C., Mosseri, R., Ingmer, H., and Cohen, S.N. (2004). SOS response induction by ß-lactams and bacterial defense against antibiotic lethality. Science *305*, 1629–1631.

Mitchell, A., Romano, G.H., Groisman, B., Yona, A., Dekel, E., Kupiec, M., Dahan, O., and Pilpel, Y. (2009). Adaptive prediction of environmental changes by microorganisms. Nature *460*, 220–224.

Mitosch, K., and Bollenbach, T. (2014). Bacterial responses to antibiotics and their combinations. Environ. Microbiol. Rep. *6*, 545–557.

Mitosch, K., Rieckh, G., and Bollenbach, T. (2017). Noisy response to antibiotic stress predicts subsequent single-cell survival in an acidic environment. Cell Syst. *4*, 393–403.e5.

Monici, M. (2005). Cell and tissue autofluorescence research and diagnostic applications. Biotechnol. Annu. Rev. *11*, 227–256.

Morones-Ramirez, J.R., Winkler, J.A., Spina, C.S., and Collins, J.J. (2013). Silver enhances antibiotic activity against gram-negative bacteria. Sci. Transl. Med. *5*, 190ra81.

Nachman, I., Regev, A., and Ramanathan, S. (2007). Dissecting timing variability in yeast meiosis. Cell *131*, 544–556.

Neish, A.S. (2009). Microbes in gastrointestinal health and disease. Gastroenterology *136*, 65–80.

Newman, D.K., and Banfield, J.F. (2002). Geomicrobiology: how molecular-scale interactions underpin biogeochemical systems. Science *296*, 1071–1077.

Newman, J.R.S., Ghaemmaghami, S., Ihmels, J., Breslow, D.K., Noble, M., DeRisi, J.L., and Weissman, J.S. (2006). Single-cell proteomic analysis of S. cerevisiae reveals the architecture of biological noise. Nature *441*, 840–846.

Ni, M., Decrulle, A.L., Fontaine, F., Demarez, A., Taddei, F., and Lindner, A.B. (2012). Pre-disposition and epigenetics govern variation in bacterial survival upon stress. PLoS Genet *8*, e1003148.

Nikaido, H., and Vaara, M. (1985). Molecular basis of bacterial outer membrane permeability. Microbiol. Rev. *49*, 1–32.

O'Boyle, C.J., MacFie, J., Mitchell, C.J., Johnstone, D., Sagar, P.M., and Sedman, P.C. (1998). Microbiology of bacterial translocation in humans. Gut *42*, 29–35.

Oehler, S., Eismann, E.R., Krämer, H., and Müller-Hill, B. (1990). The three operators of the lac operon cooperate in repression. EMBO J. *9*, 973–979.

Ozsolak, F., and Milos, P.M. (2011). RNA sequencing: advances, challenges and opportunities. Nat. Rev. Genet. *12*, 87–98.

Palmer, A.C., and Kishony, R. (2014). Opposing effects of target overexpression reveal drug mechanisms. Nat. Commun. *5*.

Parvez, S., Malik, K. a., Ah Kang, S., and Kim, H.-Y. (2006). Probiotics and their fermented food products are beneficial for health. J. Appl. Microbiol. *100*, 1171–1185.

Pedraza, J.M., and van Oudenaarden, A. (2005). Noise propagation in gene networks. Science *307*, 1965–1969.

Pedraza, J.M., and Paulsson, J. (2007). Random timing in signaling cascades. Mol. Syst. Biol. *3*, 81.

Pennacchietti, E., Lammens, T.M., Capitani, G., Franssen, M.C.R., John, R.A., Bossa, F., and De Biase, D. (2009). Mutation of His465 alters the pH-dependent spectroscopic properties of Escherichia coli glutamate decarboxylase and broadens the range of its activity toward more alkaline pH. J. Biol. Chem. *284*, 31587–31596.

Peterson, C.N., Levchenko, I., Rabinowitz, J.D., Baker, T.A., and Silhavy, T.J. (2012). RpoS proteolysis is controlled directly by ATP levels in Escherichia coli. Genes Dev. *26*, 548–553.

Pichichero, M.E., and Casey, J.R. (2007). Systematic review of factors contributing to penicillin treatment failure in Streptococcus pyogenes pharyngitis. Otolaryngol. Head Neck Surg. *137*, 851–857.

Pina, C., Teles, J., Fugazza, C., May, G., Wang, D., Guo, Y., Soneji, S., Brown, J., Edén, P., Ohlsson, M., et al. (2015). Single-cell network analysis identifies DDIT3 as a nodal lineage regulator in hematopoiesis. Cell Rep. *11*, 1503–1510.

Povolotsky, T.L., and Hengge, R. (2012). 'Life-style' control networks in Escherichia coli: Signaling by the second messenger c-di-GMP. J. Biotechnol. *160*, 10–16.

Price, M.N., Deutschbauer, A.M., Skerker, J.M., Wetmore, K.M., Ruths, T., Mar, J.S., Kuehl, J.V., Shao, W., and Arkin, A.P. (2013). Indirect and suboptimal control of gene expression is widespread in bacteria. Mol. Syst. Biol. *9*, 660.

Qiang, Z., and Adams, C. (2004). Potentiometric determination of acid dissociation constants (pKa) for human and veterinary antibiotics. Water Res *38*, 2874–2890.

Quackenbush, J. (2001). Computational analysis of microarray data. Nat. Rev. Genet. *2*, 418–427.

Ramsay, G. (1998). DNA chips: State-of-the art. Nat. Biotechnol. *16*, 40–44.

Rao, C.V., Wolf, D.M., and Arkin, A.P. (2002). Control, exploitation and tolerance of intracellular noise. Nature *420*, 231–237.

Ray, J.C.J., Tabor, J.J., and Igoshin, O.A. (2011). Non-transcriptional regulatory processes shape transcriptional network dynamics. Nat. Rev. Microbiol. *9*, 817–828.

Read, A.F., and Taylor, L.H. (2001). The ecology of genetically diverse infections. Science *292*, 1099–1102.

Richard, H., and Foster, J.W. (2004). Escherichia coli glutamate- and arginine-dependent acid resistance systems increase internal pH and reverse transmembrane potential. J. Bacteriol. *186*, 6032–6041.

Robinson, J.T., Thorvaldsdóttir, H., Winckler, W., Guttman, M., Lander, E.S., Getz, G., and Mesirov, J.P. (2011). Integrative genomics viewer. Nat. Biotechnol. *29*, 24–26.

Rolinson, G.N. (1980). Effect of β-lactam antibiotics on bacterial cell growth rate. Microbiology *120*, 317–323.

Ronen, M. (2002). Assigning numbers to the arrows: Parameterizing a gene regulation network by using accurate expression kinetics. Proc. Natl. Acad. Sci. USA *99*, 10555–10560.

Rosenfeld, N., Elowitz, M.B., and Alon, U. (2002). Negative autoregulation speeds the response times of transcription networks. J. Mol. Biol. *323*, 785–793.

Rossi, L., Silva, J.M., McGirr, L.G., and O'Brien, P.J. (1988). Nitrofurantoin-mediated oxidative stress cytotoxicity in isolated rat hepatocytes. Biochem. Pharmacol. *37*, 3109–3117.

Ryu, J.-H., and Beuchat, L.R. (1998). Influence of acid tolerance responses on survival, growth, and thermal cross-protection of Escherichia coli O157:H7 in acidified media and fruit juices. Int. J. Food. Microbiol. *45*, 185–193.

Sánchez-Romero, M.A., and Casadesús, J. (2014). Contribution of phenotypic heterogeneity to adaptive antibiotic resistance. Proc. Natl. Acad. Sci. USA *111*, 355–360.

Sangurdekar, D.P., Zhang, Z., and Khodursky, A.B. (2011). The association of DNA damage response and nucleotide level modulation with the antibacterial mechanism of the anti-folate drug Trimethoprim. BMC Genomics *12*, 583.

Scott, M., Gunderson, C.W., Mateescu, E.M., Zhang, Z., and Hwa, T. (2010). Interdependence of cell growth and gene expression: origins and consequences. Science *330*, 1099–1102.

Sengupta, S., Rahman, M.S., Mukherjee, U., Basak, J., Pal, A.K., and Chatterjee, S.N. (1990). DNA damage and prophage induction and toxicity of nitrofurantoin in Escherichia coli and Vibrio cholerae cells. Mutat. Res. Lett. *244*, 55–60.

Seo, S.W., Kim, D., O'Brien, E.J., Szubin, R., and Palsson, B.O. (2015). Decoding genome-wide GadEWX-transcriptional regulatory networks reveals multifaceted cellular responses to acid stress in Escherichia coli. Nat. Commun. *6*, 7970.

Shaner, N.C., Steinbach, P.A., and Tsien, R.Y. (2005). A guide to choosing fluorescent proteins. Nat. Methods *2*, 905–909.

Shaw, K.J., Miller, N., Liu, X., Lerner, D., Wan, J., Bittner, A., and Morrow, B.J. (2003). Comparison of the changes in global gene expression of Escherichia coli induced by four bactericidal agents. J. Mol. Microbiol. Biotechnol. *5*, 105–122.

Silander, O.K., Nikolic, N., Zaslaver, A., Bren, A., Kikoin, I., Alon, U., and Ackermann, M. (2012). A genome-wide analysis of promoter-mediated phenotypic noise in Escherichia coli. PLoS Genet. *8*, e1002443.

Sinai, L., Rosenberg, A., Smith, Y., Segev, E., and Ben-Yehuda, S. (2015). The molecular timeline of a reviving bacterial spore. Mol. Cell *57*, 695–707.

Sinha, P.K., Castro-Guerrero, N., Patki, G., Sato, M., Torres-Bacete, J., Sinha, S., Miyoshi, H., Matsuno-Yagi, A., and Yagi, T. (2015). Conserved amino acid residues of the NuoD segment important for structure and function of Escherichia coli NDH-1 (Complex I). Biochemistry (Mosc.) *54*, 753–764.

Smirnova, G.V., N. Oktyabrsky, O., V. Moshonkina, E., and Zakirova, N.V. (1994). Induction of the alkylation-inducible aidB gene of Escherichia coli by cytoplasmic acidification and N-ethylmaleimide. Mutat. Res. Repair *314*, 51–56.

Snijder, B., Sacher, R., Rämö, P., Damm, E.-M., Liberali, P., and Pelkmans, L. (2009). Population context determines cell-to-cell variability in endocytosis and virus infection. Nature *461*, 520–523.

Soupene, E., Heeswijk, W.C. van, Plumbridge, J., Stewart, V., Bertenthal, D., Lee, H., Prasad, G., Paliy, O., Charernnoppakul, P., and Kustu, S. (2003). Physiological studies of Escherichia coli strain MG1655: growth defects and apparent cross-regulation of gene expression. J. Bacteriol. *185*, 5611–5626.

Spellberg, B., and Taylor-Blake, B. (2013). On the exoneration of Dr. William H. Stewart: debunking an urban legend. Infect. Dis. Poverty *2*, 3.

Stewart-Ornstein, J., Weissman, J.S., and El-Samad, H. (2012). Cellular noise regulons underlie fluctuations in Saccharomyces cerevisiae. Mol. Cell *45*, 483–493.

Stincone, A., Daudi, N., Rahman, A.S., Antczak, P., Henderson, I., Cole, J., Johnson, M.D., Lund, P., and Falciani, F. (2011). A systems biology approach sheds new light on Escherichia coli acid resistance. Nucleic Acids Res. *39*, 7512–7528.

Storz, G., Tartaglia, L.A., and Ames, B.N. (1990). Transcriptional regulator of oxidative stress-inducible genes: direct activation by oxidation. Science *248*, 189–194.

Streker, K., Freiberg, C., Labischinski, H., Hacker, J., and Ohlsen, K. (2005). Staphylococcus aureus NfrA (SA0367) is a flavin mononucleotide-dependent NADPH oxidase involved in oxidative stress response. J. Bacteriol. *187*, 2249–2256.

Süel, G.M., Garcia-Ojalvo, J., Liberman, L.M., and Elowitz, M.B. (2006). An excitable gene regulatory circuit induces transient cellular differentiation. Nature *440*, 545–550.

Sun, Y., Fukamachi, T., Saito, H., and Kobayashi, H. (2011). ATP requirement for acidic resistance in Escherichia coli. J. Bacteriol. *193*, 3072–3077.

Sun, Y., Fukamachi, T., Saito, H., and Kobayashi, H. (2012). Adenosine deamination increases the survival under acidic conditions in Escherichia coli. J. Appl. Microbiol. *112*, 775–781.

Tagkopoulos, I., Liu, Y.-C., and Tavazoie, S. (2008). Predictive behavior within microbial genetic networks. Science *320*, 1313–1317.

Tan, C., Smith, R.P., Srimani, J.K., Riccione, K.A., Prasada, S., Kuehn, M., and You, L. (2012). The inoculum effect and band-pass bacterial response to periodic antibiotic treatment. Mol. Syst. Biol. *8*, 617.

Taniguchi, Y., Choi, P.J., Li, G.W., Chen, H., Babu, M., Hearn, J., Emili, A., and Xie, X.S. (2010). Quantifying E. coli proteome and transcriptome with single-molecule sensitivity in single cells. Science *329*, 533–538.

Tavazoie, S., Hughes, J.D., Campbell, M.J., Cho, R.J., and Church, G.M. (1999). Systematic determination of genetic network architecture. Nat. Genet. *22*, 281–285.

Thorvaldsdóttir, H., Robinson, J.T., and Mesirov, J.P. (2013). Integrative Genomics Viewer (IGV): high-performance genomics data visualization and exploration. Brief. Bioinform. *14*, 178–192.

Toprak, E., Veres, A., Michel, J.B., Chait, R., Hartl, D.L., and Kishony, R. (2012). Evolutionary paths to antibiotic resistance under dynamically sustained drug selection. Nat. Genet. *44*, 101–105.

Tsai, M.-F., McCarthy, P., and Miller, C. (2013). Substrate selectivity in glutamate-dependent acid resistance in enteric bacteria. Proc. Natl. Acad. Sci. USA *110*, 5898–5902.

Tsuru, S., Ichinose, J., Kashiwagi, A., Ying, B.-W., Kaneko, K., and Yomo, T. (2009). Noisy cell growth rate leads to fluctuating protein concentration in bacteria. Phys. Biol. *6*, 036015.

Tuomanen, E., Cozens, R., Tosch, W., Zak, O., and Tomasz, A. (1986). The rate of killing of Escherichia coli by β-lactam antibiotics is strictly proportional to the rate of bacterial growth. J. Gen. Microbiol. *132*, 1297–1304.

Uphoff, S., Lord, N.D., Okumus, B., Potvin-Trottier, L., Sherratt, D.J., and Paulsson, J. (2016). Stochastic activation of a DNA damage response causes cell-to-cell mutation rate variation. Science *351*, 1094–1097.

VanBogelen, R.A., and Neidhardt, F.C. (1990). Ribosomes as sensors of heat and cold shock in Escherichia coli. Proc. Natl. Acad. Sci. USA *87*, 5589–5593.

Venturelli, O.S., Zuleta, I., Murray, R.M., and El-Samad, H. (2015). Population diversification in a yeast metabolic program promotes anticipation of environmental shifts. PLoS Biol. *13*, e1002042.

Vogelman, B., and Craig, W.A. (1986). Kinetics of antimicrobial activity. J. Pediatr. *108*, 835–840.

Waksman, S.A. (1961). The role of antibiotics in Nature. Perspect. Biol. Med. *4*, 271–287.

Walsh, C. (2003). Antibiotics: actions, origins, resistance (Washington, DC: ASM Press).

Wang, G., and Doyle, M.P. (1998). Heat shock response enhances acid tolerance of Escherichia coli O157:H7. Lett. Appl. Microbiol. *26*, 31–34.

Weber, H., Polen, T., Heuveling, J., Wendisch, V.F., and Hengge, R. (2005). Genome-wide analysis of the general stress response network in Escherichia coli: σS-dependent genes, promoters, and sigma factor selectivity. J. Bacteriol. *187*, 1591–1603.

Wei, J.R., Krishnamoorthy, V., Murphy, K., Kim, J.H., Schnappinger, D., Alber, T., Sassetti, C.M., Rhee, K.Y., and Rubin, E.J. (2011). Depletion of antibiotic targets has widely varying effects on growth. Proc. Natl. Acad. Sci. USA *108*, 4176–4181.

Weinstein, D.H., deRijke, S., Chow, C.C., Foruraghi, L., Zhao, X., Wright, E.C., Whatley, M., Maass-Moreno, R., Chen, C.C., and Wank, S.A. (2013). A new method for determining gastric acid output using a wireless pH-sensing capsule. Aliment. Pharmacol. Ther. *37*, 1198–1209.

Young, J.W., Locke, J.C.W., Altinok, A., Rosenfeld, N., Bacarian, T., Swain, P.S., Mjolsness, E., and Elowitz, M.B. (2012). Measuring single-cell gene expression dynamics in bacteria using fluorescence time-lapse microscopy. Nat. Protoc. *7*, 80–88.

Young, J.W., Locke, J.C.W., and Elowitz, M.B. (2013). Rate of environmental change determines stress response specificity. Proc. Natl. Acad. Sci. USA *110*, 4140–4145.

Youngman, R.J., Osswald, W.F., and Elstner, E.F. (1982). Mechanisms of oxygen activation by nitrofurantoin and relevance to its toxicity. Biochem. Pharmacol. *31*, 3723–3729.

Ysern, P., Clerch, B., Castańo, M., Gibert, I., Barbé, J., and Llagostera, M. (1990). Induction of SOS genes in Escherichia coli and mutagenesis in Salmonella typhimurium by fluoroquinolones. Mutagenesis *5*, 63–66.

Yurkovsky, E., and Nachman, I. (2013). Event timing at the single-cell level. Brief. Funct. Genomics *12*, 90–98.

Zampar, G.G., Kümmel, A., Ewald, J., Jol, S., Niebel, B., Picotti, P., Aebersold, R., Sauer, U., Zamboni, N., and Heinemann, M. (2013). Temporal system-level organization of the switch from glycolytic to gluconeogenic operation in yeast. Mol. Syst. Biol. *9*, 651.

Zampieri, M., Zimmermann, M., Claassen, M., and Sauer, U. (2017). Nontargeted metabolomics reveals the multilevel response to antibiotic perturbations. Cell Rep. *19*, 1214–1228.

Zaslaver, A., Mayo, A.E., Rosenberg, R., Bashkin, P., Sberro, H., Tsalyuk, M., Surette, M.G., and Alon, U. (2004). Just-in-time transcription program in metabolic pathways. Nat. Genet. *36*, 486–491.

Zaslaver, A., Bren, A., Ronen, M., Itzkovitz, S., Kikoin, I., Shavit, S., Liebermeister, W., Surette, M.G., and Alon, U. (2006). A comprehensive library of fluorescent transcriptional reporters for Escherichia coli. Nat. Meth. *3*, 623–628.

Zhang, X., McDaniel, A.D., Wolf, L.E., Keusch, G.T., Waldor, M.K., and Acheson, D.W.K. (2000). Quinolone antibiotics induce shiga toxin-encoding bacteriophages, toxin production, and death in mice. J. Infect. Dis. *181*, 664–670.

Zieg, J., Silverman, M., Hilmen, M., and Simon, M. (1977). Recombinational switch for gene expression. Science *196*, 170–172.